DEFINING THE FUNCTION OF AN UNCHARACTERIZED CBASS GENE IN THE REGULATION OF 3'3'-CGAMP SIGNALING IN *VIBRIO CHOLERAE*

By

Soo hun Yoon

A DISSERTATION

Submitted to
Michigan State University
in partial fulfillment of the requirements
for the degree of

Microbiology and Molecular Genetics – Doctor of Philosophy

2022

ABSTRACT

Bacteria compete with phages in a myriad of environments for survival. This constant arms race has led to the acquisition of cyclic oligonucleotide based antiphage signaling system (CBASS) throughout all bacterial phyla. Phage infection activates CBASS which results in altruistic suicide of the host to save the clonal community, a process termed abortive infection. In *Vibrio cholerae* El Tor, CBASS is comprised of DncV, CapV, Vc0180, and Vc0181. DncV is activated following phage infection to synthesize 3'3'-cGAMP which activates CapV, a phospholipase that degrades the cellular membrane. Though evidence suggests VC0180 and VC0181 allow for response against broader range of phages, their function in relation to DncV remains undefined.

To determine their role, we investigate the effect of VC0180 and VC0181 on the stability of DncV in vivo. During this pursuit, we discovered a novel protein which we named Bumo, for Bacterial Ubiquitin Modifier, encoded upstream of *capV* that is a component of the CBASS operon. We show a novel regulatory network of DncV, in which Bumo protects DncV from degradation and that VC0181 is a protease that degrades DncV. We also show evidence that VC0180 interacts with DncV.

To expand our knowledge of CBASS, we also explored the function of CBASS systems encoding HNH-SAVED effectors in other Gram-negative bacteria. We discovered *E. coli* EDEC13E and *P. fluorescens* SRM1 have active CBASS systems that affect the growth capacity of heterologous hosts. We also show their nucleotide substrate specificity. Interestingly, the *E. coli* EDEC13E HNH-SAVED effector is inactivated following the

addition of nucleotide signals, which is distinct from all previously described CBASS systems.

In conclusion, Bumo is a newly discovered component of the CBASS operon that protects DncV from degradation by Vc0181. VC0180 and VC0181 both regulate DncV in separate ways. Moreover, the function of CBASS is conserved in other Gram-negative species, even though they may have adapted to respond differentially to cyclic oligonucleotide signals. The results of my thesis work lead to a better appreciation of the complexity in the regulation of CBASS signaling and the diversity in evolution of CBASS across species.

This thesis is dedicated to my parents and family both biological and non-biological.
Thank you all for your love, support, and encouragements throughout the years.
Merci pour votre courages et support durant mon entrainement.
엄마, 아빠, 누나, 동생과 가족들 사랑과 기도 감사합니다.

ACKNOWLEDGEMENTS

I want to acknowledge first and foremost my family and close friends who have been there through the rough times and the good times, for their unconditional love and support. The time that you spend encouraging, supporting and loving me have helped me persevere. I want to thank Dr. Chris Waters, my PI, who have been so kind in guiding and sharing his wisdom with me throughout my training and creating a safe space for me to reach my potential. I especially want to acknowledge the patience and understanding he showed when I was going through multiple health crises throughout my training and how supportive he is of my aspirations and vision. I want to acknowledge members of the Waters lab, both former and current who have been there to create a safe, loving, and supportive environment that helped me thrive and achieve all that I did. I especially want to thank Brian Hsueh who have been a great friend and colleague I could bounce ideas with and share in the down and up sides of research and life. I also want to specially acknowledge my undergraduate associates Ram Sanath-Kumar and Elise Trost who have been amazing student, enthusiastic about science, ready to learn and being great implementers of knowledge. I want to thank Geoffrey Severin, who have been an awesome lab mate, encourager, and scientist to bounce ideas off of with. I would like to thank my close friend Alex Moauro, Meng-lun Hsieh and Michael Maiden who have made this journey worthwhile and memorable. I would like to acknowledge my close friends from around the world who gave me their time, encouragement, memories of travel and food. I would like to acknowledge the Chauvancy family for their unconditional love, encouragement, and hospitality. I would also like to give a shout out to my undergraduate mentor Dr. Greg Powell and Dr. Cynthia Powell for their wisdom, guidance and encouragement that helped me persevere.

I would like to thank my committee members Dr. Kristen Parent, Dr. Neal Hammer, Dr. Sean Crossen and Dr. Shannon Manning for their guidance, wisdom, and support. I would like to acknowledge Dr. Anthony Schilmiller and Dr. Lijun Chen of the Michigan State University Metabolomics and Mass Spec Core for the patience and help in my project throughout the years even though I continue to struggle with Mass Spec.

TABLE OF CONTENTS

LIST OF ABBREVIATIONS

Bumo	Bacterial ubiquitin-like modifier
cAMP	Cyclic AMP
CBASS	Cyclic/oligonucleotide based antiphage signaling system
cdN	Cyclic di nucleotide
c-di-AMP	Cyclic di adenosine monophosphate
c-di-GMP	Cyclic di guanosine monophosphate
cDNA	Complementary DNA
CD-NTase	cGAS/DncV-like nucleotidytransferase
cGAMP	Cyclic guanosine monophosphate - adenosine monophosphate
CIP	Calf intestinal phosphatase
coN	Cyclic oligonucleotide
CT	Cholera toxin
ctN	Cyclic trinucleotide
DAC	Diadenylate cyclase
dCMP	Deoxycytidine monophosphate
dCTP	Deoxycytidine triphosphate
DHF	Dihydrofolate
DGC	Diguanylate cyclase
DUB	Deubiquitinase
dUMP	Deoxyuridine monophosphate
EDEC	*E. coli* EDEC13E
EOP	Efficiency of plaquing
NTP	Nucleotide triphosphates

OMV	Outer membrane vesicles
PCR	Polymerase chain reaction
PDE	Phosphodiesterase
Pf	*P. fluorescens* SRM1
PLE	phage-inducible chromosomal island-like elements
PUP	Prokaryotic ubiquitin-like modifier
SUMO	Small ubiquitin-like modifier
TCP	Toxin-coregulated pilus
THF	Tetrahydrofolate
TLC	Thin layer chromatography
TSS	Transcriptional start site
Ubl	Ubiquitin-like protein
Vc	*Vibrio cholerae*
VPI-1	*Vibrio* pathogenicity island 1
VSP-I/II	*Vibrio* seventh pandemic island I or II

CHAPTER 1:

INTRODUCTION

Part of this chapter was published in:

Yoon S hun, Waters CM. 2019. Vibrio cholerae. Trends Microbiol 27:806–807.

Yoon SH, Waters CM. 2021. The ever-expanding world of bacterial cyclic oligonucleotide second messengers. Curr Opin Microbiol 60:96–103.

1.1 *Vibrio cholerae*: The Diarrheal Pathogen

Vibrio cholerae is the primary bacterial pathogen responsible for the Cholera pandemic worldwide (1). Plaguing many developing nations and areas of poor sanitation, it causes about 2.9 million cases and ~95,000 deaths annually that are worsened in times of natural disasters and humanitarian crises (2, 3). Characterized by its curved-shaped rod, this Gram-negative bacterium causes "rice-watery" stools upon consumption of contaminated food or water (**Fig. 1.1**).

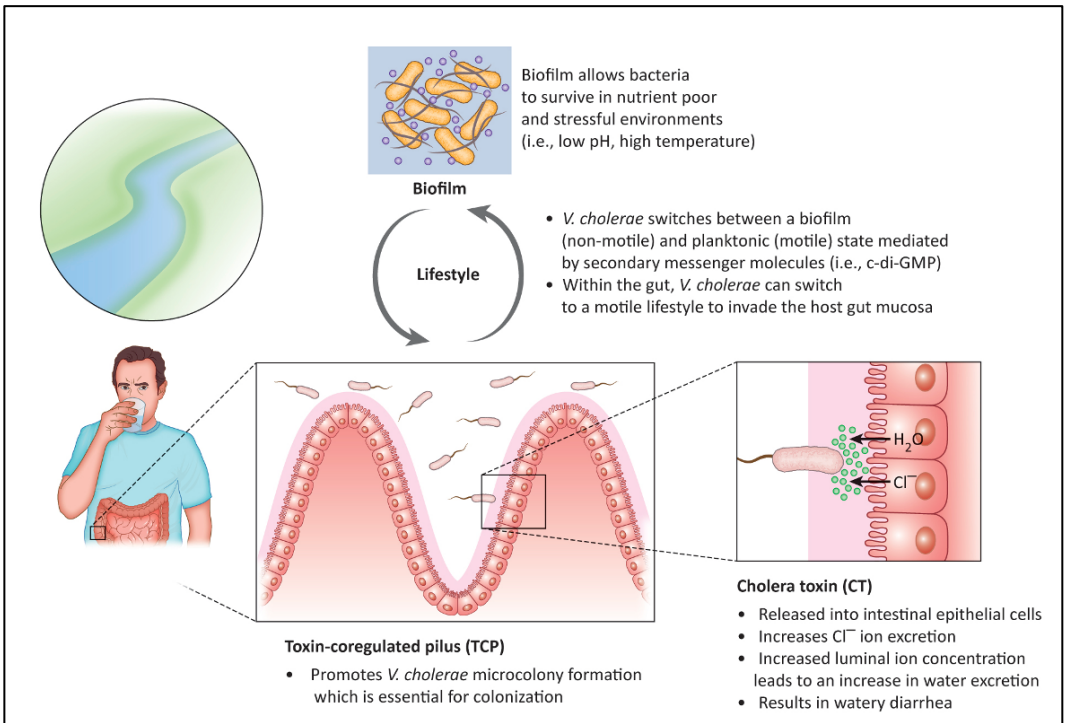

Figure 1.1 *Vibrio cholerae* is a diarrhea causing pathogen spread by contaminated water. *V. cholerae* switches between a motile and biofilm lifestyle depending on the environment. After colonization of the human mucosa, they release virulence factors TCP and CT to cause diarrhea.

A previously healthy host can succumb to the illness due to two major virulence factors released: toxin-coregulated pilus (TCP) and cholera toxin (CT) (1, 4). TCP is important for colonization of the host gut mucosal layer where CT is released and passes through the gastro-endothelial wall to cause watery diarrhea (5, 6). CT binds to and

activates the G-alpha protein via ADP-ribosylation which induces adenylate cyclase to synthesize cAMP (7–9). CT induction leads to cAMP levels hundreds of fold over normal physiological levels leading to downstream activation of chloride ion channels, primarily the cystic fibrosis transmembrane conductance regulator (CFTR) (8, 10, 11). This results in massive efflux of chloride ions and expulsion of water, sodium, potassium and bicarbonates and diminished absorption that leads to dehydration and diarrhea characteristic of the disease (12, 13) (**Fig. 1.1**). If not adequately attended to, mass dehydration can lead to hypovolemic shock and metabolic acidosis that can prove fatal. Oral rehydration therapy is the main course of treatment with antibiotics as adjunct in case of prolonged or severe diarrhea (1, 3, 12). However, water sanitation and proper hygiene are the best proven preventative measures for cholera. Proper hygiene methods and treatment can decrease mortality from 50% to less than 1% (3, 13, 14). Though easy to treat and less lethal than other well-known bacterial pathogens such as *Mycobacterium tuberculosis*, cholera continues to be a threat in resource poor and endemic regions especially during times of natural disasters, wars as in Yemen and seasonal heavy rainfall as seen in many endemic Sub-Saharan African countries (2, 3).

Vibrio cholerae is found in a myriad of environments. It often resides in saline waters along coasts and estuaries in association with shellfish and zooplanktons. Biofilm formation provides protection and a means of transportation for the bacteria to colonize and survive in these diverse environments (15, 16). They aggregate as biofilms, entering a dormant state to safeguard against varying pH, temperature, low nutrients or predations and propagate when conditions are optimal (13, 16–18). Chitin is the main carbon source of *Vibrio cholerae* in the aquatic environment and the lack thereof can facilitate biofilm formation (19, 20). *V. cholerae* is used as a model organism to study virulence in Gram-

negative bacteria due to its high infectious dose, ease of genetic manipulation, and rapid replication time (21–23). *V. cholerae* is also a model for studying chemical signaling such as cell-to-cell communication via quorum sensing and cyclic di-nucleotide signaling, both of which facilitate the lifestyle switch between motile and biofilms states of the bacterium in response to the environment (15, 24).

Cholera is caused by two serogroups of *Vibrio cholerae,* the O139 and O1 serogroups, with the latter being the main causative agent. The O1 serogroup can be further divided into the classical and El Tor biotypes (1, 25). The El tor biotype is the primary agent accountable for the current 7th Cholera pandemic while the classical biotype was responsible for the previous six pandemics from the early 1800s to the start of the current pandemic in 1961 (26–29). Unlike the classical biotype, it had acquired two pathogenic islands, VSP-1 and VSP-2 that allow for its prominence (26, 30). The functions of the majority of the genes encoded in the islands are unknown. Recent work has shown the presence of two potential bacteriophage defense islands, AvcID and CBASS (31, 32). My thesis research used *V. cholerae* as a model system to better understand cyclic dinucleotide signaling and its connection to phage defense. I will review this topic in this chapter.

1.2 Diverse world of Cyclic di nucleotide signaling

Elucidating the molecular underpinnings of how bacteria sense and respond to their environment is central to understand their evolution and adaptation. Given their ecological diversity, it is therefore not surprising that bacteria encode a myriad of strategies to respond to ever changing challenges including transcription factors(33, 34), two-component and phosphorelay pathways (35), mechanosensing (36), and chemotaxis (37). Of primary importance to environmental sensing and adaptation are second messenger signaling pathways. These pathways recognize and respond to a "first" signal that modulates the activity of a synthesis or degradation enzyme that controls the level of an intracellular signal molecule. Second messengers in bacteria are primarily purine derived modified nucleotides, which exert global regulatory effects by altering transcription, translation, or even protein activity (38).

Second messenger systems have long been recognized as global regulatory networks in bacteria (and all living systems), but we have just begun to fully appreciate their diversity and central importance to many aspects of bacterial physiology. The original second messenger systems discovered include cyclic AMP, which is primarily associated with the regulation of carbon utilization (39, 40) as well as other central traits such as biofilm formation, virulence, and central metabolism (41–43), and guanine penta/tetraphosphate that drives the bacterial stringent response (44, 45). However, this chapter will focus on the more recent additions to this chemical lexicon, cyclic di- and trinucleotide (cdN and ctN) second messengers (**Fig. 1.2**).

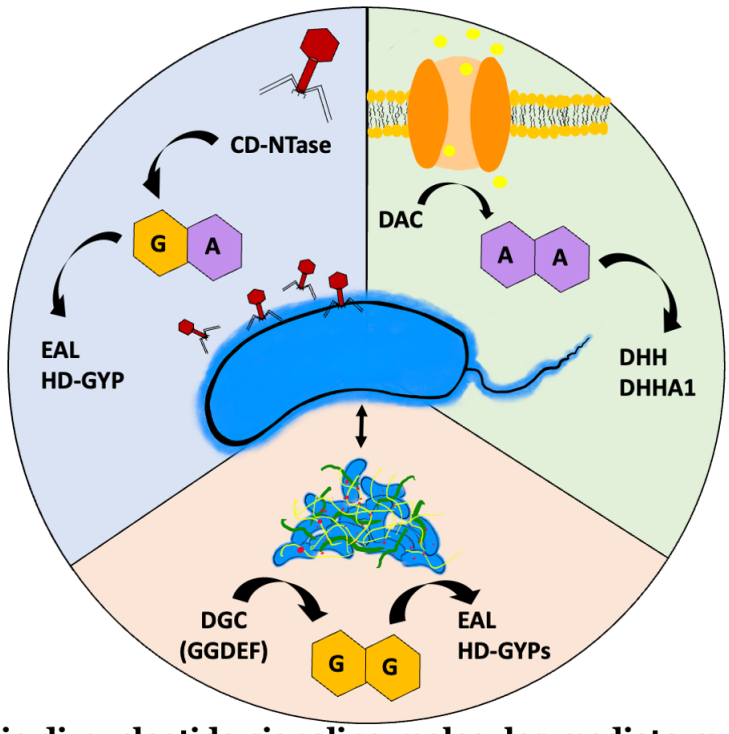

Figure 1.2. Cyclic di nucleotide signaling molecules mediate multiple response pathways in bacteria. Top left: cGAMP is synthesized by CD-NTases in response to phage infection and is broken down by EAL and HD-GYP phosphodiesterases. Top right: c-di-AMP mediate osmoregulation in Gram-Positive bacteria. They are synthesized by DAC family of proteins and broken down by DHH and DHHA1 enzymes. Bottom: c-di-GMP is synthesized by DGCs and metabolized by EAL and HD-GYP phosphodiesterases. They are the major molecular signal mediating biofilm formation and motility in *V. cholerae*.

Cyclic di-GMP (c-di-GMP) controls transitions from motility to biofilm formation.

The first described cdN in any living organism is 3'-5', 3'-5' c-di-GMP. This second messenger was first identified and characterized by Moshe Benziman's laboratory studying cellulose biosynthesis in *Komagataeibacter xylinus* (46–48), although the prevalence of this cdN was not widely appreciated until 2000 – 2005 with the advent of bacterial genome sequencing and a renewed interest in understanding the molecular mechanisms that regulate biofilm formation (48). Analysis of bacterial genomes revealed a widely conserved domain of unknown function that was homologous to Benziman's c-di-GMP synthases (49–51). This domain, which possess diguanylate cyclase (DGC) activity, was named the "GGDEF" domain for the key amino acids in its active site (52). The corresponding c-di-GMP phosphodiesterase (PDE) that degrades c-di-GMP was soon shown to be another widely conserved enzymatic domain that was named the "EAL" domain (53, 54). Moreover, a second PDE domain termed the HD-GYP domain was demonstrated to also degrade c-di-GMP (55). GGDEF, EAL, and HD-GYP enzymes are present in the vast majority of bacteria, and in addition to being widely conserved, bacterial genomes can encode up to dozens of enzymes involved in c-di-GMP synthesis or degradation (56). Seminal studies of biofilm formation and motility in *Escherichia coli, Vibrio cholerae, Salmonella* Typhimurium *sp.*, and development in *Caulobacter crescentus* demonstrated that c-di-GMP regulated by DGCs and PDEs was associated with the transitions between motile and sessile lifestyles (50, 57, 58).

C-di-GMP signaling enzymes typically are multidomain proteins consisting of an N-terminal sensory domain and a C-terminal enzymatic domain (48). The N-terminal domain is proposed to bind specific environmental cues that regulate the synthesis and degradation of c-di-GMP, such that in specific environments a sessile lifestyle is

initiated or inhibited. Although a handful of environmental cues are known (for example oxygen (59), spermine (60), bile and bicarbonate (61), and reducing conditions (62)), the majority of environmental signals regulating DGCs and PDEs remain to be discovered (**Fig. 1.3**). Changes in the intracellular concentration of c-di-GMP is sensed by a myriad of transcription factors, riboswitches, and protein complexes whose activity is controlled by directly binding to c-di-GMP (48, 63). Although classically known as an inducer of biofilm formation and repressor of motility, c-di-GMP functions as a global regulator controlling numerous phenotypes including but not limited to bacterial predation (64), virulence (65), development (66), DNA repair (67), and cell shape (68). C-di-GMP signaling systems are primarily found in bacteria, although stalk cell formation in the slime mold *Dictyostelium discoideum* is dependent on c-di-GMP (69).

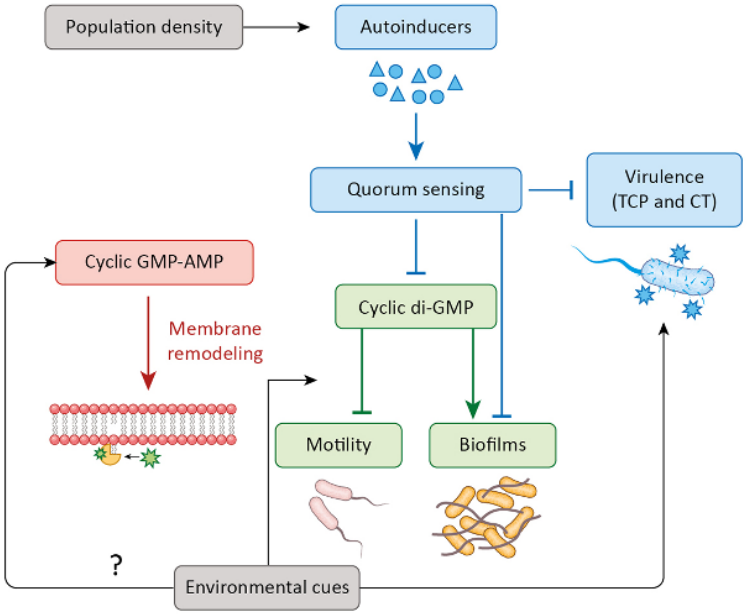

Figure 1.3. cGAMP and c-di-GMP respond to environmental stimuli in *V. cholerae*. Cyclic di-GMP responds to multiple environment stimuli such as population density. It mediates multiple downstream effectors that regulate biofilm formation and inhibition of motility. cGAMP responds to multiple environmental signals, many of which are unknown. One signal is phage infection which leads to abortive infection.

Cyclic di-AMP (c-di-AMP)

The next cdN to be discovered in 2008 was 3'-5', 3'-5' c-di-AMP, first observed to be synthesized by the DNA integrity scanning protein DisA (70). As excellent reviews of c-di-AMP have been recently published, we will only briefly summarize it here (71, 72). C-di-AMP is found in many bacterial and archaeal species, and it is notable for having been identified in many Gram-positive bacteria not known to use c-di-GMP (73, 74). C-di-AMP is synthesized by diadenylate cyclase enzymes (DAC) and degraded by PDEs that have a DHH-DHHA1 domain (71) (**Fig. 1.2**). C-di-AMP has notable differences from c-di-GMP including that most bacteria encode only one or a few DACs (73), and c-di-AMP is essential in many but not all bacterial species including the *Firmicutes* (71, 75). This requirement for growth stems from c-di-AMP as a regulator of cellular osmolarity that controls the import and export of potassium and other osmoprotective molecules (76). Although the mechanism of this sensing is not fully understood, high extracellular concentrations of potassium increase DAC activity and intracellular c-di-AMP, which then functions to limit potassium uptake while promoting potassium export (76–78). C-di-AMP plays an analogous role in controlling the intracellular concentrations of other water-soluble osmoregulatory molecules such as certain amino acids and sugars (77, 79). Thus, in the absence of c-di-AMP, cells are not able to appropriately balance their osmotic state. Accordingly, c-di-AMP is not essential in rich media with lower salt concentrations or defined minimal media (76, 80).

1.3 Cyclic GMP-AMP Signaling and CD-NTases in Bacteria

Bacterial 3'-5', 3'-5' cGAMP (3'3'cGAMP), the third known cdN was first discovered in 2012 from the El Tor Biotype of *Vibrio cholerae*, which is the causative agent of the 7th and current cholera pandemic (30). 3',3' cGAMP is synthesized by DncV, which interestingly is encoded on the Vibrio Seventh Pandemic-1 (VSP-1) genomic island that is unique to El Tor (81). DncV was reported to influence *V. cholerae* motility and colonization, but the receptor for 3',3'cGAMP in *V. cholerae* was unknown (30). However, we recently demonstrated that 3',3' cGAMP directly binds to and activates CapV, a patatin-like phospholipase encoded directly adjacent to *dncV* on the VSP-1 island. 3',3' cGAMP binding to CapV activates this enzyme, leading to degradation of the cell membrane (82). 3',3' cGAMP synthesized by a DncV homolog also modulates biofilm formation in *Escherichia coli* ECOR1, an animal commensal, suggesting this signal may regulate broader functions (83). DncV is structurally analogous to the eukaryotic enzyme cyclic GMP-AMP synthase (cGAS), and both enzymes evolved from a common ancestor (84). Together, they belong to a novel protein superfamily termed cGAS/DncV like nucleotidyltransferase (CD-NTases), which is genetically conserved throughout all bacterial phyla (85, 86). In stark contrast to DGC and DAC protein families, CD-NTases produce an extensive array of nucleotide signals utilizing all four ribonucleotides to form linear oligonucleotides to cdN and ctN molecules, allowing for specificity and diversity in downstream pathways (86). In bacteria, recent *in vitro* studies revealed the first examples of pyrimidine containing cdNs including cyclic UMP-AMP and cyclic di-UMP, and ctNs such as cyclic tri-AMP (cAAA) and cyclic AMP-AMP-GMP (cAAG) (86–88). A bioinformatic analysis by Burroughs et al predicted such nucleotide synthases might participate in biological conflicts (85). Indeed, Cohen et. al. showed that *dncV* and *capV*

initiate altruistic suicide by restricting cell growth upon phage infection, thereby aborting phage replication and limiting phage spread within the bacterial population (89). Furthermore, 3',3'-cGAMP synthesis by DncV is induced upon phage infection via an unknown mechanism (89). CD-NTases like DncV are found genetically associated with putative effector proteins that suggest their primary function is phage defense (**Fig. 1.2**). Such signaling modules were renamed as cyclic oligonucleotide (coN)-based anti-phage signaling systems (CBASS) (89). Millman et al proposed a classification system that organizes CBASS systems according to their operonic architecture, effector function and dominant signaling nucleotide (31). However, a major outstanding question is how phage infection modulates nucleotide synthesis by CD-NTases.

The enzymes that degrade 3',3' cGAMP remain relatively unstudied although a few examples of 3',3' cGAMP PDEs have emerged. 3',3' cGAMP is degraded via hydrolysis by the V-cGAP1/2/3s in *V. cholerae* and PmxA in *Myxococcus xanthus*, both of which are HD-GYPs (90, 91) . VcEAL is the first 3',3' cGAMP specific EAL type PDE encoded by *V. cholerae* (20). Unlike the V-cGAP1/2/3 PDEs, VcEAL and PmxA hydrolyze both c-di-GMP and 3',3' cGAMP. 3',3' cGAMP and Hypr GGDEFs (20, 91). Bacterial 3'3'-cGAMP has also been studied in delta-proteobacteria. Although, in these bacteria 3'3'-cGAMP is not synthesized by a CD-NTase, but by hybrid promiscuous GGDEF (Hypr GGDEF), a GGDEF-like enzyme with active site residue variations that coordinate synthesis of 3',3' cGAMP rather than c-di-GMP (Figure 3) (92). 3',3' cGAMP binds riboswitches to modulate iron(III) oxide metal reduction in *Geobacter sulfurreducens* and mediates osmotic stress response in *M. xanthus* (92, 93). Interestingly, in *Geobacter* c-di-GMP activates biofilm formation and energy production on electrode surfaces, suggesting 3',3' cGAMP and c-di-GMP are antagonistic signaling pathways that induce alternative

lifestyles in this bacterium (94). Structural analyses revealed Hypr-GGDEFs have a symmetric active site whose nucleotide product is dependent on substrate availability, in contrast to DncV, which has an asymmetric active site that preferentially binds ATP and GTP as substrates (94, 95). However, 3',3' cGAMP is the major nucleotide signal for both enzymes.

2',3' cGAMP as an immune modulator.

In human cells, a structural isomer of bacterial 3'3'- cGAMP, 2'-5', 3'-5'-cGAMP, is synthesized by the CD-NTase cGAS upon binding cytosolic DNA introduced via viral invasion or intracellular damage (96). 2'3'-cGAMP then activates the STING receptor which upregulates Type I interferon production, leading to an anti-viral or anti-cancer response (97, 98). STING is also capable of sensing extracellular c-di-AMP released by the intracellular pathogen *Listeria monocytogenes,* leading to increased interferon response (74, 97). A second eukaryotic cdN receptor named RECON, which specifically recognizes adenine containing cdNs, was also recently discovered, suggesting an intricate recognition and response of eukaryotic cells to cdNs (99).

CD-NTase – the newest enzyme family that synthesizes coNs.

In contrast to c-di-AMP and c-di-GMP, 3',3' cGAMP regulation and effector functions are not as well described. Given the diversity of CD-NTases, characterization of these signaling modules is an exciting new frontier in understanding the evolution of coN signaling systems across biological kingdoms and its adaptation to modulate specific response pathways in different environments from seawater to human hosts. Many CD-NTases that have been identified do not exhibit nucleotide synthesis activity and their function is unknown(86, 100). Evidence of CD-NTases mediating signaling pathways vital for cellular adaptation and virulence present novel therapeutic targets amid growing

concerns with antibiotic resistance. In theory, abortive infection driven by CBASS can be manipulated to limit infection by human pathogens.

DncV and cGAS, cGAMP synthases have been shown to be regulated by two mechanisms thus far. cGAS, the eukaryotic synthase, is activated upon binding of DNA or RNA nucleic acids to its protein backbone to initiate cGAMP production(98). This results in regulated response to invading pathogenic nucleic acids in the cell cytoplasm such as viruses and endocytosed bacteria (98, 101). In *V. cholerae* folate-like molecules inhibit cGAMP production by binding to corresponding backbone pocket (95). Thus, CD-NTase regulation is categorized into to DNA/RNA activated Type I or Folate inhibited Type II systems.

1.4 Adaptive Phage Defense and CBASS in Pathogenic *V. cholerae*

Bacteria live in the environment in conjunction with predatory viruses known as phage in the environment (102). Bacterial phages are in a constant arms race with their hosts for survival leading to a continuous cycle of adaptation and co-evolution. Horizontal gene transfer has allowed for acquisition of novel DNA for the survival of *V. cholerae* (23). Pathogenic *V. cholerae* is distinguished by the production of TCP and CT that are encoded on mobile pathogenicity island, VPI-1 and lysogenic bacteriophage within its chromosome (4, 102). Pathogenic strains of *V. cholerae* employ various phage defense mechanisms such as decoy outer membrane vesicles (OMV) (103, 104), phage-inducible chromosomal island-like elements (PLEs) (18), and the cyclic/oligonucleotide based antiphage signaling system (CBASS) (82, 89). The 7th pandemic pathogenic El Tor strains notably have two genetic islands VSP I and II (for *Vibrio* Seventh Pandemic) that can also excise from the chromosome to make circular intermediates (81). Although the functions of the majority of these genes are unknown, recent evidence has shown the presence of two potential phage defense systems, AvcID and CBASS. The constant battle for survival of environmental *Vibrio* phage with these elements may have led to the prominence of three lytic vibrio phages, ICP1, 2 and 3, in clinical samples allowing for detailed exploration of phage defense mechanism in this system (18, 23, 105).

V. cholerae release OMV coated in specific receptors that neutralize all three ICP phages (103, 104). OMV isolated from *V. cholerae* encoding mutant O1-antigen (104), specific for ICP1 or mutant *ompU* (23), specific for ICP2, showed lower levels of inhibition

while increased expression led to higher inhibition. Though the receptor for ICP3 is unknown, WT vesicles was able to neutralize ICP3 albeit at a lower level than ICP1.

Phage-inducible chromosomal island-like elements (PLE) are *V. cholerae* specific mobile genetic islands that protects the bacterium from ICP1 infections (18, 105). PLE are excised from the chromosome following ICP1 infection and expressed to reduce phage replication and induce earlier cell lysis resulting in lower phage generation (18). Excised PLEs are packaged into virions and are transferred to neighboring cells and integrated to host genomes in an O-antigen dependent manner (18). This leads to sharing of phage defense islands among neighboring populations. PLEs are activated in response to ICP1 encoded CRISPR-Cas system (105). CRISPR-Cas is a form of bacterial adaptive immune response in which a small effector RNA "guides" Cas endonucleases to specific genetic targets for degradation (106). Though typically used by bacteria to identify and degrade invading phage DNA, studies of phage-host evolution have revealed that ICP1 phages utilizing a CRISPR-Cas system to counteract and degrade PLEs in *V. cholerae* (23, 105).

On the VSP-1 island, our lab has recently uncovered the function of AvcID, a novel toxin antitoxin phage defense system in *V. cholerae* (32). AvcD is a dCTP/dCMP specific deaminase that decreased the dCTP and dCMP pools while increasing cellular dUMP following phage infection (32). However, in the absence of stimuli, AvcD is inhibited by a small RNA AvcI found upstream of AvcD. The AvcI degradative enzyme and mechanism of phage defense is yet undefined; however, it is hypothesized it biases cellular dNTP pool to decrease phage replication (32).

A rather novel form of adaptive bacterial phage response is CBASS. First described in 2019, these are operons characterized by a cyclic/oligonucleotide synthase (CD-NTase) and its effector at its core (89). The CD-NTase is a synthase that utilize nucleotide

triphosphates (NTPs) to produce cdNs and ctNs that act as signals to bind and activate the associated effector in response to phage infection (31, 89). CD-NTases are associated with a variety of putative effectors such as phospholipases, endonucleases, and transmembrane proteins. Patatin-like phospholipases are the most common effector found associated with CD-NTases (31). Many effector enzymes are fused to putative cdN and ctN sensing domains such as STING and SAVED, and binding of the nucleotide signal to these domains modulates effector function (85, 88). The SAVED domain, which contains two CRISPR-associated Rossman folds (CARF), binds the specific nucleotide signal produced by their cognate CD-NTase to activate the fused effector function (88). This was recently demonstrated with the widespread Cap4 endonuclease that is activated after specifically binding to cyclic tri-AMP synthesized by its CD-NTase, CdnD, following phage infection (87).

The majority of CBASS exist as a two gene operon, comprised of a CD-NTase and effector, predicted to confer phage defense (31). Since its introduction, CBASS is classified into 4 types. Type 1 comprises the core CD-NTase and effector operon (31). Type 2 contains ubiquitin like E1/E2 and DUB-like ancillary genes (31). Type 3 s TRIP13 and HORMA-like ancillary genes (31). The most rare type 4 is only found in Archaea and Firmicutes with potential nucleotide modifying enzymes encoded ancillary to the core (31). Many bacterial CBASS operons exist with ancillary domains such as eukaryotic-like ubiquitination or HORMA/TRIP13 ancillary systems predicted to modulate cdN or ctN synthesis in phage infection (31, 107). These accessory genes enhance bacterial resistance to more phage in addition to the CD-NTase and its effector. Bacterial HORMA1 initiates cAAG synthesis by binding its associated CD-NTase and TRIP13 dissociates the two. The role of eukaryotic ubiquitination-like systems, however, remains undefined in bacteria

(107). In eukaryotes, cGAS sensitivity to cytosolic DNA is modulated by small ubiquitin-like modifiers (SUMO) through E3 ubiquitin ligase and deubiquitinase (108). DncV does not sense cytosolic DNA, however, crystal structure analyses showed folate-like molecules inhibiting the enzyme in the corresponding structural backbone (95). Thus, a hypothetical function of eukaryotic-like ancillary proteins might be to modulate CD-NTase sensitivity to activating nucleic acids as in cGAS, or inhibitory molecules such as folates in DncV.

1.5 Ubiquitin-like Systems in Bacteria

Ubiquitin-like (Ubl) post-translational protein modification pathways modify protein activities or target them for degradation by proteases (109, 110). Extensive studies in eukaryotes have shown Ubl signaling systems compose of E1, E2 and E3 enzymes that work together to activate, conjugate and transfer the Ubl modifier to their target proteins (110–114). Many systems include a deubiquitinase (DUB) which cleaves the substrate from the target (115).

Ubiquitination involves activation of the Ubl modifier by an E1-like enzyme (110). Ubl have a characteristic C-terminal glycine (-GG) motif or in some, serine glycine (-SG) motifs (111, 116–118). The E1 enzyme adenylates the C-terminal glycine using ATP, forming a thiosester bond with an E1 cysteine (111, 117, 119). The activated Ubl is then to transferred to an E2 conjugating enzyme via a transesterification reaction (120–122). In the presence of an E3 enzyme, E2 conjugates the Ubl to the E3 which identifies and catalyzes the ligation of Ubl to a lysine residue on its target (110, 114, 120). Proteins can be monoubiquitinated as in many signaling pathways or polyubiquitinated when destined for degradation.

In bacteria, a prokaryotic ubiquitin-like protein (Pup) that is structurally distinct from other Ubls, tags proteins for degradation (123, 124). Pup is activated at its C-terminus similar to Ubl proteins, however a -GGE/Q motif is found unlike the Ubl characteristic -GG motif (123, 125, 126). The terminal asparagine residue is ligated to its substrate at a lysine residue via the PafA ligase, which then directs the substrate to the Mpa-protease complex for degradation (118, 126, 127). Pup is cleaved by depupylase (125). Pup is ligated and cleaved in a biochemical mechanism similar to eukaryotic Ubl however using just one enzyme in the ligation process (126). This hints at the possibility that

ancestral ubiquitin-like systems were more simplified, less involved versions of the now more involved eukaryotic process found.

In the degradative Ub-ligase pathway, the E3 ligase transfers the modifier to a target protein to signal it for degradation by proteasome complexes (110). Polyubiquitination allows for specific targeting and protein recycling. Sae1 and Sae2, E1 and E2-like yeast enzymes, form a complex with SUMO to modulate target I-kappa B-alpha protein activity blocking NF kB dependent transcriptional activation (128). Unlike other Ubl systems, Sae1 and Sae2 can conjugate SUMO to its target without the presence of an E3 ligase in vitro (128). MoeB and ThiF, molybdenum and thiamine synthase respectively, are bacterial precedents of eukaryotic E1 with beta-grasp folds (119, 129–131). They are activated by sulfur transfer upon binding of their ubiquitin-like modifiers MoaD and ThiS which allows for conjugation with E2 equivalents (119, 129, 131–133). These E2 equivalents then transfer the modifier, a thiocarboxylate group, to a target protein to alter their activity without an E3 ligase (119, 129, 131–133).

V. cholerae's CBASS have *vc0180* and *vc0181* ancillary genes downstream of *dncV*. VC0180 is predicted to have an E2-like N-terminal domain and a C-terminal E1-like domain. VC0181 encodes a JAMM motif DUB-like domain. Together they are suggesting a ubiquitin-like post-translational modification of CBASS. However, *V. cholerae*'s CBASS system lack an E3 ligase suggesting a more modulatory role of these enzymes than targeting for degradation.

1.6 Chapter 1 Summary

In summary, *Vibrio cholerae* is an pathogen of concern in developing nations, especially in areas of poor sanitation and healthcare access (134, 135). It causes the diarrheal disease cholera through release of various virulence factors such as TCP and CT (4, 136). It survives in various environment such as aquatic reservoirs and humans hosts through lifestyle modification mediated by cyclic di-nucleotide signaling (15, 16). In a constant battle for survival with phage predators, they have acquired various genetic island that encode phage defense mechanisms such as AvcID and CBASS (31, 32, 89, 102). In particular V. cholerae CBASS has produces cGAMP in response to phage infection in order to activate CapV, which degrades the host cell membrane (82). This altruistic suicide of the infected host leads to survival of the clonal community leading to aborted infection. Even though the function of DncV and CapV is well studied, the function of cognate genes VC0180 and VC0181, E1/E2-like enzyme and DUB-like enzyme are not well defined. We do know that they confer defense against a broader range of phages, however, their mechanism and actions are not yet known (89). Thus, to better understand the regulation of 3'3'-cGAMP signaling in response to phage predation, we explore the function of VC0180, VC0181 and an uncharacterized gene I discovered in modulating CBASS response.

CHAPTER 2:

DEFINING THE FUNCTION OF AN UNCHARACTERIZED GENE IN THE REGULATION OF 3'3'-CGAMP SIGNALING IN *VIBRIO CHOLERAE* EL TOR

For this research portion of my thesis, many individuals were involved. Undergraduate associate of Waters lab Elise Trost cloned and performed cell viability assays of various *Vibrio cholerae* El Tor mutants. Another undergraduate associate Ram Sanath-Kumar performed cloning of *Vibrio cholerae* El tor CBASS for phage studies, infection assays and transposon screening under the combined guidance of Kaylee Wilburn.

2.1 Introduction

Vibrio cholerae is a diarrheal pathogen found in a large array of environments from the human host, to shellfish and chitin surfaces of aquatic reservoirs (15, 16, 19). It is able to adapt to and survive in different conditions due to cyclic di-nucleotide signaling pathways that respond to environmental stimuli (24, 68). Cyclic di-GMP, modulates the switch between bacterial motile and biofilm lifestyles through various transcriptional and post-translational mechanisms (137, 138). 3'3'-cyclic GMP-AMP (cGAMP) is another cyclic di-nucleotide in *V. cholerae* synthesized by the enzyme DncV to mediate phage defense in a system known as CBASS (cyclic/oligonucleotide based antiphage signaling system) (30, 95). CBASS activity commences with activation of DncV upon phage infection via an unknown signaling mechanism (89). cGAMP then binds and activates CapV, a patatin-like phospholipase that specifically degrades phosphotidylethanolamine and phosphotidylglycerol, the major phospholipids found in *V. cholerae*, cleaving off 16:1 and 18:1 free fatty acids (82) (**Fig. 2.1**). High activation of CapV leads to degradation of the membrane, making the cell no longer viable (82). This response has been coined abortive infection as phage infection is halted via host suicide thereby preserving neighboring cells from phage attack. DncV and CapV together form the core part of the CBASS system (89).

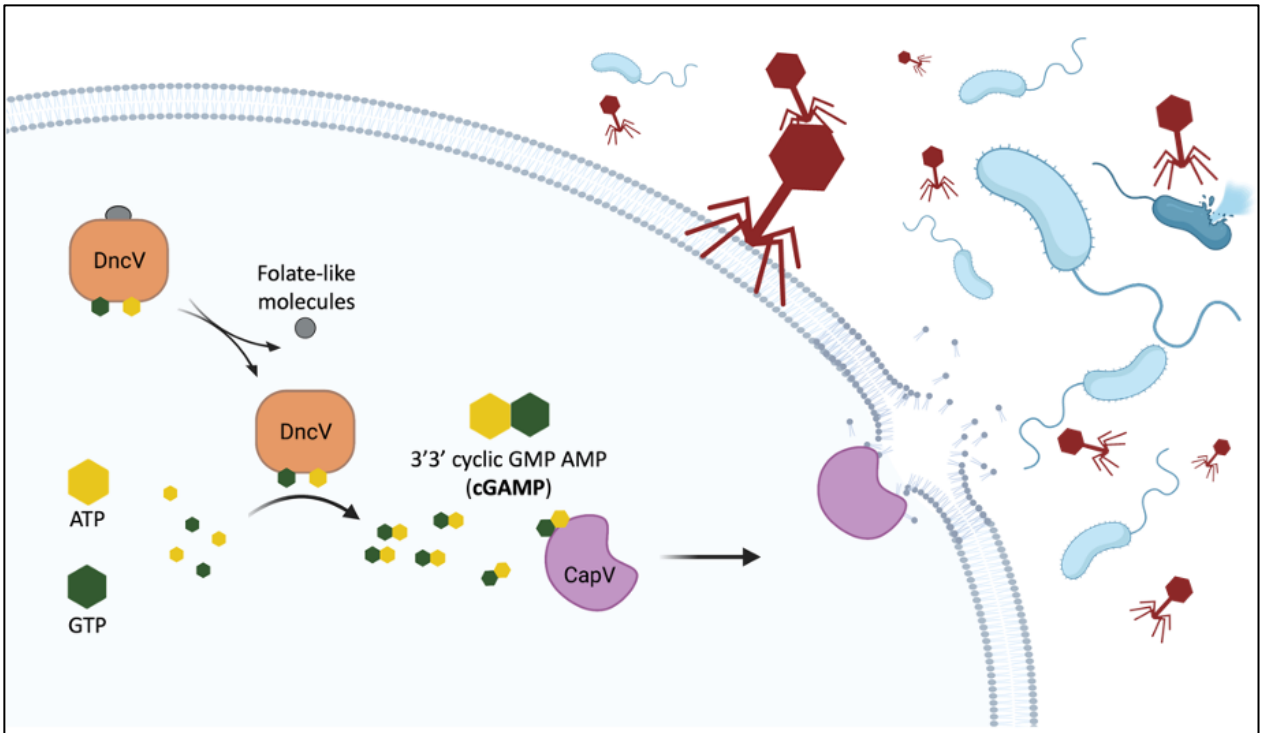

Figure 2.1. 3'3'-cGAMP mediate abortive infection in phage-infected host. DncV is inhibited by folate-like molecules in the cells. Following phage infection, DncV is activated and produces 3'3'-cGAMP which binds to CapV, a phospholipase that degrades the phospholipid membrane. Sufficient activation leads to death of the infected host called abortive infection, a form of altruistic suicide that saves the nearby bacterial community.

CBASS is encoded in *V. cholerae* on a genetic island called VSP-1, unique to the current and 7th pandemic strains of *V. cholerae* El Tor (30, 81). The function of many of the genes encoded on VSP-1 has not been determined. However, it has recently been discovered that VSP-1 harbors a second antiphage defense system mediated by the *avcID* in which the AvcD cytidine deaminase is activated upon phage infection to deplete dCTP and dCMP nucleotides in the cell, thereby inhibiting phage replication (32). VspR, a transcriptional regulator of CBASS, is also encoded on VSP-1 (30) (**Fig. 2.2**).

One limitation to studies of CBASS antiphage defense is that study of these systems has almost exclusively been carried out in heterologous hosts such as *Escherichia coli,* and not in the native context in which they are discovered (88, 89, 139, 140). This

limitation is because there is often a scarcity of phages available to infect the natural hosts, whether they be *V. cholerae* or other species, while coli phages are generally more well characterized and available. Moreover, in *V. cholerae,* there are only three predominant phages found in the environment to infect pandemic strains of V. cholerae, ICP1, ICP2, and ICP3, all three of which our laboratory has shown are not effected by CBASS or the aforementioned AvcID (23, 32, 105). We are therefore interested in studying CBASS defense island in the context of its native *V. cholerae* host.

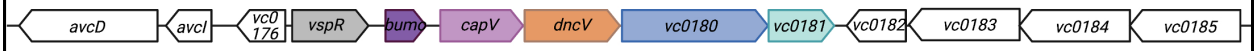

Figure 2.2. CBASS is part of the VSP-1 genetic island. The function of many VSP-1 island genes are yet unknown. It includes the recently described *avcID* operon, VspR (*vc0177)* shown to regulate CBASS expression and CBASS. The function of an uncharacterized gene we named *bumo* between *vc0177* and *capV,* and *vc0182 – vc0185* are yet to be defined.

In that regard, our laboratory has established that sulfamethoxazole treatment can be used as a proxy to study DncV activity in its native *V. cholerae* context (Severin, in preparation). *V. cholerae* El tor is 1,000 – 5,000 times more sensitive to sulfamethoxazole than classical *V. cholerae* (141). The main difference between the two strains being inclusion of VSP-1 and VSP-2 islands in *V. cholerae* El Tor, we investigated the possibility of VSP-1 being responsible for this difference (26, 81). Sulfamethoxazole inhibits dihydropteroate synthetase which synthesizes dihydropteroic acid, an important precursor of dihydrofolate (DHF) (141, 142). DHF is then synthesized into tetrahydrofolate (THF) (142, 143). DncV is inhibited by THF-like molecules, specifically 5'-methylTHF and 5'-methylTHF-diglutamate, both downstream products of THF synthesis pathways (95). Our lab established that deletion of VSP-1 rendered *V. cholerae*

El Tor more resistant to sulfamethoxazole treatment equivalent to the resistance of classical strains (Severin, in preparation). Thus, we hypothesize sulfamethoxazole treatment reduces the concentrations of intracellular folates that repress DncV, and therefore sulfamethoxazole sensitivity serves as a proxy for DncV synthesis of cGAMP and CapV activation. In this report, we support this hypothesis showing that DncV activation of CapV is the main modulator of sulfamethoxazole sensitivity. I also demonstrate that the accessory CBASS genes *vc0180* and *vc0181* impact CBASS activation.

Given how detrimental it would be if DncV and CapV were unregulated, it is likely they are activated by a specific stimulus that is yet unidentified. The ancillary genes, *vc0180* and *vc0181* encoded downstream of DncV likely play a role in this regulation by conferring broader phage defense as CapV/DncV homologs only provided protection against 1/10 lytic phage in *E. coli* whereas addition of VC0180 and VC0181 homologs increased that protection to 6/10 phage (89). The mechanism by which they function is unknown. As VC0180 encodes E1 and E2-like ubiquitin modifying domains and VC0181 encode deubiquitinase-like domain, it is plausible they play a regulatory role in modifying CBASS response via protein modification (31, 89).

E1, E2c and DUBs are part of the ubiquitin post-translational modification system (110, 114, 120). However, a vital component of this system is a ubiquitin like protein modifier. A ubiquitin-like protein is activated at its C-terminal -GG or -SG motif via adenylation reaction by E1 enzymes, which then conjugates and passes it on to E2 conjugating enzyme (116, 118–120, 144). In most well studied pathways, the Ubl is then passed onto an E3 ligase that works to identify then ligate the Ubl to its target protein (114, 125). Ubl have been shown to polyubiquitinate a protein to signal it for protease complexes that will degrade the protein (110). However, small ubiquitin like modifiers

(SUMO) can modify protein activity without driving degradation following binding to their target substrate, a process called SUMOylation (108, 128, 145, 146). In either system, a DUB-like enzyme exists to counteract this signaling, allowing for protein recycling or reversal of SUMOylation (115, 147). VC0180 and VC0181 likely function similar to their eukaryotic counterparts in activating, conjugating, and reversing those reactions. It is important to note no E3-like ligase enzyme exists in CBASS or *V. cholerae*; however, Ube2I, a SUMO E2-like enzyme previously called Ubc9, has been shown to directly bind its corresponding ubiquitin to ligate it to its protein targets (148). With the lack of an E3-like enzyme, and the existence of both E1 and E2-like domains, VC0180 might represent an ancestral prokaryotic post-translational system that did not yet diverge into multiple component systems similar to that of eukaryotes. VC0181 encodes a DUB-like domain that might function to reverse the effects of VC0180.

In addition to no identified E3 ligase, no Ubl encoding gene has been identified for the *V. cholerae* CBASS (30, 89). Thus, the exact mechanism of VC0180 and VC0181 regulation, their targets, and the specific modifier remain elusive. It is important that we explore the targets and potential modifiers of these enzymes to better understand how they modulate 3'3'-cGAMP signaling to confer broader phage response. In search of the potential Ubl, we have identified two possible candidates. The most probable is DncV. Ubl proteins are generally small (<100 aa) and have characteristic C-terminal -GG motifs or -SG motifs in some bacteria and archaea. Though DncV is not small, and is a cGAMP synthase, it does have a C-terminus -SG motif similar to Ubl-proteins (118). Ubl domains have also been found encoded within multi-domain proteins to confer Ubl-like functions (147). Thus, it is not unfathomable that DncV might have a Ubl-like C-terminus that might be a target for activation and modification by VC0180 and reversal by VC0181. Another

candidate *bumo* (bacteria ubiquitin-like modifier), a small open reading frame upstream of CapV that I discovered during my thesis research that will be described below. It consists of 284 bases (84 amino acids), consistent with the size range of ubiquitin-like proteins, and its proximity to the CBASS operon makes it a likely candidate as a modifier. The two other flanking genes are less likely, as *vspR* is a transcriptional regulator of CBASS expression and *vc0182* encodes an integrase-like domain (30). Thus, DncV and this uncharacterized gene represent two potential candidates to start studying VC0180 and VC0181 regulation of cGAMP signaling.

We have designed both a broad top down, unbiasedand target-specific bottom-up approach to determine whether these two proteins are targets of VC0180 and VC0181 modification. Our laboratory has a transposon library of VSP1 which can be used to screen for mutants that reverse phage susceptibility to non-CBASS harboring levels (82). These selected mutants can be sequenced for identification of mutation sites and further exploration of VSP1 island genes responsible for phage defense. The more targeted approach is to manipulate these genes specifically, creating single mutants and testing phage susceptibility patterns.

Our efforts show evidence that *bumo* is part of the CBASS operon and protects DncV from degradation by VC0181. We also show evidence that VC0181 is not on the same transcript as the rest of CBASS and seems to be working independently of VC0180 in modifying DncV.

2.2 Results

2.2.1 El tor CBASS leads to defense against T2, T4 and T5 phages

Previous studies on CBASS systems have not utilized the CBASS operon from the laboratory strain of *V. cholerae* we use, El Tor C6706. To first explore whether this CBASS confers phage defense, a cosmid encoding the VSP-1 island, containing CBASS, which was previously isolated from a genetic screen, was inserted into *Escherichia coli* DH10B cells, which lack the island (82). This cosmid contains both the upstream and downstream intergenic regions that preserve its natural promoters, terminators, and other regulatory sequences. The VSP-1 harboring *E. coli* cells were then infected with a panel of 10 *E. coli* lytic phages to determine whether it conferred any difference in phage susceptibility. We tested host range against double stranded DNA phages: T2, T4, and T6 phage of the *Myoviridae* family, T3 of the *Autographiviridae* family, T5, lambda-vir, SECphi18 and SECphi27 of the *Siphoviridae* family, T7 of the *Podoviridae* family, and the single stranded DNA phage SECphi17 of the *Microviridae* family .

The VSP-1 island conferred phage defense against multiple families of phages. There was a 1000-fold reduction in T2 phage titer and 100-fold reduction in T5 phage titer (**Fig. 2.3**). Smaller reductions of ~10 fold were seen for phages T4 and T7. No other phage showed significant difference in comparison to the control empty vector.

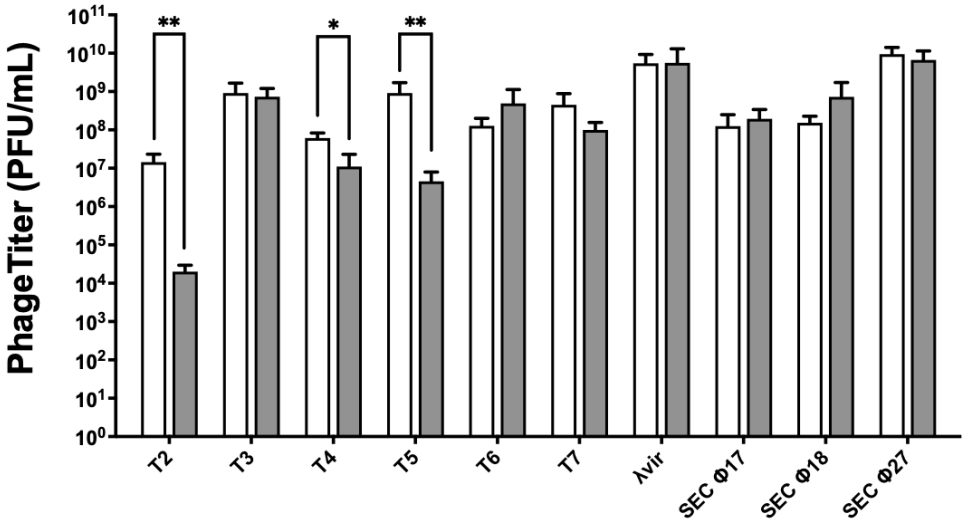

Figure 2.3. VSP-1 island confers protection against T2, T4 and T5 phages. VSP-1 island cloned (pCCD7) into *E. coli* DH10B cells lead to lower phage titers compared to empty vector (pLAFR) cloned cells when infected with T2, T4 and T5 phages.

To determine which part of the VSP-1 island was responsible for the phage defense, the VSP-1 encoding cosmid was subjected to mutagenesis by a Tn5 transposome *in vitro*, electroporated into *E. coli* cells, and screened for efficiency of plaquing (EOPs). Cosmids that showed reversion of phage titers to that of empty vector were then sequenced using a primer to the transposon to determine the location of the transposon insertion. There were 54 clones that were sequenced for T2 and T5. There were 15 positive hits in VSP-1, 12 of which had differential EOPS for both T2 and T5 infections positive hits, 1 transposon insertion that altered defense for only T2, and 2 transposon insertions that altered defense for only T5. Most of the transposon insertions in VSP-1 were in the CBASS operon as shown in (**Fig. 2.4**). Transposon mutations that reduced infection of both T2 and T5 were found in each gene of CBASS including the upstream intergenic region with single hits on other genes of the VSP-1 island. This supports CBASS as the major contributor of

phage defense in the VSP-1 cosmid in these conditions. Interestingly, two of the transposon insertions that significantly impaired phage defense were in the upstream intergenic region of *capV* and *vspR* upstream of the uncharacterized gene (**Fig. 2.4**).

A.

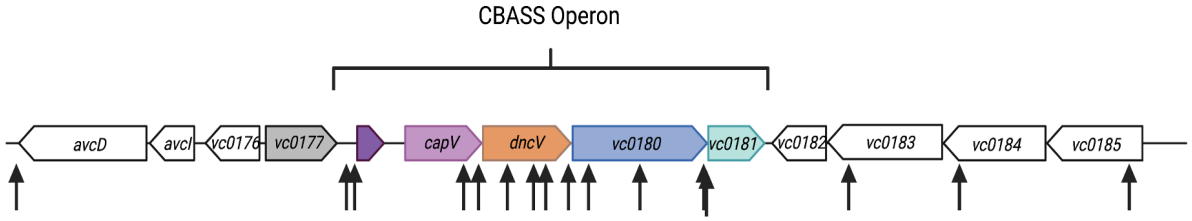

B.

Hits	Transposon Location	T2 Titer	T5 Titer
C	pLAFR	6.00E+06	4.00E+08
C	pCCD7	2.50E+04	3.00E+05
1	*vc0174*	5.00E+05	1.30E+10
2	CBASS promoter (DS vspR)	1.00E+08	1.10E+12
3	CBASS promoter (DS vspR)	1.50E+07	1.30E+11
4	*capV*	2.00E+08	2.60E+11
5	*capV*	5.00E+08	6.10E+11
6	*dncV*	1.00E+09	9.00E+06
7	*dncV*	5.00E+07	5.00E+09
8	*dncV*	4.50E+07	8.00E+08
9	*vc0180*	5.00E+06	1.00E+11
10	*vc0180*	6.70E+11	2.00E+08
11	*vc0180/181 overlap*	4.50E+09	5.00E+04
12	*vc0180/181 overlap*	5.00E+07	2.00E+10
13	*vc0183*	5.00E+04	6.50E+10
14	*vc0184*	1.50E+05	4.50E+10
15	*vc0185*	1.00E+05	4.00E+10

Figure 2.4. CBASS is the major contributor of phage defense seen with VSP-1. **A.** Screening of VSP-1 island transposon library in DH10B cells that with phage titers reversed similar to that of EV, revealed hits mostly in the CBASS operon of the VSP-1 island. **B.** EOP of transposon mutagenesis clones show insertions into *capV, dncV, vc0180* and *vc0181* had difference in both T2 and T5 phage titers. Blue boxes show titers significantly different from that of pCCD7. Yellow boxes show transposon insertions that affected both T2 and T5 vulnerability.

2.2.2 An uncharacterized gene, *bumo*, upstream of *capV* is part of the CBASS operon

The intergenic region between *vspR* and *capV* is 913 base pairs. Prediction for putative open reading frames (ORFs) identified an uncharacterized ORF of 284 bp that we named *bumo* for Bacterial Ubiquitin-like Modifier (**Fig. 2.5**). To establish whether the upstream intergenic region including *bumo* is part of the CBASS operon, we extracted

RNA and used random hexamers to generate complementary DNA (cDNA). The cDNA was then PCR-amplified using primers spanning two genes to determine whether they were originally encoded on the same mRNA transcript and thus present in an operon. Primers specific for *vspR, bumo*, CBASS genes, and *vc0182* were used to confirm which genes transcribed with CBASS. Genomic DNA was used a positive control for the PCR reaction, and a no reverse transcriptase reaction functioned as a negative control for DNA contamination of the RNA sample.

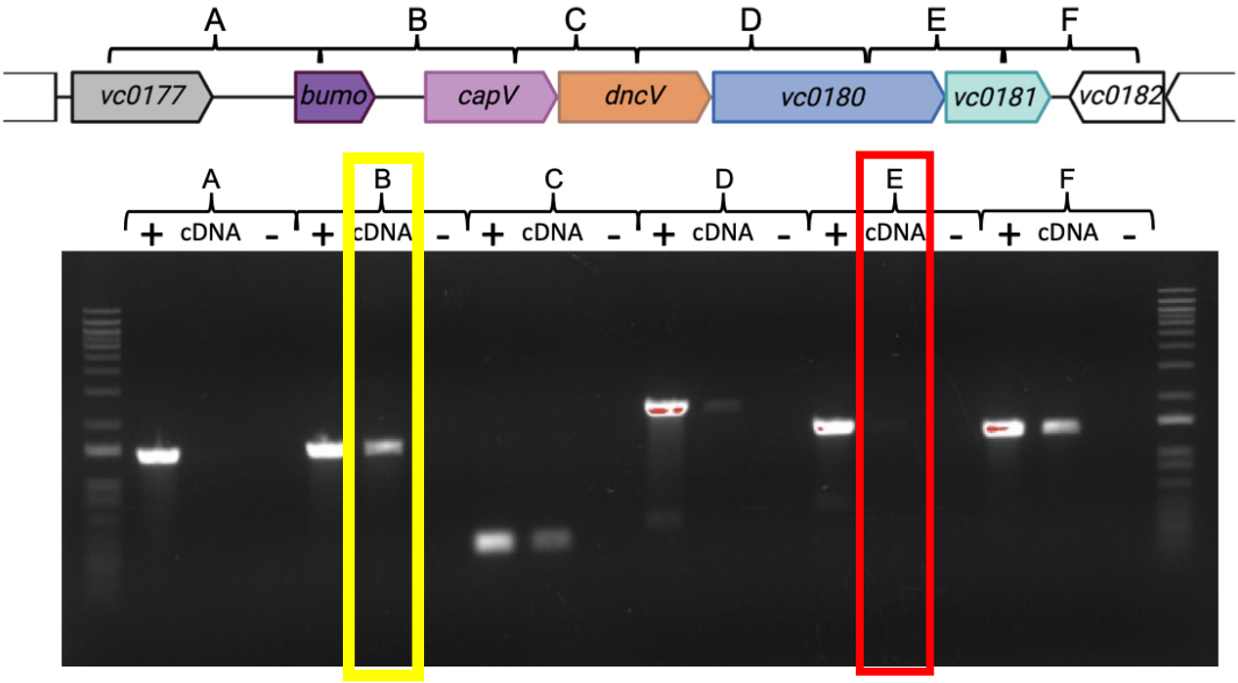

Figure 2.5. *bumo* is part of the CBASS operon. PCR amplification of cDNA synthesized from mRNA extracts spanning two genes, reveal that *bumo* is part of the same transcript is *capV, dncV* and *vc0180* (yellow box). However, *vc0181* is not on the same transcript as the rest of the CBASS operon (red box) but instead on the same transcript as *vc0182*.

As expected, no bands were seen in reactions using primers spanning *vspR* and *capV* (**Fig. 2.5**). Similarly, no bands were seen for reactions with primers spanning *vspR*

and *bumo* suggesting that *vspR* is not part of an operon with CBASS. However, a band of the expected size for primers spanning *bumo* and *capV* was amplified from the cDNA, confirming *bumo* is indeed part of the CBASS operon (**Fig. 2.5 yellow box**). Bands of the expected sizes amplified from cDNA were seen for genes spanning *capV* and *dncV,* and *dncV* and *vc0180* confirming they are on the same transcript (**Fig. 2.5**). Unexpectedly, no bands were seen when primers spanning *vc0180* and *vc0181* were used on the cDNA, suggesting they are not on an operon. Interestingly, a band is present when primers spanning *vc0181* and *vc0182* were used to amplify the cDNA. Since *vc0182* is encoded on the opposite strand, these genes are not in an operon, but this result suggests that transcription of *vc0181* extends into *vc0182*.

To confirm that the absence of a band from *vc0180* to *vc0181* is not due to primer error or low abundancy of cDNA, PCR amplifications were repeated for longer cycles and

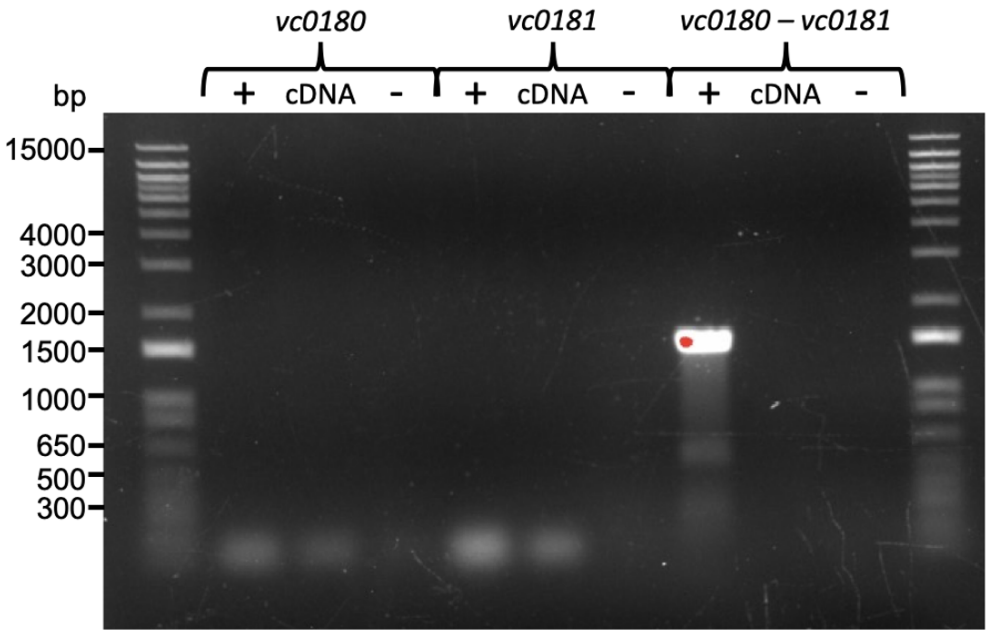

Figure 2.6. *vc0181* is not part of the CBASS operon. PCR amplification using primers spanning *vc0180* and *vc0181* reveal that *vc0181* is not on the same transcript as *vc0180*. The absence of a band is not attributable to a defect in primers as can be seen by the presence of bands in single gene amplifications (~100 bps).

using internal primers to confirm RNA was originally present when the cDNA was generated. Additional cycles resulted in brighter bands on gel electrophoresis for *dncV* to *vc0180;* however, no bands were apparent in wells containing the reaction for *vc0180* to *vc0181* (**Fig. 2.6**). Moreover, internal primers for both *vc0180* and *vc0181* yielded positive bands similar to the genomic DNA control suggesting that both genes were transcribed. These results show for the first time that *vc0181* is not part of the CBASS operon, and more generally suggest that the DUB component of Type II CBASS systems may not be cotranscribed with the rest of the genes.

With evidence that *bumo* is on the same transcript as *capV, dncV,* and *vc0180* while *vc0181* is not, I performed 5'RACE (rapid amplification of cDNA ends) to determine the transcriptional start site (TSS) of the CBASS operon and *vc0181*. We were unsuccessful in determining the TSS of *vc0181* using both *vc0181* internal and external primers. However, only one TSS of the CBASS operon was detected using reverse primers that annealed to *capV*. This TSS was found encoded 210 bp upstream of *bumo* further

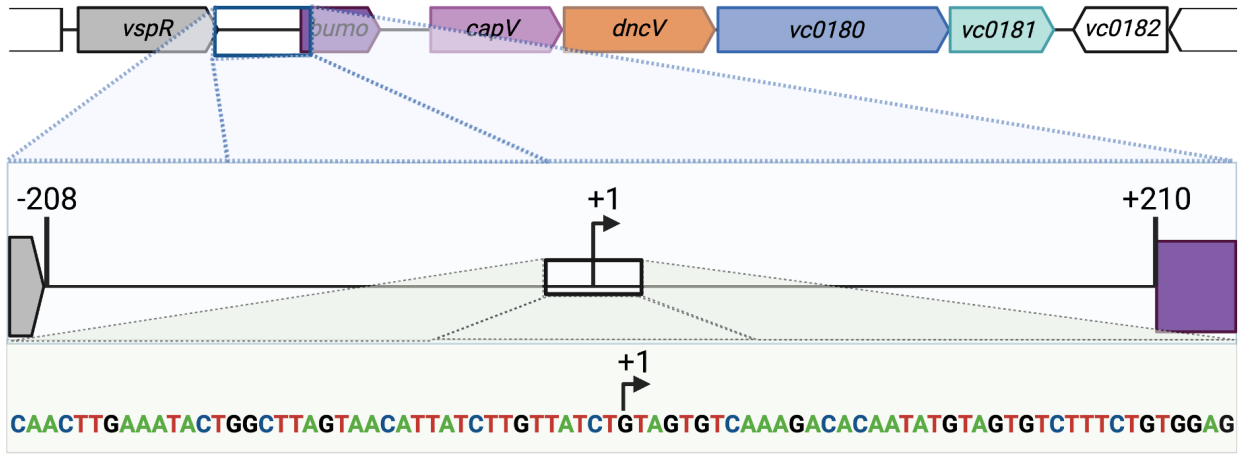

Figure 2.7. The transcriptional start site (TSS) of CBASS is between *vspR* and *capV*. 5'RACE of *capV* led to the identification of the TSS between *vspR* and *bumo*.

supporting the fact that it is part of the CBASS operon (**Fig. 2.7**). The TSS is situated about midway between *vspR* and *bumo*.

2.2.3 Nonsense mutation of *bumo* leads to sulfamethoxazole resistance

To ascertain whether the uncharacterized gene impacts CBASS activation, we first made a strain with *bumo* deleted and challenged it with sulfamethoxazole. We had established that El Tor strains encoding VSP-1 were more sensitive to sulfamethoxazole treatment (100 μg/mL). This sensitivity is dependent on *dncV* as deletion of the cGAMP synthase is highly resistant to sulfamethoxazole (Serverin et Al. , in preparation) (**Fig. 2.8A**). Therefore, sensitivity to sulfamethoxazole can be used as a proxy for CBASS activation to study CBASS in its native *V. cholerae* context. The Δ*bumo* mutant exhibited earlier and lower cell growth following sulfamethoxazole treatment in comparison to WT strains and Δ*dncV*, suggesting this mutation increased DncV activity (**Fig. 2.8A**).

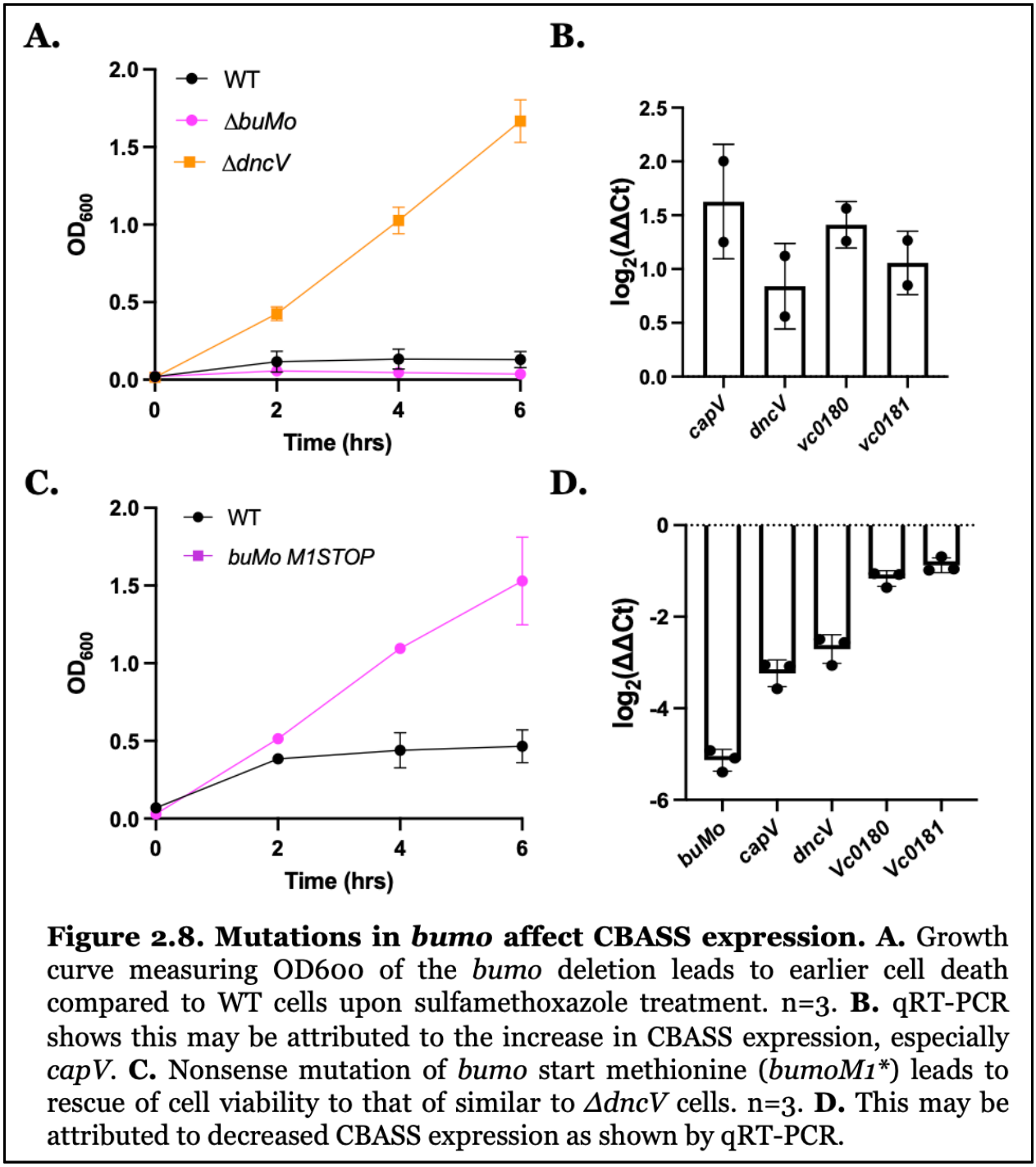

Figure 2.8. Mutations in *bumo* affect CBASS expression. A. Growth curve measuring OD600 of the *bumo* deletion leads to earlier cell death compared to WT cells upon sulfamethoxazole treatment. n=3. **B.** qRT-PCR shows this may be attributed to the increase in CBASS expression, especially *capV*. **C.** Nonsense mutation of *bumo* start methionine (*bumoM1**) leads to rescue of cell viability to that of similar to *ΔdncV* cells. n=3. **D.** This may be attributed to decreased CBASS expression as shown by qRT-PCR.

We hypothesized that such increased sensitivity upon deletion of *bumo* could be due to an impact on expression of the CBASS operon. To test this, we extracted mRNA from WT and Δ*bumo* to measure gene expression. qRT-PCR revealed increased

abundance in CBASS (two to four-fold) gene transcripts, suggesting the earlier and lower cell death might be a result of increased CBASS transcription in the cells (**Fig. 2.8B**). There was no difference in CBASS and *bumo* expression profiles between sulfamethoxazole treated and non-treated cells confirming sulfamethoxazole does not affect CBASS gene expression (**Fig. 2.9**).

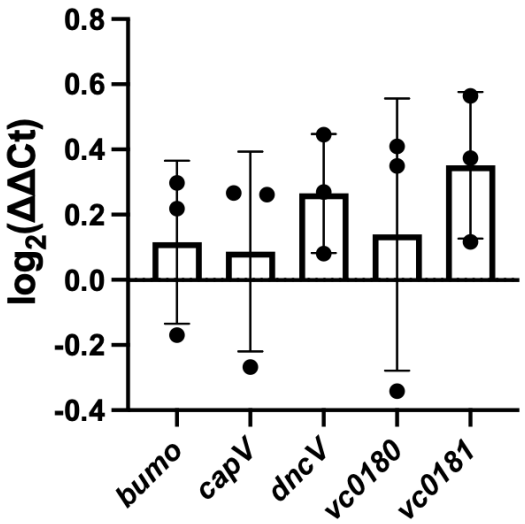

Figure 2.9. Sulfamethoxazole (100 µg/mL) treatment does not affect CBASS expression. There is no difference in CBASS expression upon sulfamethoxazole treatment of *V. cholerae* El Tor.

To mitigate the effect of the deletion, we made a nonsense mutation to the first codon of *bumo* (*bumoM1**). The nonsense mutant showed bacterial proliferation similar to Δ*cbass* and Δ*dncV* strains in contrast to WT strains that showed cell death following sulfamethoxazole treatment (**Fig. 2.8C, Fig. 2.10**). This result suggests that DncV is not active in the *bumoM1** mutant. However, qRT-PCR of extracted mRNA from this mutant showed four-to-sixteen-fold reduction CBASS mRNA at both 2 and 4 hours post treatment and a 32-fold decrease in the transcript of *bumo* as expected (**Fig. 2.8D**). This

suggests that the proliferation of the cell in the *bumo* mutant upon sulfamethoxazole treatment might be due to decreased expression of CBASS genes and not a direct result of the deletion mutation.

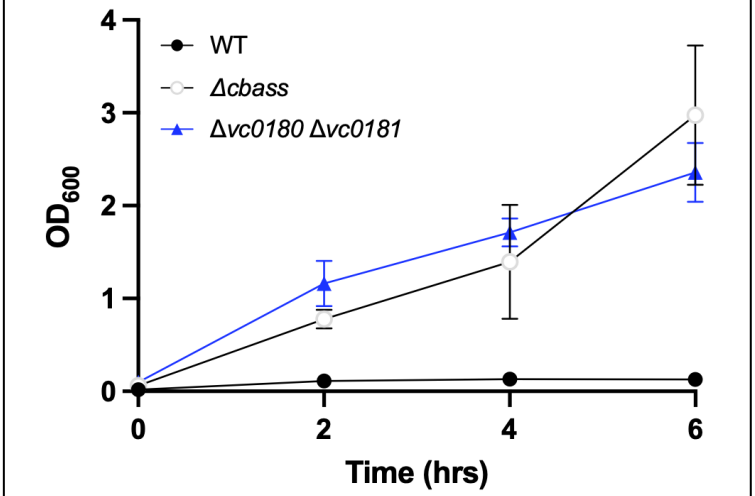

Figure 2.10. Δ*cbass* and Δ*vc0180Δvc0181 V. cholerae* are resistant to sulfamethoxazole. Δ*cbass* and Δ*vc0180Δvc0181* mutants of *V. cholerae* El Tor are insensitive to sulfamethoxazole (100 µg/mL) treatment compared to WT. n=3

We tried to compliment the nonsense phenotype by introducing a vector overexpressing either the WT or nonsense mutant of *bumo*. Although the transcript of *bumo* increased four to eight-fold when expressed from the complementation strain, there was no significant difference in the expression of the other CBASS genes, suggesting that the *bumoM1** mutation functions *in cis* to alter CBASS expression (**Fig. 2.11**). Even though nonsense mutation of *bumo* leads to sulfamethoxazole resistance similar to a CBASS deletion, due to its differential effects on CBASS expression, it is unclear how *bumo* impacts sulfamethoxazole resistance. This would have to be further explored.

To assess the role of *vc0180* and *vc0181* in regulation of DncV activity, I generated a double deletion mutant of these genes. The Δ*vc0180-vc0181* also showed increased

resistance to sulfamethoxazole, similar to Δ*dncV*, suggesting they might be important together with *bumo* for enhancing DncV activity (**Fig. 2.10**).

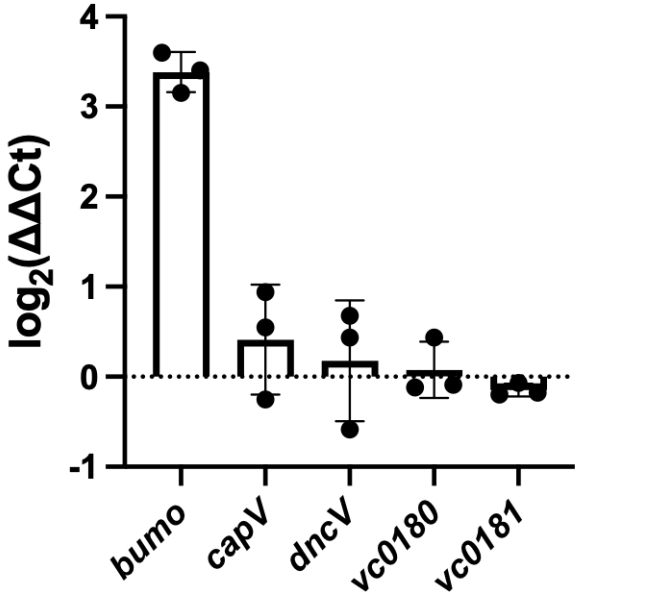

Figure 2.11. *bumo* affects CBASS expression in a cis manner. Complementation of *bumo M1STOP* with WT *bumo* leads increased *bumo* transcripts but no changes in *capV, dncV, vc0180* and *vc0181* expression.

2.2.4 *bumo* encodes for a protein

To explore the nature of *bumo*, I fused its coding sequence to an intein-tag containing chitin binding domain expression system and induced its expression in *E. coli* BL21. I affinity purified the product using chitin resin in a column. The product was cleaved from the intein tag using DTT to purify *bumo* alone. The resulting elution showed a robust band on SDS-PAGE gel corresponding to its predicted molecular weight of ~10 kDa (**Fig. 2.12**).

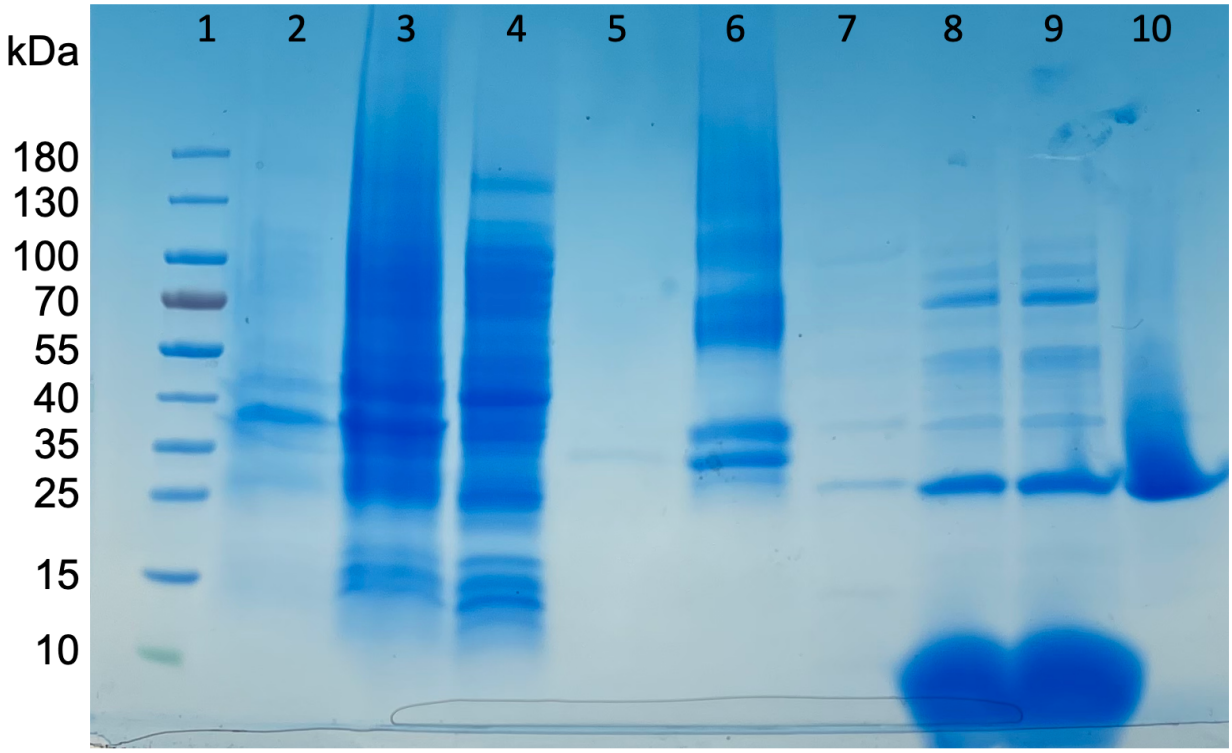

Figure 2.12. *bumo* may encode for a protein ~10 kDa. Bumo can be purified via affinity purification on chitin resin column following induced expression in *E. coli* BL21 cells. Coomassie staining of SDS-PAGE gel of protein purification samples. Lane 1: ladder Lane 2: Induced cell culture Lane 3: Whole cell lysates Lane 4: Column flowthrough during loading Lane 5: Flowthrough after heavy wash of column with column buffer Lane 6: Chitin resin sample Lane 7: Cleavage buffer flowthrough Lane 8 & 9: Elutions 1 and 2 after 18 hrs of incubation Lane 10: Chitin resin after elution.

Moreover, immunoblotting of the protein fusion tagged with intein-CBD domains with an antibody directed against the CBD detects a similar sized band from cell lysates (**Fig. 2.13**). Although this is not direct evidence that *bumo* encodes a protein, we can state that the peptide produced from *bumo* can be stably expressed in a cell. This gave us some confidence that the uncharacterized gene produces a stable protein rather than a small RNA or substrates.

2.2.5 Bumo is stable *in vivo*

To explore whether Bumo is stable in vivo and whether it is impacted by the absence of other CBASS components, a tagged Bumo was cloned into both an intein tag and 6XHis-tag overexpression vectors introduced and introduced into *V. cholerae* A1552 strains. A1552 encodes an IPTG-inducible T7 RNA polymerase on its genome, allowing induction of proteins using the T7 expression system. C-terminally intein/Chitin Binding Protein (CBP)-tagged Bumo was stable in both WT and Δ*dncV* strains, with two bands seen in both strains. A lower band corresponding to the intein/CBP tag (~27 kDa) and the Bumo fusion as a monomer (~37 kDa total) (**Fig. 2.13A**). Analysis of C-terminal 6XHis-tagged Bumo revealed only one major band ~10 kDa in WT, Bumo M1*, Δ*vc0181* and *bumoM1**Δ*vc0181* corresponding to the size of a Bumo monomer with the C-terminus 6X-His tag (**Fig. 2.13B**). Together, this result suggests the stability of Bumo is not dependent on the presence of other components of CBASS. However, Bumo stability remains to be tested in the Δ*capV* and Δ*vc0180* strains.

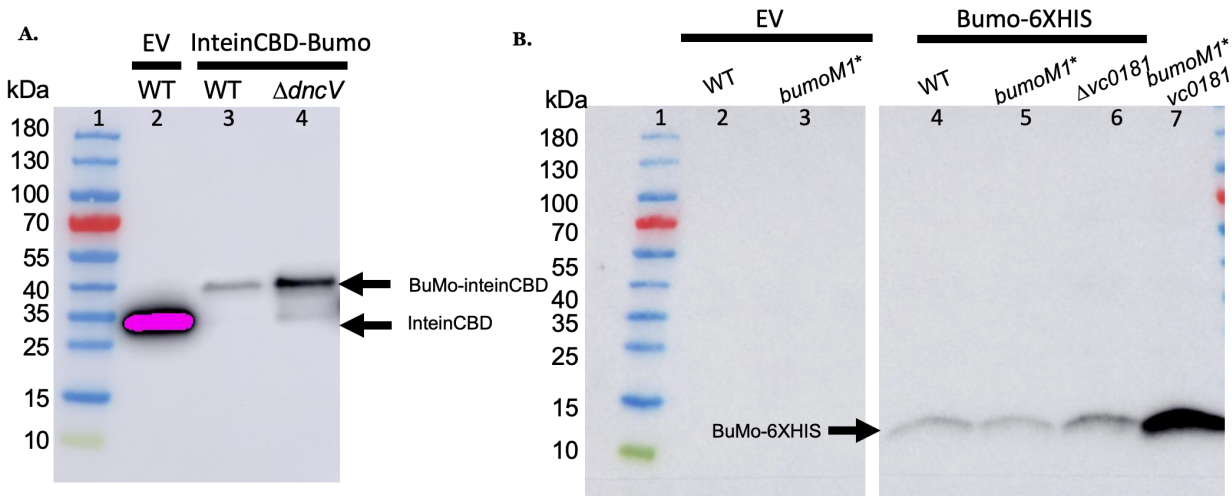

Figure 2.13. Bumo is not dependent on DncV and Vc0181 for stability. A. αCBD detection shows no change in Bumo signal between WT and Δ*dncV* cells. Lane 1: ladder Lane 2: pTXB1 EV showing InteinCBD at ~34 kDa. Lane 3-4: pTXB1 bumo showing Bumo-InteinCBD signal >~40kDa. **B.** αHIS detection of Bumo show no change in signal between WT and Δ*dncV, bumoM1** and *Δvc0181* strains. Lane 1: ladder Lanes 2-3: pET28B EV show no signal. Lanes 4-7: BuMo-6XHIS is detected in all three strains.

2.2.6 VC0180 and VC0181 stabilize DncV

DncV is predicted to be modified by VC0180 and VC0181 in an undefined manner. Before we explore whether *bumo* works in relation with VC0180 and VC0181, we needed to define their function in cGAMP signaling. We first studied the effect of VC0180 and VC0181 on DncV stability. A 6x histidine C-terminal tagged fusion of DncV that is expressed using the T7 expression system from pET28 was electroporated into various CBASS mutant strains generated in *V. cholerae* El Tor A1552. DncV was then induced using IPTG in WT, Δ*vc180,* and Δ*vc0181* mutants and detected from cellular lysates via Western immunoblotting using an anti-6X-His primary antibody.

The EV control did not generate a signal. Interestingly, there were no bands seen in *Δvc0180* lysates, suggesting VC0180 is vital for DncV stability in the cell. The Δ*vc0181* strain showed both DncV bands observed from the WT at higher intensities (**Fig. 2.14**). The lower ~50 kDa band was darker than the higher band. These results suggests that VC0180 positively influences abundance of DncV while VC0181 negatively influences its abundance.

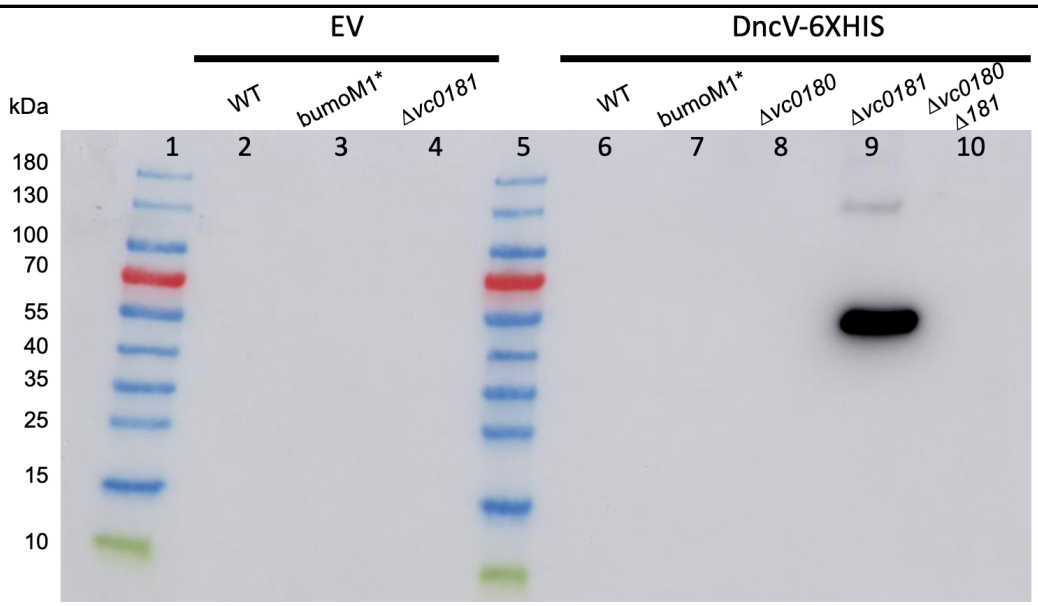

Figure 2.14. DncV phenotype in Δ*vc0180* is not suppressed by *Δvc0181* deletion. αHIS detection of DncV-6XHIS in *V. cholerae A1552* reveal a very faint signal in WT (high exposure of another band overshadows). DncV is absent in both *bumoM1** and *Δvc0180*. However, DncV and a possible dimeric band is detected in *Δvc0181*. The absence of DncV in Δ*vc0180* is not suppressed by the additional deletion of Δ*vc0180Δvc0181*. Lane 1 & 5: Ladder Lane 2-4: pET28b EV containing cells. Lane 6-10: Strains with pET28b DncV-6XHIS vectors. Representative of three images.

E1 and E2 domains (i.e., VC0180) are the mediators of protein interaction in ubiquitin like networks with DUBs (i.e., VC0181) acting to undo the interaction. Interestingly, the first few amino acids of *vc0181* overlaps with the C-terminus of *vc0180* with no other potential start codons further downstream for *vc0181*. This overlap suggests there might be interdependency between VC0180 and VC0181. We tested a double KO

strain of VC0180 and VC0181 to determine how complete removal of this system affects DncV abundance. Given the potential role of VC0180 as an activator and conjugator and VC0181 as a negative driver of DncV stability, we hypothesized that DncV would be detected only in its monomeric form. Unexpectedly, no DncV bands were detectable in the Δ*vc0180-vc0181* mutant, suggesting that VC0180 is required for the stability of DncV in vivo. Given differential dependency of DncV on these ancillary proteins, we next explored the impact of *bumo* on its stability.

2.2.7 Bumo is required for DncV stability

Following our findings that both VC0180 and VC181 are required for DncV stability and existence *in vivo,* we tested to see whether *bumo* also affects DncV stability. Similar to the above experiments, a T7-promoter overexpression vector of 6X-His tagged *dncV* was electroporated into *V. cholerae* encoding the Δ*bumo* (**Fig. 2.15B**)or *bumoM1**(**Fig. 2.18B**) mutations. Induced cell lysates of these mutants were then blotted for DncV using an anti-6X-His primary antibody. Both *bumo* mutations showed a complete loss of the DncV signal similar to that of ΔVC0180, suggesting a relationship in the role of VC0180 and *bumo* in the abundance of DncV in the cell (**Fig. 2.15** and **Fig. 2.18**).

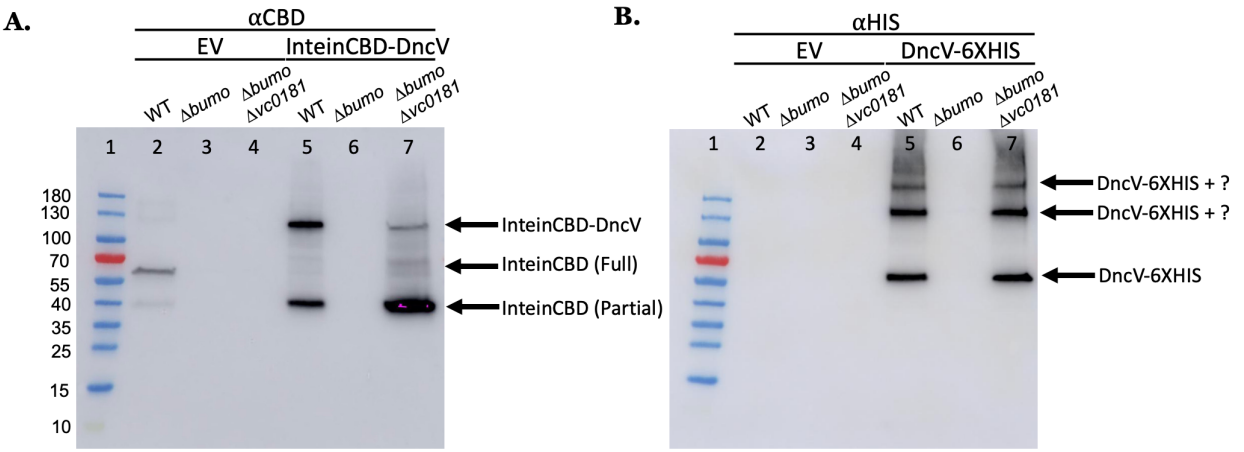

Figure 2.15. DncV is dependent on Bumo. Western blot analyses of **A.** N-terminus InteinCBD-tagged (αCBD) and **B.** C-terminus 6xHIS (αHIS) tagged DncV. DncV show signal corresponding to monomeric DncV in WT VcA1552 strains which are missing in Δ*bumo*. This suggests DncV is unstable and degraded in the absence of Bumo. The lack of any signals is surprising given DncV is being expressed from a vector. **A.** Lane 1: ladder Lane 2-4: pTYB21 EV showing full and partial Intein-CBD tag (~55 kDa) Lane 5-7: pTYB21 DncV showing partially cleaved Intein-CBD tag and full InteinCBD-DncV (~110 kDa). InteinCBD-DncV signal is absent in Δbumo but revived with the additional deletion of vc0181. **B.** Lane 1: Ladder Lane 2-4: pET28b EV Lane 5-7: pET28B DncV. C-terminal tagging of DncV show a band corresponding to a DncV monomer and higher MW bands suggesting multimers containing DncV-6XHIS. These are depleted with Δbumo. However, this is suppressed by the deletion of vc0181. Representative of 3 images.

2.2.8 VC0180 is stabilized by Bumo, DncV and VC0181

Following the dependency of DncV on Bumo and VC0180 and the role of VC0181 in destabilizing DncV, we tested whether VC0180 stability is dependent on the presence of the other CBASS components. A C-terminus 6X-His tagged VC0180 was induced from a T7-promoter vector and cell lysates collected for detection via western immunoblotting. Three major bands were visible in the WT strain: ~70 kDa corresponding to a VC0180 monomer, another between ~130 and 180 kDa and another >~180 kDa suggesting the presence of VC0180 multimers. A Δ*capV* mutant also exhibited similar bands to the WT (**Fig. 2.16**).

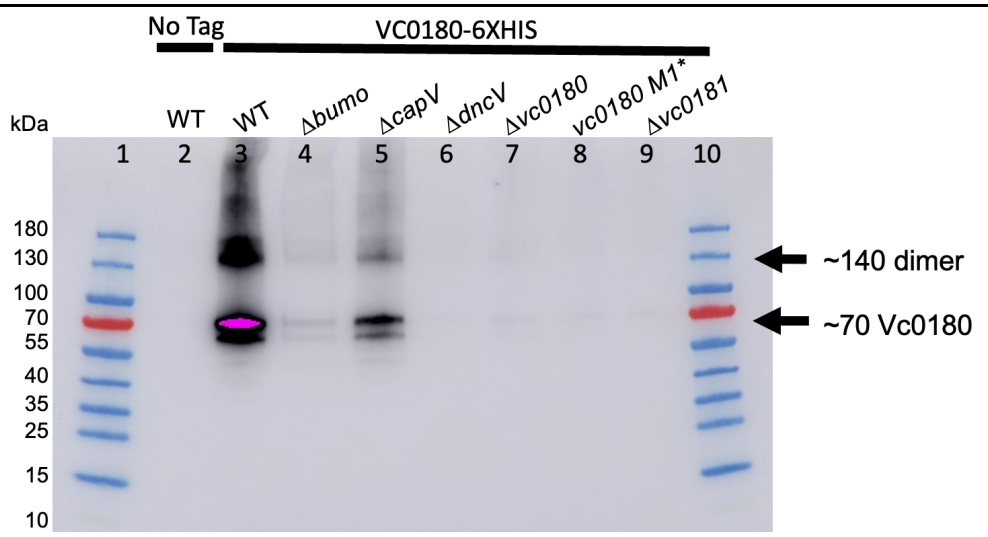

Figure 2.16. VC0180 is more stable with Bumo, DncV and VC0181. αHIS detection of VC0180 show monomeric and possible dimer MW signals in WT and Δ*capV*. However, the only faint monomeric signals are seen in Δ*bumo, ΔdncV, Δvc0180, vc0180 M1stop,* and *Δvc0181*. This suggests that VC0180 is not dependent on CapV for stability but the rest of the CBASS components. The presence of a monomeric signal is not surprising as VC0180 is being expressed from a vector. The multiple bands seen in Δ*bumo* is likely a spill over effect. Image is representative of n=3.

However, the *Δvc0180, ΔdncV, Δvc0180, and ΔVC0181* mutants all showed a very faint band at ~70 kDA corresponding to VC0180 (**Fig. 2.16**). Given VC0180 is being expressed from a plasmid, it is important to note that the lack of detection is not due to polar effects. However, it is interesting the Δ*vc0180* mutant does not look like the WT, as expression of VC0180-His should complement this mutation, suggesting that either deletion of *vc0180* is polar on expression of *vc0181* or the fusion protein is not functional. To address a possible polar effect of Δ*vc0180* on *vc0181* expression, we made a first codon nonsense mutant of *vc0180*. However, the same phenotype was seen in this VC0180 M1STOP mutant (**Fig. 2.16**). This result suggests translation of *vc0180* might be important for expression of *vc0181*. Overall, immunoblot imaging for VC0180 suggests CapV is not necessary for its stability; however, Bumo, DncV and VC0181 are important in its abundance and stability to form multimers.

2.2.9 VC0181 stability is dependent on VC0180

We also tested whether VC0181 stability is dependent on the presence of the other CBASS components. A C-terminus 6X-histidine tagged VC0181 was induced from a pTAC IPTG inducible promoter containing pEVS143 vector (**Fig. 2.17A**) and T7-promoter vector pET28b (**Fig. 2.17B**), and cell lysates collected for detection via western immunoblotting.

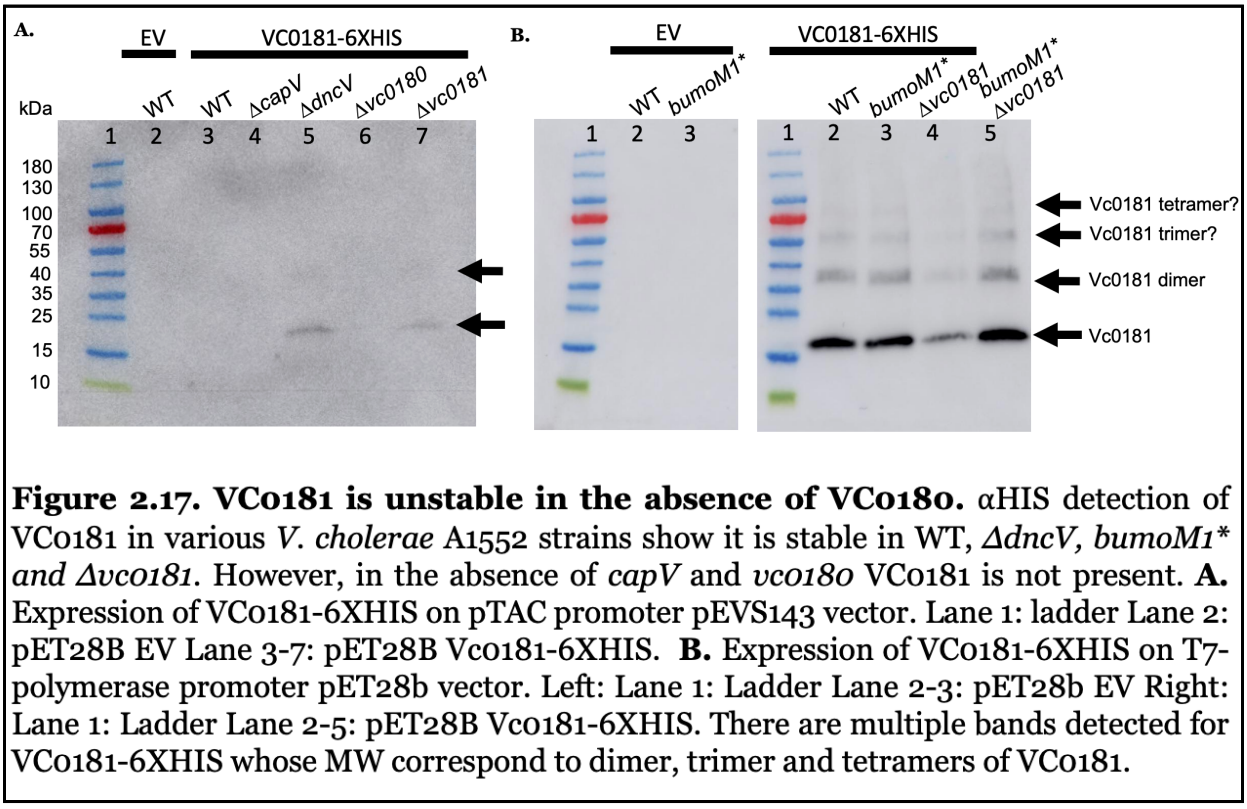

Figure 2.17. VC0181 is unstable in the absence of VC0180. αHIS detection of VC0181 in various *V. cholerae* A1552 strains show it is stable in WT, *ΔdncV, bumoM1* and Δvc0181*. However, in the absence of *capV* and *vc0180* VC0181 is not present. **A.** Expression of VC0181-6XHIS on pTAC promoter pEVS143 vector. Lane 1: ladder Lane 2: pET28B EV Lane 3-7: pET28B Vc0181-6XHIS. **B.** Expression of VC0181-6XHIS on T7-polymerase promoter pET28b vector. Left: Lane 1: Ladder Lane 2-3: pET28b EV Right: Lane 1: Ladder Lane 2-5: pET28B Vc0181-6XHIS. There are multiple bands detected for VC0181-6XHIS whose MW correspond to dimer, trimer and tetramers of VC0181.

Expression from pEVS143 showed a single faint band slightly larger than ~15 kDa in both the *ΔdncV* and *Δvc0181* strains with no bands visible for WT, Δ*capV* or *Δvc0180* (**Fig. 2.17A**).

Due to the poor signal in this expression system, I fused the his-tagged VC0181 into a vector to drive expression using T7 polymerase and electroporated this vector into the *V. cholerae* A1552 strains. I did subsequent blots of cell lysates from *bumoM1** and

Δvc0181. Blot analyses of the WT strain showed a major band >~15 kDa, corresponding to a VC0181 monomer, predicted to be ~18 kDa (**Fig. 2.17B**). Two fainter bands were seen, one between ~35 kDa and ~45 kDa, and the other between ~55 kDa and ~70 kDa corresponding to possible dimer and tetramer forms of VC0181. There are a couple of higher but very faint bands suggesting a higher order complex of VC0181 (**Fig. 2.17B**). The Bumo M1* mutant strain and the Δ*vc0181* strain had similar bands. Both blots taken together suggests VC0181 stability is dependent on VC0180 and possibly CapV, while its stability is independent of Bumo, DncV, and WT chromosomal VC0181.

2.2.10 DncV is depleted by VC0181

The stability of DncV is impacted by Bumo and VC0180, which are required for DncV to be observed, and VC0181 which reduces its stability. C-terminal 6X-His-tagged DncV is detectable as both a monomer and multimer in the WT and Δ*vc0181* strains, with the latter showing greater abundance (**Fig. 2.14**). However, no bands were visible in the *bumo*M1* (**Fig. 2.14**), the Δ*bumo* (**Fig. 2.15B**) and Δ*vc0180* strains (**Fig. 2.14**). We thus explored how these ancillary proteins controlled DncV. Given VC0181 encodes deubiquitinase-like domains, we hypothesized that VC0180 and Bumo function together to modify and stabilize DncV while VC0181 undoes that modification to destabilize the enzyme.

To test whether VC0180 and Bumo can form a complex with DncV, we tested the ability of DncV to form a multimer in the absence of Bumo, the *bumoM1** and Δ*bumo* mutants, the Δ*vc0181* mutant, and a double *bumoM1**Δ*vc0181* mutant. In all strains, VC0180 was present, and thus we could test the necessity of Bumo and its effect on DncV stability in the presence and absence of VC0181. C-terminal His-tag fusion analyses showed the presence of both the monomer and two multimer bands in the WT strains

(**Fig. 2.15B, Fig 2.21C**). These DncV bands were missing in the two Bumo mutants, suggesting Bumo is important for DncV existence in vivo (**Fig. 2.15B, Fig 2.18B**) . The absence of VC0181 lead to a highly intense monomer band ~55 kDa and ~70 kDa with a faint band between ~130 kDa and ~180 kDa (**Fig. 2.15, Fig 2.18B**). Surprisingly, the double mutant of Bumo and VC0181 revealed major monomer and multiple higher bands, one between ~ 130 kDa and ~180 kDa as seen in WT and Δ*vc0181* but also another higher band >~180 kDa (**Fig. 2.15, Fig 2.18B**). This suggests the formation of higher order structures that do not contain Bumo or VC0181.

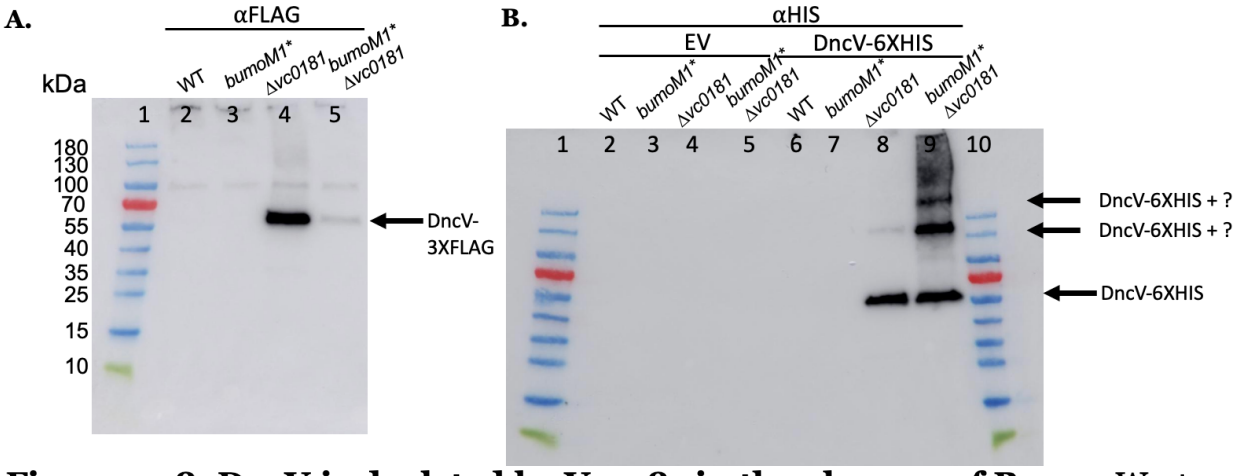

Figure 2.18. DncV is depleted by Vc0181 in the absence of Bumo. Western blot analyses for DncV in various *V. cholerae* A1552 strains show absence of DncV bands in Δ*bumo,* which is suppressed by Δ*vc0181*. DncV prominent in its monomeric form in Δ*vc0181*, however, higher MW bands are present in the double *bumoM1*Δvc0181* mutant for αHIS detection of vector expressed DncV but not chromosomal FLAG-tagged strains. These are representative images of three trials. **A.** DncV was fused at its C-terminus with 3X-FLAG tag on the genome. WT and *bumoM1** had no bands except for nonspecific bands present in all strains (~100 kDa). Deletion of *vc0181* resulted in detection of DncV in both the single Δ*vc0181* with smearing and double *bumoM1*Δvc0181,* though fainter in the latter. ***B.*** αHIS detection of DncV. Lane 1&10: ladder Lane 2-5: pET28b EV showing no bands (6Xhis is <1 kDa). Lane 6-9: pET28b DncV expressing cells. WT cells showed very faint DncV signal which was absent even with overexposure (not shown) in *bumoM1**. DncV is detected in *Δvc0181* suppressing *bumoM1** phenotype. Higher MW bands are present in the double *bumoM1*Δvc0181* mutant absent in *Δvc0181*.

To confirm these findings, we tested the stability of DncV under its natural expression in these mutants. To do this, I generated a chromosomal C-terminal FLAG tag fusion of DncV under control of its natural promoter and collected cell lysates at similar time points. FLAG-tagged DncV was detected in all strains. The WT strain had a very faint band between ~55 kDa and ~70 kDa corresponding to monomeric DncV. This band was missing in the *bumoM1** strain but revived in both the Δ*vc0181* and *bumoM1*Δvc0181* strains in line with the previous two studies (**Fig. 2.18A**). The DncV signals were more intense in both Δ*vc0181* and BumoM1STOP*Δvc0181* compared to WT with Δ*vc0181* exhibiting the most intense bands (**Fig. 2.18A**). This confirms that expression of *dncV* from its native promoter is unstable in the absence of Bumo and is even more stable in the additional absence of VC0181, confirming our findings expressing DncV from a plasmid.

The sum of this evidence support that DncV abundance is depleted by VC0181 and Bumo negatively impacts this interaction. This suggests Bumo is not functioning through VC0180 as the presence of a C-terminus fusion tag on Bumo did not impact its ability to prevent VC0181 degradation of DncV. Given that DncV signal is depleted in vivo for both N-terminal and C-terminal fusions, VC0181 seems to be acting as a protease in degrading DncV regardless of placement of the fusion tag and that the cleavage target of VC0181 might be internal to the protein or nonspecific. We were thus interested in exploring the role of VC0181 as a potential protease.

2.2.11 VC0181 is a DncV protease

Protein structure predictions by I-TASSER revealed similarities of VC0181 to other protease-like enzymes in both in silico predictions and structural database-based predictions. One well studied candidate found was 26S proteasome regulatory subunit N11-like protein in yeast with well characterized active sites. Amino acid sequence alignment with VC0181 revealed E39, a glutamine residue as an important protease active site residue (not shown).

To determine whether VC0181 is a DncV specific protease, I made chromosomal mutation of the active site glutamine residue into alanine (E39A). C-terminus 6X-Histidine-tagged DncV vector was cloned into this strain and compared to the WT strain. The VC0181 E39A strain revealed a band between ~55 and ~70 kDa similar to known monomeric his-tagged DncV. However, no bands were detected in the normal WT strain (**Fig. 19**).

This confirms that VC0181 is a protease that targets DncV. Given previous evidence that DncV stability is enhanced in a double deletion of *bumo* and *vc0181*, we then tested whether a double *bumo* and *vc0181* E39A mutant would affect DncV activity. In line with previous results, there were stronger bands in this double mutant (Fig. 19). DncV also exhibited higher order bands in the absence of Bumo or VC0181, supporting previous findings that VC0181 might be acting as a peptidase to deform multimeric complexes and that Bumo is not required for these multimers.

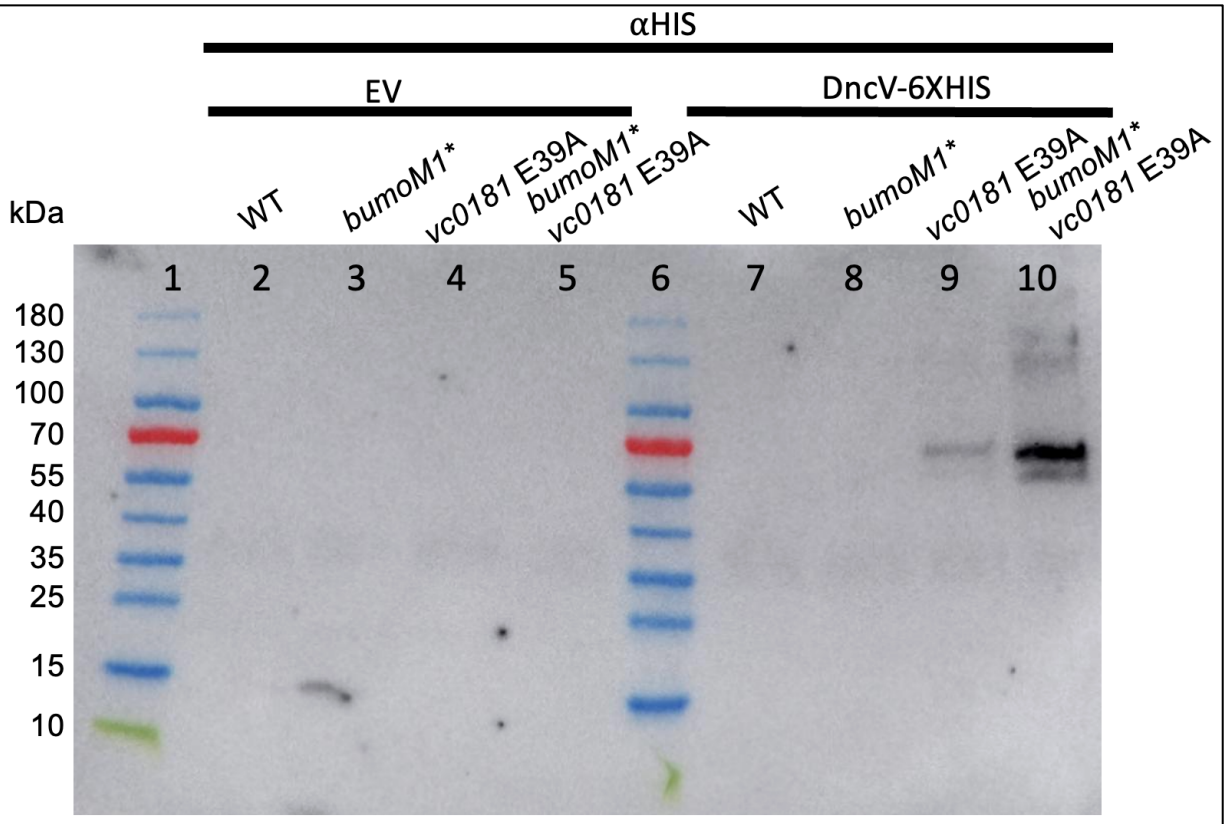

Figure 2.19. VC0181 is a DncV protease. αHIS western blot analyses for DncV in various *V. cholerae* A1552 strains show absence of DncV bands in WT and *bumoM1**. Active site mutation of Vc0181 E39A leads to detection of DncV. DncV is even more prominent in *bumoM1* V*c0181 E39A double mutant and there are higher MW bands. Thus, Vc0181 is a DncV specific protease. These are representative images of three trials. Lane 1&6: ladder Lane 2-5: pET28b EV showing no bands (6Xhis is <1 kDa). Lane 7-10: pET28b DncV expressing cells.

Another line of evidence to support that VC0181 degrades DncV is the lack of monomeric DncV isolated when purified from *V. cholerae*. We have attempted purification of DncV from both BL21 *E. coli* and A1552 *V. cholerae* strains both containing IPTG inducible T7 polymerase promoter. Following column elution, a major band corresponding to ~50 kDa can be isolated from Bl21 cells with some contamination of noncleaved fusion protein and the intein-tag itself. However, following protein production, and affinity column purification of cell lysates from *V. cholerae* A1552 cells,

I saw many multiple bands throughout the entire well (**Fig. 2.20**). After multiple attempts at optimizations and purifications, all attempts at isolating DncV from A1552 was abandoned. However, VC0181 is lacking in *E. coli* Bl21 but present in *V. cholerae* A1552, resulting in DncV produced in *V. cholerae* being degraded by VC0181. This might explain the difficulty associated with purification and the multiple bands seen upon SDS-PAGE staining of purified column elution of *V. cholerae* isolated samples.

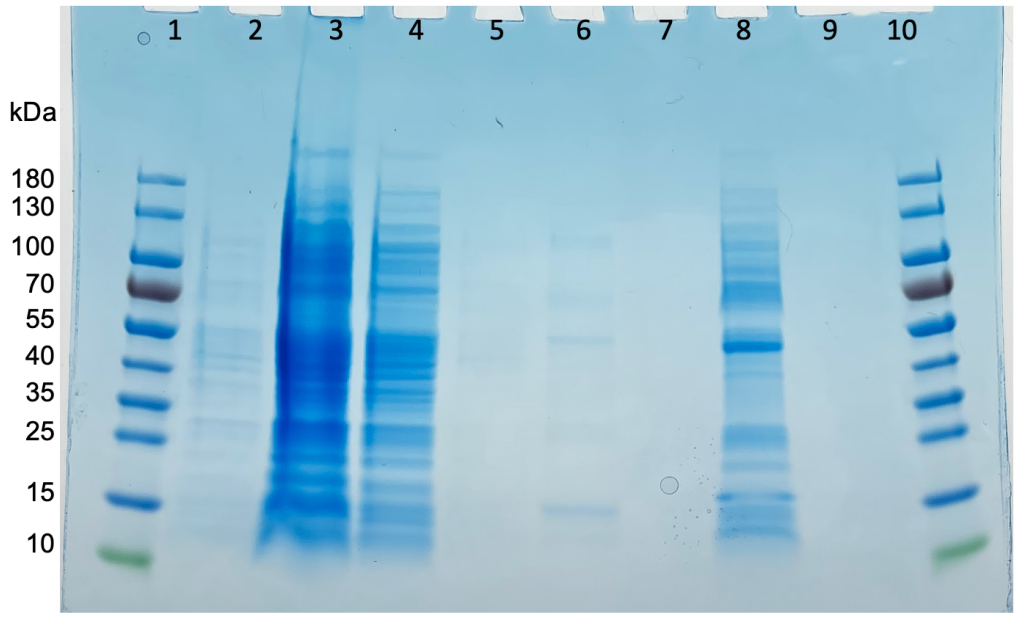

Figure 2.20. DncV expressed in *V. cholerae* A1552 show degradative pattern on SDS-PAGE gel. DncV purified via affinity purification on chitin resin column following induced expression in *V. cholerae* A1552 cells show multiple bands and smearing indicating multiple size forms of DncV. Coomassie staining of SDS-PAGE gel of protein purification samples. Lane 1&10: ladder Lane 2: Induced cell culture Lane 3: Whole cell lysates Lane 4: Column flowthrough during loading Lane 5: Flowthrough after heavy wash of column with column buffer Lane 6: Chitin resin sample Lane 7: Cleavage buffer flowthrough Lane 8: Elutions 1 and 2 after 18 hrs of incubation Lane 9: Chitin resin after elution.

2.2.12 Bumo inhibits formation of DncV and VC0180 heteromultimers.

VC0181 has a predicted DUB-like domain. NCBI BLAST search of VC0181 showed other DUB-like and protease-like domain containing enzymes. With evidence that Bumo, DncV ,and VC0180 might interact, we explored whether Bumo negatively impacts the interaction of DncV and VC0180. Due to previous findings that DncV in the Δ*vc0181* and *bumoM1*Δvc0181* mutants was produced at high levels to overshadow the DncV signal from the WT strain, we exposed the Western blot for a longer period of time (13 min vs 30s) to assess DncV signal in strains in which it was not as highly expressed. In the raw immunoblot alone, we can see that three bands exist in WT strains, the lowest corresponding to a possible monomer, a higher band between ~100 kDa and ~130 kDa presenting a possible dimer or multimer of DncV and VC0180 and a third high band >~180 kDa (**Fig. 2.21C**). No DncV signal was visible even at greater exposure levels for *bumoM1** strain (**Fig. 2.21C**). However, in the Δ*vc0181* strain, the two lower bands of DncV were visible (**Fig. 2.21A&C**). All three bands however can be seen at high intensities in the double *bumoM1*Δvc0181* strain (**Fig. 2.21C**). When we look at VC0180 levels however, we can see that though there are reduced levels in all mutant strains, especially Δ*vc0181,* the band indicative of a monomer and possible dimers and heteromer are found in all strains (**Fig. 2.21D**). In ubiquitination pathways, E2 holds onto to their Ubl or substrates until they find an E3 ligase or target protein to pass it onto. With this logic in mind, it is possible, that in the WT strain where both VC0180 and VC0181 exists, you find all three forms of DncV: DncV alone, conjugated to E2, and in a complex with VC0180 and either Bumo or VC0181.

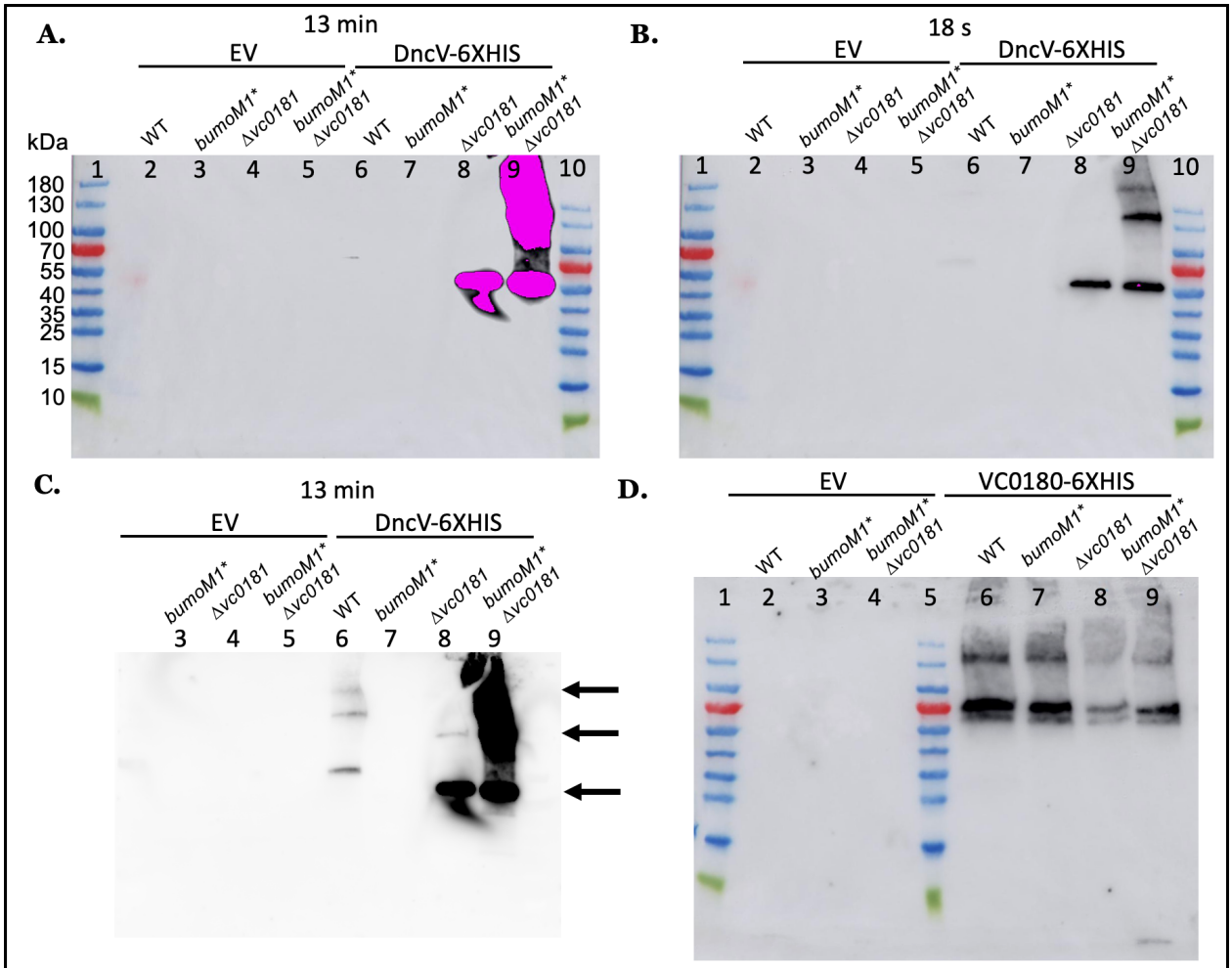

Figure 2.21. Lack of higher order complexes in the presence of Bumo. A. αHIS detection of DncV-6XHIS exposed for 13 min show no bands in EV controls (Lanes 2-4). Very faint DncV monomer and heteromer bands in WT and no bands visible in *bumoM1**. DncV monomer and one higher MW band is present in *Δvc0181*. Even higher bands are present in double *bumoM1*Δvc0181*. **B.** Same blot as A exposed for 18 sec. **C.** Raw immunoblot only of A showing three distinct bands in WT and *bumoM1*Δvc0181* but only 2 lower bands in the *Δvc0181*. **D.** VC0180-6XHIS expressed on pET28B show VC180 monomeric and possible dimer/heteromer MW signals in all strains. However, the signals are fainter with *Δvc0181*. Suggests Vc0180 might be dependent on Vc0181 for stability. Lane 1&6: Ladder Lane 2-5: pET28B EV. Lane 7-10: pET28B Vc0180-6XHIS. Image is representative of n=3.

I have previously established that Bumo and VC0181 remain stable in these strains (**Fig. 2.13**). Thus, depletion of DncV in the absence of Bumo but with functional VC0180 and VC0181 present show that Bumo protects DncV from degradation. In the double *bumoM1*Δvc0181* mutant, detection of DncV and VC0180 yield higher bands of similar MW (**Fig. 2.21B&C lane 9, Fig. 2.21D lane 9**). This suggests the higher bands might be a heterodimer of DncV and VC0180. That band however is absent in the Δ*vc0181* strain where *bumo* is present but present in the *bumoM1*Δvc0181* mutant indicating that Bumo might inhibit the formation of these heteromultimers. I have tested if only the monomeric DncV band is detected in Δ*vc0180,* but DncV is not produced in this mutant rendering this experiment unfeasible. Thus, further experiments are necessary as DncV is not detected in a Δ*vc0180* background (**Fig. 2.14 lane 8**).

2.2.13 VC0180 specifically utilizes ATP

E1-like enzymes activate their target via an adenylation reaction utilizing ATP. We tested whether VC0180 can adenylate target substrates using ATP in vitro by detecting nucleotide triphosphates (NTP) turnover. I purified VC0180 and incubated it with ATP, GTP, CTP and UTP alone and in different combination. In vitro reaction of VC0180 with different triphosphate nucleotides led to turnover of only ATP containing reactions when visualized on silica gel TLC (**Fig. 2.22**). This confirmed to us that VC0180 is functioning like other E1 like enzymes in vitro in preferentially turning over ATP for possible adenylation reaction.

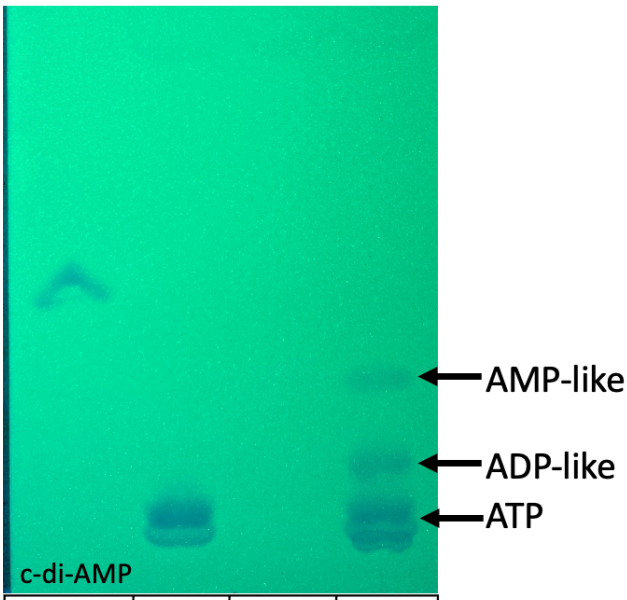

ATP	+	-	+
Vc0180	-	+	+

Figure 2.22. Vc0180 hydrolyzes ATP. Incubation of Vc0180 with ATP resulted in turnover to bands like AMP and ADP controls (not shown) but not c-di-AMP. This supports Vc0180 uses ATP as substrates as other E1-like enzymes.

2.3 Discussion

Bacteria adapt to various environments through cdN signals that regulate numerous adaptive phenotypes (15, 24, 65). *V. cholerae* must respond to multiple challenges in aquatic conditions including viral predators for survival (102, 105). cGAMP leads to communal protection from phages via abortive suicide of the infected host (89). Upon phage infection, cells are killed by DncV synthesis of cGAMP which leads to membrane degradation by CapV (82). Neither the activating signal nor the full regulation of this signaling network has been identified. Previous work on cGAMP's antiphage function showed that VC0180 and VC0181, two ancillary genes found, contribute to broader phage defense, hinting at a modulatory function of these enzymes, but their exact mechanism has yet to be determined (30, 85, 89). Moreover, no ubiquitin-like protein or modifier have been identified to be associated with CBASS, though such modifiers are an important component of ubiquitination biochemistry.

We identified DncV and an uncharacterized upstream gene we name *bumo* as potential candidates for VC0180 and VC0181 modifications. DncV has the characteristic ubiquitin -SG motif in its C-terminus while *bumo* is a small ORF in the vicinity of CBASS. We show that *bumo* is part of the CBASS operon being present on the same RNA transcript as *capV*, *dncV*, and *vc0180* **(Fig 2.5)**. Surprisingly, *vc0181* is not found to be on the same transcript as the other members of the CBASS operon (**Fig. 2.5 & 2.6)**. It is possible that Q-RT PCR cannot amplify the junction between *vc0180* and *vc0181* even if they are on the same transcript due to the formation of hairloop pins or other structures that inhibit synthesis of continuous cDNA. However, is it interesting that the transcript of *vc0181* extends into the ORF of *vc0182* (**Fig. 2.5**), although on the opposite strand, suggesting transcription termination of *vc0181* extends well past the translation stop site

for this gene. Given the proximity of *bumo* to *capV* and their existence on the same transcript, it is highly possible that VspR also negative regulation *bumo* expression.

In line with our observation, previous studies into VspR, a transcriptional inhibitor of CBASS only showed negative regulation of *vc0178* (*capV*), *vc0179* (*dncV*) and *vc0180* (30). This is supported by our observation that *vc0181* is not on the same transcript as the rest of CBASS thus is not coordinately regulated. Analysis of *Pseudomonas fluorescens* SRM1 and *Escherichia coli* ECOR31 containing orthologous VC0180 and VC0181 ancillary domains show there are also overlaps in the ORFs indicating that differential transcriptional regulation and post-translational interdependency might be evolutionarily conserved.

Bumo plays an important role in promoting DncV stability within the cell. A nonsense mutation in *bumo* decreases CBASS transcription while a deletion of *bumo* increased CBASS transcription (**Fig. 2.8 B & D**). These effects on CBASS expression can be seen phenotypically by the survival of nonsense mutants and earlier cell death of deletion mutants (**Fig. 2.8 A & C**). We were unable to complement these mutations suggesting they impact transcription *in cis*. Due to the differential effect of the mutation on sulfamethoxazole viability, it is not a suitable model to study the phenotypic effects of Bumo in relation to CBASS.

I show that Bumo is a post translational modifier of DncV that protects it from degradation specifically by VC0181. In the WT strain, DncV and its multimeric bands are present, which are completely missing in either the Δ*bumo* or *bumo* M1STOP mutants(**Fig. 2.15 & 2.18**). Evidence suggests that VC0181 targets and cleaves DncV as an endopeptidase as both C-terminal and N-terminal tagged fusions of DncV were completely cleared in the absence of Bumo. Furthermore, no peptide fragments

containing the tag were visible on the Western blot indicating that the protein was completely degraded. This phenotype is also independent of CBASS expression, as both *bumoM1** and Δ*bumo* lack DncV (**Fig. 2.15B** and **2.18B**). It is interesting to note that the same higher bands of DncV are present when detecting VC0180, suggesting these higher bands might be heterodimers and multimers of DncV and VC0180 (**Fig. 2.21**). It is quite remarkable that DncV is the potential target of VC0180, as most E1 and E2 enzymes target ubiquitin-like small proteins for activation and conjugation as seen by the presence of the same higher bands when detecting for DncV or VC0180. In contrast DncV, is a larger protein and does not encode a predicted Ubl domain like some larger protein.

Regulation of DncV by VC0181 also represents a rather novel mechanism of control. Instead of acting like other DUBs that only remove ubiquitin tags from target lysine residues or dissociate E1/E2 enzymes from SUMO, it acts to degrade DncV entirely in the absence of Bumo (115). This is in contrast to other prokaryotic deubiquitinase-like enzyme DOP which remove PUP from its target protein or DRJAMM, another JAMM motif containing DUB-like enzymes, known to cleave MoaD and MoaE (149). It is still possible that VC0181 cleaves VC0180 from DncV, which would be best investigated *in vitro* using a double terminal tagged DncV, in which cleavage of the C-terminal end would not affect its ability to be detected using an antibody against the N-terminal tag.

Bumo seem to be inhibiting formation of even higher order multimers of DncV and VC0180 as seen by the lack of high bands in the Δ*vc0181* mutant but presence in the double *Bumo*M1STOP, Δ*vc0181* mutant (**Fig. 2.21**). Though the DncV and VC0180 heterodimer is present, the higher multimeric bands are not (**Fig. 2.21**). E1 enzymes MoaD and ThiS generally function as a homodimer, so it is likely that the two higher bands represent a single DncV and VC0180 heterodimer and then a dimer of DncV and

VC0180 heterodimers (129, 131, 132). This is supported by the fact that these higher multimeric bands are present in both DncV and VC0180 immunoblots. The absence of the band indicative of a dimer of dimers in the presence of Bumo but absence of VC0181 (Δ*vc0181* strain) imply that Bumo inhibits the formation of the DncV-VC0180 dimer. The purpose of this inhibition might be to avoid targeting by VC0181. This can easily be tested with complementation of VC0181 *in vivo*. *In vitro*, these individual components can be combined to determine whether these higher order structures form based on MW band shifts of different combinations. We can also test VC0181 endopeptidase activity by adding purified enzyme and seeing whether DncV his-tag signal disappear.

VC0180 preferentially utilizes ATP, supporting that it might be activating its substrate with adenylation (116). This is also further supported by the fact that the fusion of the C-terminus of DncV to a rather bulky 3X FLAG TAG does not lead to a formation of the higher bands comprising the multimer. However, the use of the smaller His-tag, the higher bands are formed.

CBASS is an important antiphage defense system for bacteria to counteract phage in different environments. Though activating signals of CBASS have not been identified, we now know that activity of the DncV is regulated at multiple levels. VspR regulates *capV*, *dncV*, and *vc0180* expression at the transcription level while at the post-translational level, VC0180 and Bumo stabilize DncV with the latter also protecting DncV from degradation by VC0181, a DncV-specific protease. We can further appreciate the diversity in ubiquitin-like post translational modification systems in bacteria to regulate vital pathways include that of 3'3'-cGAMP and the importance of cyclic di nucleotide signaling in bacterial survival.

2.4 Materials and Methods

Strains and Growth Conditions

Escherichia coli DH10b (Invitrogen) was used for cloning, protein expression, transposon library screening and phage plaque assays. *Vibrio cholerae* El Tor strain C6706 and its genetic derivatives were used for sulfamethoxazole treatment assay, mRNA extractions, cGAMP quantification and protein expression. *E. coli* BL21(DE3) was used for protein expression and production. *V. cholerae* A1552 and its genetic derivatives were used for protein production and expression studies.

All strains were grown in 2 mL of Luria-Bertani (LB) broth (0.5 % yeast extract, 1% tryptone, 1% NaCl, pH 7.5) overnight at 37˚C unless indicated otherwise. LB agar medium was used with 1.5% agarose. Antibiotic selections were at the following dosages: Ampicillin [100 μg/mL], Kanamycin [100 μg/mL], Gentamycin [10 μg/mL], Spectinomycin [100 μg/mL], Sulfamethoxazole [100 μg/mL], and Trimethoprim [30 μg/mL].

Mutations

For DNA base substitutions, we followed the previously established method called SPRINP as described (150). Plasmids harboring our gene(s) of interest were PCR amplified in sets of twos with each containing either a forward or reverse base substituted primer. They were then combined into a single reaction tube and incubated as described. They were then diluted with water on dialysis membranes and electrotransformed into E. coli DH10B cells as described previously (82). They were then recovered in 500 μL of SOC for 1 – 2 hours and spread on LB selective agar. They were incubated overnight, and positive colonies were PCR amplified and sequenced for the mutagenesis.

Genetic manipulation in *V. cholerae* El Tor was done following chitin-competent transformation and EXO-MUGENT protocol (151–153). *V. cholerae* strains were grown overnight then sub-cultured (1:100) into fresh LB media. They were grown to an OD600 of 0.5 – 0.9 and collected at 15,000 g for 5 min. The top media was aspirated, and the pellet resuspended in 1X Instant Ocean (IO). In a 1.5 mL Eppendorf tube, 150 µL of chitin slurry, 750 µL of 1X IO, and 100 µL of resuspended cultures were mixed together and incubated at 30˚C for 18 hrs. For plasmid transformations, 0.5 µL to 1 µL were added and mixed to transform into cells. For EXO-MUGENT ~3000 bases upstream and downstream of the gene of interest were PCR amplified and ligated together using Gibson cloning. They were then PCR amplified using internal primers for the combined product. For genomic editing, 10 – 15 µL of ligated PCR are added along with 1 µL of either Spec or Trim PCR amplified antibiotic cassettes which replaces Vc01807 a frameshifted transposase on the chromosome. For gene KI or replacement, primers spanning ~2-3 kb US to ~2-3 kb DS of the gene of interest are used to amplify the region then added along with 1 µL of PCR amplified antibiotic cassettes. The mixture is incubated at 30˚C for 18 hours. 500 µL of LB was added to each mixture and transferred into sterile glass tubes. The culture was the grown at 37˚C for 2-3 hours shaking at 210 rpm. Each culture (300 – 500 µL) was then spread on LB selective agar plates and incubated at 30˚C overnight. Isolated colonies were checked for insertions or deletions via colony GoTaq PCR and checked on agarose gel. Colonies with appropriate deletion or insertion size were confirmed via sequencing.

Phage plaque assay

E. coli DH10B clones were challenged with T2, T3, T4, T5, T6, T7, lambda vir, SECphi17, SECphi18 and SECphi27 coli phages. Subsequent infection studies utilized T2 and T5 phages.

Overnight culture of *E. coli* DH10b was subcultured 1:1000 into 10-15 mL of LB and grown to OD600 of 0.02 – 0.08. 250 µL of grown culture was transferred into a new test tube and mixed with liquified 15 – 18 mL of MMB agar. The mixed solution was immediately poured into large agar plate and swirled to cover the entire surface. While the plate solidifies, we prepared 10-fold dilutions of each phage to be tested. After solidification of the agar, we added 5 µL of each phage dilution onto the agar surface. The plate was incubated for 18 hours and then observed for plaque formation.

mRNA extraction and cDNA synthesis

Overnight cultures were back diluted to OD600 = 0.01 in 3 mL of LB and grown in experimental conditions in large glass tubes. Sample cultures (1.5 mL) were collected at designated timepoints and pelleted at 15,000 g for 5 min at RT. The solution was aspirated, and pellet was redissolved in 1 mL of Trizole (Invitrogen™ Cat.# 15596018). mRNA was extracted following manufacturer guidelines to "Isolate RNA." Extracted mRNA were quantified by NanoDrop and stored at -20˚C.

DNA contaminations in the mRNA extract was removed using TURBO DNA-*free*™ Kit (Invitrogen™ Cat.# AM1907) following manufacturer protocol. cDNA was synthesized using the SuperScript™ III Reverse Transcriptase (Invitrogen™ Cat.# 18080044) following manufacturer protocol. Prepared 2x volume for each RNA sample

to be used in reverse transcription reaction and half-volume no reverse transcriptase control reactions.

qRT-PCR

qRT-PCR of cDNA samples were performed using SYBR™ Green PCR Master Mix (Applied Biosystems™ Cat.# 43-091-55) following the manufacturer's protocol. No template and no RT samples were included as negative controls and *gyrA* as a positive control for standardization of results. Sample data was collected using QuantStudio3 following previous methods (67, 68).

5' RACE

5' rapid amplification of cDNA ends (5' RACE) was carried out using Template Switching RT Enzyme Mix (NEB™ Cat.# M0466L) following the manufacturer's protocol. For CBASS 5' RACE, Random Primer (Promega™ Cat.#C1181) was used for the initial second strand synthesis and CapV qPCR Rvs primer was used for cDNA PCR amplification and sequencing. For Vc0181 5' Race, Vc0181 qPCR Rvs Primer and Vc0182 US primers were used for cDNA PCR amplification.

Sulfamethoxazole Treatment Assay

Overnight cultures were back diluted to OD600 of 0.01 in 3 mL of fresh LB liquid media in large glass tubes. Cultures requiring induction were inoculated with IPTG [100 μg/mL]. They were grown for 1 hr at 37˚C shaking at 210 rpm then treated with sulfamethoxazole [100 μg/mL]. Cultures were continuously grown and collected every

two hours until the 6th hour post treatment. The OD600 was recorded for each sample at their designated time points.

Protein Purification

Proteins of interests were purified using the IMPACT™ Kit (NEB™ Cat.# E6901S) following the manufacturer's protocol. Each gene was cloned to be expressed by a T7 polymerase promoter containing Amp^R vectors. For C-terminal fusions of intein-CBD tag, the gene was cloned into the pTXB1 vector at the NdeI and SapI restriction sites. For N-terminal fusion of intein-CBD tag, genes were cloned into the SapI site of pTYB21 vector.

Overnight cultures of *E. coli* BL21 or *V. cholerae* A1552 were sub-cultured 1:1000 into 1 L of LB liquid media supplemented with Amp (100 μg/mL). They were then grown shaking at 210 rpm for at 37˚C until OD600 reached ~0.500. The culture was then induced with IPTG (100 μg/mL) and grown shaking at 210 rpm for 4-6 hours at 30˚C or 37˚C depending on the optimal conditions determined for each protein. Bumo was induced for 4 hrs at 30˚C. DncV and Vc0181 were induced for 6 hrs at 30˚C. And Vc0180 was induced for 6 hrs at 37˚C. The cultures were then collected in 300 mL centrifuge bottles and pelleted at 5000 g for 1 5 min at 4˚C. Cells were harvested in 100 mL of column buffer (20 mM HEPES/Tris-HCl, 500 mM NaCl pH 8.5) and homogenized using Microfluidics M-110P. They were then spun down at 25,000 g for 20 min at 4˚C. A chitin resin (NEB™ Cat.# S6651S/L (20 mL/100 mL) column was prepared, and samples were prepared and loaded following manufacturer recommendation. Cleavage buffer consisted of 100 mM DTT in the column buffer used. Loaded columns were incubated at either 4˚C or 23˚C for 40 – 60 hours before elution. A third of the column volume was eluted using column buffer. Eluted proteins were quantified by Quick Start™ Bradford 1x Dye

Reagent (BIO-RAD™ Cat.# 5000205) following manufacturer protocol using BSA standards.

Protein samples were concentrated using Amicon® Ultracentrifugal Filters following manufacturer protocol. Utilized Amicon® Ultra-4 Centrifugal Filter Units 3 kDa (Millipore™ Cat.# UFC800324), 30 kDa (Millipore™ Cat.# UFC801024) and 50 kDa (Millipore™ Cat.# UFC805024) and Amicon® Ultra-15 Centrifugal Filter Units 3 kDa (Millipore™ Cat.# UFC900308), 30 kDa (Millipore™ Cat.# UFC903008) and 50 kDa (Millipore™ Cat.# UFC905008).

SDS-PAGE

Each sample was mixed with 4X SDS-PAGE dye (200 mM Tris-HCl pH6.8, 8% SDS, 4.3 M glycerol, 6 mM bromophenol blue) with or without 400 mM DTT to 1X and boiled at 60˚C for 10 min or 95˚C for 5 min. Boiled samples were loaded onto 4–20% Mini-PROTEAN® TGX™ Precast Protein Gels, 10-well, 50 µl (BIO-RAD Cat.# 4561094) and ran for 90 min at 90 V constant or 30 min at constant 200 V. Samples were run in 1X TG-SDS PAGE running buffer (10X buffer: 0.2501 M Tris base, 1.924 glycine, 0.03467 M SDS). PageRuler™ Prestained Protein Ladder (Thermo Scientific™ Cat.# 26616) was used for all gels.

Protein Gel Coomassie Staining

Protein gels were stained using Coomassie stain (0.1% Coomassie Brilliant blue, 50% MeOH, 10% glacial acetic acid (vol/vol), 40% water) overnight shaking at 100 rpm at RT. They were then decanted and de-stained using warm destaining solution (20% MeOH, 10% glacial acetic acid in water) overnight. Destaining solution was refreshed at

least once when solution seemed concentrated. Images were captured using a personal iPhone 12 Pro Max.

Western Blot

Overnight cultures were sub-cultured (1:100) into LB liquid broth (3 mL) and grown until the OD600 reached ~1.0. Cultures needing induction were induced with IPTG (100 μg/mL) before subculture. Samples (1.5 mL) were centrifuged at 15,000 g for 3 min and aspirated. Pellets were normalized in 1X Dulbecco's Phosphate Buffered Saline (SIGMA™ Cat.# RNBH5973) to an OD600 of 1.0.

Protein gels were transferred onto nictrocellulose membranes in transfer buffer (20% MeOH in 1X Tris-glycine buffer) for 2 hrs at 250 Amp using a transfer sandwich or semi-dry blot transferred at 250 Amp for 1 hr. Membranes were blocked in 5% milk 1X TBST (1% Tween20, 200 mM Tris, 1.5 M NaCl pH 7.6) for 2 hours shaking at 100 rpm at RT. Each membrane was then blocked-in primary antibodies diluted into 5% milk 1X TBST buffer at 4˚C for 18 hrs. They were then rinsed in 1X TBST buffer for 5 min shaking at 100 rpm at RT three times. Membranes needing secondary antibody treatment were blocked in secondary antibody mixed into 5% milk 1X TBST solution for 2 hours at RT shaking at 100 rpm. They were then rinsed in 1X TBST buffer for 5 min shaking at 100 rpm at RT three times. Membranes were imaged using the Amersham Imager 600 using semi-auto exposure to determine optimal exposure periods. Images were prepared using Microsoft Powerpoint and BioRender.

His-tag proteins were detected using Mouse IgG αHA (GenScript® Cat.# A00186) at 1:5000 and αFLAG HRP-conjugated antibody (GenScript® Cat.# A01869) was used at 1:5000 in 5% milk 1X TBST solution. αRabbit/Mouse IgG H&L (HRP) (abcam™ Cat.#

ab6721/ab97023) secondary antibody was diluted 1:5000 in 5% milk 1X TBST solution. Bands were detected using Pierce™ ECL Western Blotting Substrate kit (Thermo Scientific™ Cat.# 32106) following manufacturer protocol.

cGAMP Extraction

Overnight cultures were sub-cultured (1:100) into LB liquid broth (3 mL) in large glass tubes and grown shaking at 210 rpm at 37˚C until the OD600 reached ~1.0. Cultures needing induction were induced with IPTG (100 μg/mL) before subculture. Samples (1.5 mL) were centrifuged at 15,000 g for 3 min and aspirated. They were resuspended in 100 μL of cdN extraction buffer (MeOH:MeCN:water:0.1N Formic acid, 4:4:4:0.2, vol:vol:vol:vol) and incubated at -20˚C for 30 min. The samples were centrifuged at 15,000 g for 5 min then the supernatants were transferred into new 1.7 mL Eppendorf tubes. The solvent was then evaporated via rotary evaporation overnight. Dried pellets were stored at -20˚C until needed for mass spec. Sulfamethoxazole samples were prepared following the appropriate protocol and harvested following the protocol above. We made 10-fold dilutions of each culture and pipetted 5 μL of each onto LB plates to determine CFU/mL of our cells.

Mass Spectrometric Analysis

Following cGAMP extraction as outlined above, thawed pellets were resuspended in 100 μL of HPLC-grade water. They were then analyzed on a Waters Xevo TQ-S using UPLC/MS/MS at the Michigan State University Mass Spectrometry and Metabolomics Core following the method outlined in Massie et al (154). cGAMP was detected with

electrospray ionization in negative ion mode at *m/z* 674.1 -> 337.05. Standards were prepared ranging from 1.95 to 125 nM.

Nucleotide Utilization Assay

Purified Vc0180 [5 μM] was mixed with $MgCl_2$ [2.5 mM], ATP [1.25 mM] in column buffer (20 mM HEPES, 500 mM NaCl pH 8.5) in a PCR reaction tube for a total of 50 μL. No enzyme control and no substrate controls were also prepared of equal total volume. They were incubated at 37˚C for 16 hrs before TLC analysis.

Thin Layer Chromatography

Samples were blotted (10 μL) onto silica gel thin layer chromatography glass plates (250um, THICK, 60A. FLUORES. IND.) (ANALTECH Cat. C09622) with nucleotide standards (1 μL of 10 mM or 100 mM) . The TLC plate was incubated with running solution of n-propanol:ammonium hydroxide:water in 11:7:2 (vol:vol:vol) until the solvent front was about 1 cm from the top. The plate was then dried and visualized under UV light (254 nM). Images were captured using an iPhone 12 Pro Max and prepared using BioRender and Microsoft PowerPoint.

CHAPTER 3:

DETERMINING THE FUNCTION OF CBASS IN OTHER GRAM-NEGATIVE BACTERIA

For this research portion of my thesis, many individuals were involved. John Dover and Kendal Tinney of the Parents laboratory conducted growth curves and phage infection assays of *Escherichia coli* EDEC13E, *Vibrio cholerae* 2631-78 and *Pseudomonas fluorescens* SRM1 CBASS systems cloned into *Shigella flexineri* Y and *Salmonella typhimirium*. Q-TOF Mass Spectrometry was performed by Dr. Anthony Schilmiller of the Michigan State University Metabolomics and Mass Spec Core.

3.1 Introduction

Bacterial pathogens must adapt to a wide variety of environmental conditions and predators. Phages compete with their bacterial hosts in these micro-environments to ensure their survival (23). This constant battle between the bacterial host and phage for survival has led to the development of various phage defense mechanisms. Many bacteria have acquired the cyclic-oligonucleotide based antiphage system (CBASS) that utilizes a nucleotide signal to mediate a phage infection response (31, 89). These systems have two core components comprising of the cGAS/DncV-like nucleotidyltransferase (CD-NTase), and its effector that senses and is activated by that signal (31, 89). Activation of the effector typically results in the death of the infected host, a process termed abortive infection, in which the infected host commits altruistic suicide to prevent infection of its clonal neighbors (31, 89). Majority of CBASS have these two primary components while many have ancillary domains hypothesized to play a crucial role in enhancing or regulating the CBASS response.

CBASS has been categorized into Types 1, 2, 3 and 4 (31). Type 1 comprises just the synthase and effector, type 2 comprises E1/E2-like and JAB-like ancillary domains, type 3 comprises HORMA/TRIP13 ancillary domains, and Type 4 contains potential nucleotide modifying enzyme domains (31). There are variations of Type 2 and Type 3 called Type 2 short in which only a short E2-like domain is found and no E1 or JAB-like domains and Type 3 double HORMA domains (31).

Putative CD-NTases have been identified in all bacterial phyla (31, 85, 88, 89). cGAS and DncV, cGAMP synthase in humans and bacteria, respectively, belong to 2 of 7 clades of the CD-NTase protein family divided based on 10% nucleotide sequence similarities (31, 85, 89, 100). CD-NTases are also classified into two different classes

based on whether they sense and respond to DNA or RNA or are inhibited by folate-like molecules (95, 98, 100). cGAS and OAS, a cGAS-like enzyme that produces 2'5'-oligoadenylate (pApA), are activated upon sensing double stranded DNA and RNA, respectively (31, 97, 155, 156). DncV, a cGAS-like bacterial structural homolog was shown to have folates attached in the corresponding backbone region and was active in the absence of such stimuli. *In vitro* screening of numerous bacterial CD-NTases showed synthesis of nucleotide signaling molecules utilizing all four nitrogenous bases, contrary to the previous thought that only purines were utilized as was the case for cyclic di-GMP, cyclic di-AMP, and cyclic GMP-AMP (cGAMP) (86, 100). CD-NTases can make a diverse set of cyclic oligo-nucleotides as *in vitro* c-di-UMP is synthesized by CdnE02 from *Legionella,* cUMP-AMP (cUAMP) and cAAA are synthesized by CdnD and CdnC from various *E. coli* strains (86, 88, 139). This demonstrates that we are just beginning to understand the variety of cdN produced in bacteria and their role in bacterial physiology.

CD-NTases are found associated with a variety of potential effector domains. There are phospholipases, transmembrane domains, endonuclease domains, toll-like receptor domains, phosphorylase domains, and peptidase domains (31). Abortive infection has been observed experimentally in some of these systems but only hypothesized in others (87–89). The majority of Type 1 and 4 systems harbor transmembrane-like domains, type 2 systems encode patatin-like phospholipase domains, while type 3 system harbor endonucleases (31). There are three subtypes of endonucleases found throughout the CBASS system, the HNH-SAVED endonuclease family, NucC nuclease family, and the PF14130 family (31). It is interesting to note that patatin-like phospholipases, such as CapV, and HNH-SAVED endonuclease have only been identified in Type 1 and Type 2 systems (31, 88). Patatin-like phospholipase is the most abundant effector followed by

HNH-endonuclease (31). My primary goal of this research is to explore the function of the HNH-SAVED effector and its relation to the Type 2 CBASS systems.

Though cells may harbor CBASS systems, is it not definitive that they are active. Given the vastness of CBASS, we have developed a funnel approach in first screening for active systems before further investigating their cyclic di-nucleotide (cdN) and effector function. Active CBASS systems were screened by induced expression in heterologous hosts. Previous studies in our lab have shown overexpression of El Tor CBASS led to reduced viability of the host (Severin, in preparation). Thus, we first acquired three different strains of Gram-negative bacteria harboring yet uncharacterized CD-NTases associated with HNH-SAVED effectors of Type 1, Type 2, and Type 2 short. These three CBASS systems came from *Pseudomonas fluorescens* strain SRM1 (157)(Type 2B), *Escherichia coli* strain EDEC13E (158) (Type 1), and *Vibrio cholerae* strain 2631-78 (159) (Type 2 short B). These CBASS operons were inserted into inducible vectors and cloned into *E. coli* DH10b and *Shigella flexinerii* cells to see whether they impacted cell viability. Moreover, we also studied phage infection by infecting the host with coli or ICP phages expressing the CBASS under their native promoter in their respective hosts. ICP phage 1, 2, and 3 are the dominant *Vibrio cholerae* specific phages isolated from pandemic cholera samples (23, 105). The reason for their dominance in both clinical samples and environment are not yet known, but they are seen to infect pathogenic *V. cholerae*.

For those CBASS systems with activity, we tried to determine their signaling nucleotide used in vitro via mass spectrometry and thin layer chromatography. *In vitro* detection of novel nucleotides was achieved via purification of the CD-NTase and synthesis of the novel nucleotide in vitro with different combinations of nucleotide triphosphates (NTPs): ATP, UTP, CTP and GTP. The resulting reaction would be analyzed

via thin layer chromatography for a novel product band and quantitative time-of-flight mass spectrometry to determine novel mass profiles.

For this chapter of my thesis, I identify active CBASS systems in *E. coli* EDEC13E and *P. fluorescens* SRM1 that affect heterologous host viability. We show EDEC CD-NTase utilizes ATP and GTP *in vitro* to produce two novel bands on TLC screening while *P. fluorescens* utilizes ATP *in vitro* to produce novel bands that are susceptible to phosphatase treatment. We show that EDEC HNH-SAVED endonuclease activity is inhibited by the addition of cdN synthesis mixture, indicating a possible inhibitory role of the unidentified cdN.

3.2 Results

3.2.1 *In vivo* overexpression *P. fluorescens* SRM1 and *E. coli* EDEC13E CBASS systems leads to growth defects in heterologous systems

Overexpression of DncV and CapV within an *E. coli* heterologous host leads to growth defects caused by membrane degradation. I assessed whether the putative CBASS systems from other species impacted growth within *E. coli* DH10B cells. I constructed overexpression vectors of *P. fluorescens* SRM1, *E. coli* EDEC13E (EDEC) and *V. cholerae* 2631-78 (VC) CD-NTase systems and overexpressed these in a laboratory strain of *E. coli* DH10b or *Shigella flexneri* serotype Y.

Overexpression of the putative CD-NTase signaling operon of *P. fluorescens* resulted in growth inhibition in *E. coli* DH10b (**Fig. 3.1F**), but no observable growth changes were observed with EDEC and *V. cholerae* operons (**Fig. 3.1C & 3G**). However, the Parent Laboratory observed growth defect upon overexpression of the EDEC CD-NTase operon in *S. flexneri* (Sf) (**Fig. 3.1B**). These results suggest that the *P. fluorescens* and EDEC CD-NTase are active in different species of bacteria and warrants future analyses within multiple bacterial species. Preliminary analyses identified these two out of three CD-NTase operons exhibiting *in vivo* activity in a heterologous system, supporting screening of *in vivo* activity as a useful tool in prioritizing CD-NTase systems for further study.

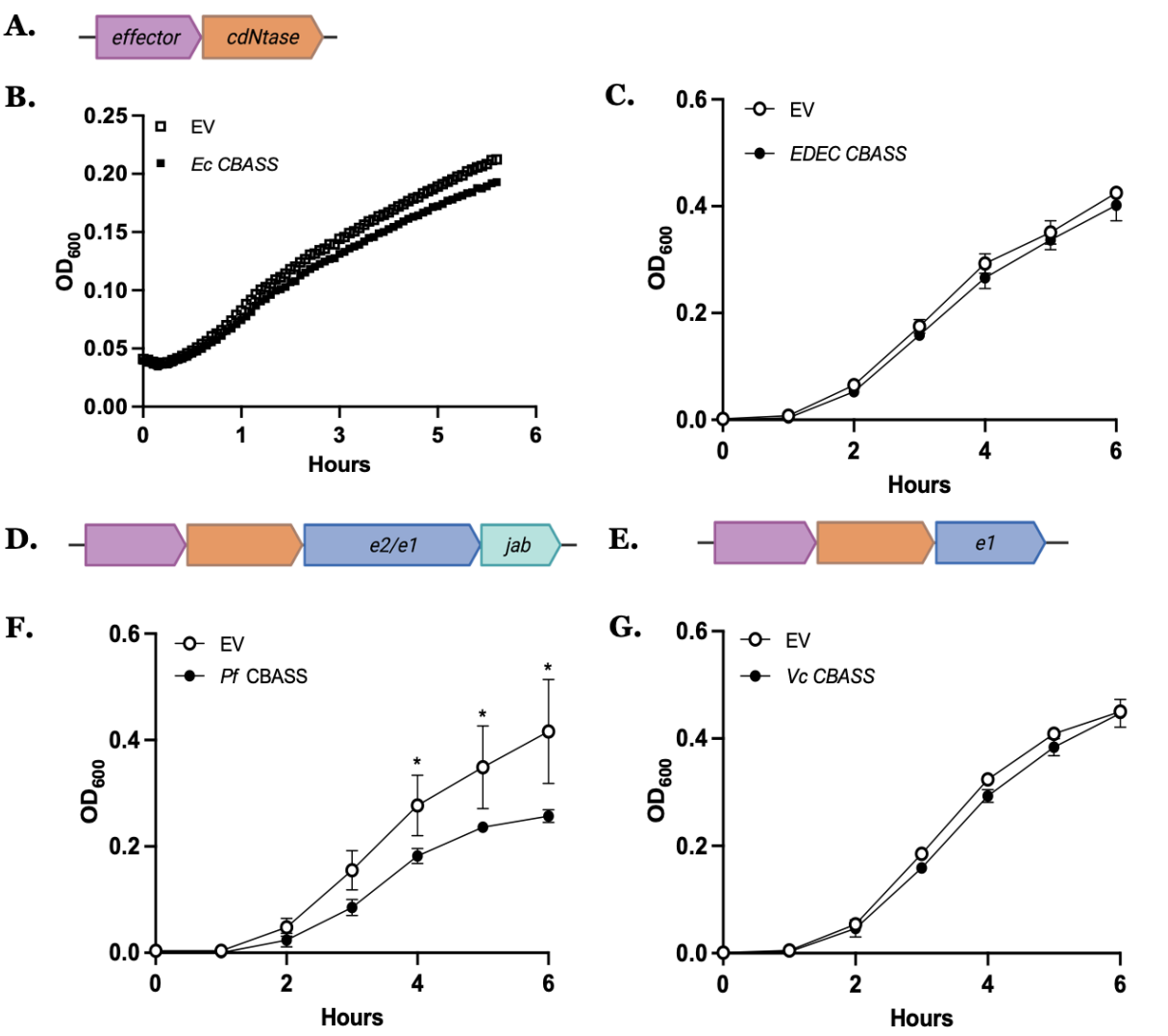

Figure 3.1. *E. coli* EDEC13E and *P. fluorescens* SRM1 CBASS affect growth of heterologous hosts. Growth curve measuring OD600 over 6 hrs following induction of various CBASS in heterologous hosts on 96-well plates. **A.** *E. coli* EDEC13E CBASS operon (type I). **B.** Expression of EDEC13E CBASS in *S. flexineri* resulted in slight decrease in growth of the host over time compared to the EV control (Parent Lab). Representative growth curve. **C.** Expression of EDEC13E CBASS in *E. coli* DH10B results in no visible difference in growth phenotype compared to EV containing hosts. n=3 **D.** *Pseudomonas fluorescens* SRM1 CBASS operon (type II). **E.** *Vibrio cholerae* 2631-78 CBASS operon (type II short). **F.** *P. fluorescens* SRM1 CBASS expression in *E. coli* DH10B cells result in decreased viability of the host compared to EV containing cells over time. N=3 **G.** *V. cholerae* 2631-78 CBASS expression led to no significant change in cell viability between CBASS expressing and EV containing hosts. n=3.

3.2.2 HNH-SAVED is the main perpetrator of *P. fluorescens* SRM1 CBASS growth inhibition

Following growth defects seen with overexpression of *P. fluorescens* CBASS in *E. coli* DH10B cells, we next investigated which component was the main perpetrator of the phenotype. Given the core component are the CD-NTase and HNH-SAVED effector, I generated active site mutations in the HNH motif of HNH-SAVED and the DND aspartic active sites of the CD-NTase then tested these individual component impacts on cell viability. The CD-NTase D79A, D81A active site mutant showed growth defect in its heterologous host similar to that of CBASS expressing cells (**Fig. 3.2**). The HNH H56A H91A mutant however, showed cell viability similar to that of EV control. This suggests HNH-SAVED is active in the cell and is the main cause of the cell viability defect seen in WT CBASS and HNH-SAVED expressing cells and this effector, when overexpressed, does not need a functional synthase to produce a cdN. A double mutant displayed no discernible cell viability defect.

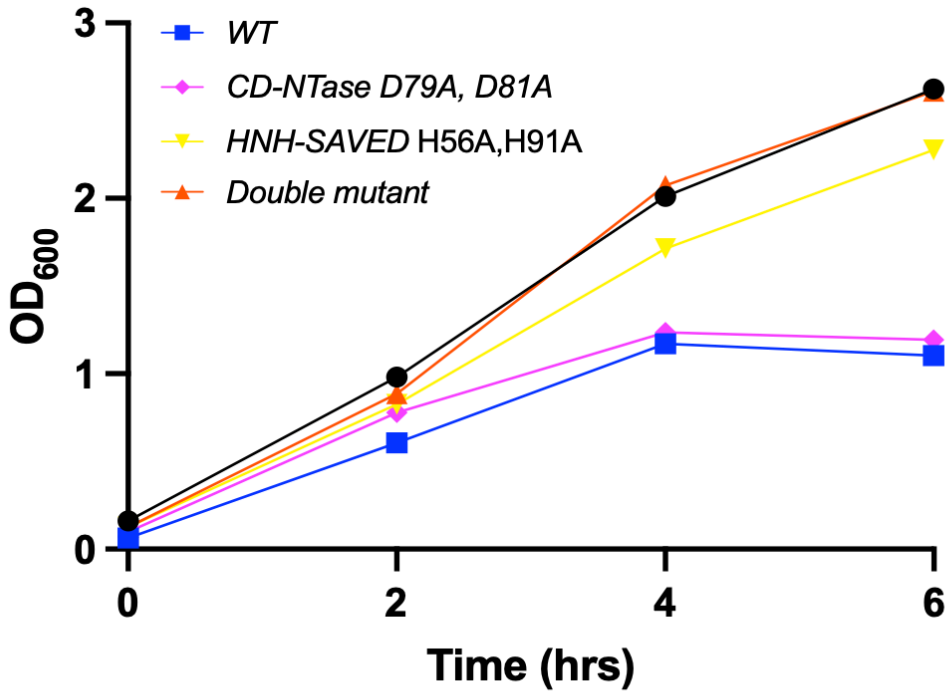

Figure 3.2. HNH-SAVED is the main effector of growth defect seen in *P. fluorescens* SRM1 CBASS expressing DH10B cells. Growth curve measuring OD600 over 6 hrs following induction of various CBASS in heterologous hosts in large test tubes. *P. fluorescens* CBASS expression in *E. coli* DH10B cells result in decreased viability of the host compared to EV containing cells over time. Active site mutation of the CD-NTase D79A, D81A does not rescue that phenotype. However, an HNH H56A, H91A active sites mutation suppresses this phenotype. HNH-SAVED mutation alone also leads to EV like growth phenotype. n=3.

3.2.3 *Pseudomonas fluorescens* SRM1 CD-NTase utilize ATP as substrates *in vitro*

When purified *P. fluorescens* CD-NTase was incubated with nucleotide triphosphates (NTPs), only ATP containing reactions showed novel bands, indicating formation of a novel cyclic or linear oligonucleotide (**Fig. 3.3A**). These bands were similar to c-di-UMP and slightly higher than c-di-GMP. Interestingly it was much lower than c-di-AMP. The top band was lined up with the AMP control on subsequent TLCs, as well as 5'-pApA-3'. Reactions with novel bands were repeated and treated with Calf intestinal phosphatase (CIP) to determine whether the cdN products contain any free 5' or 3' phosphates or P1 nuclease, a ssDNA and RNA nuclease with 3'-phosphomonoesterase activity to determine whether they have 3'-5' cyclic peptide bonds. These ATP utilizing products were CIP-susceptible indicating they have 5' or 3' exposed phosphates with complete turnover into a single band corresponding to adenosine (**Fig. 3.3B**). C-di-AMP was not susceptible to CIP treatment as expected. We are continuing to enhance Quadrupole Time-of-Flight mass spectrometry (Q-TOF MS) detection methods and analyses to identify the masses of our products.

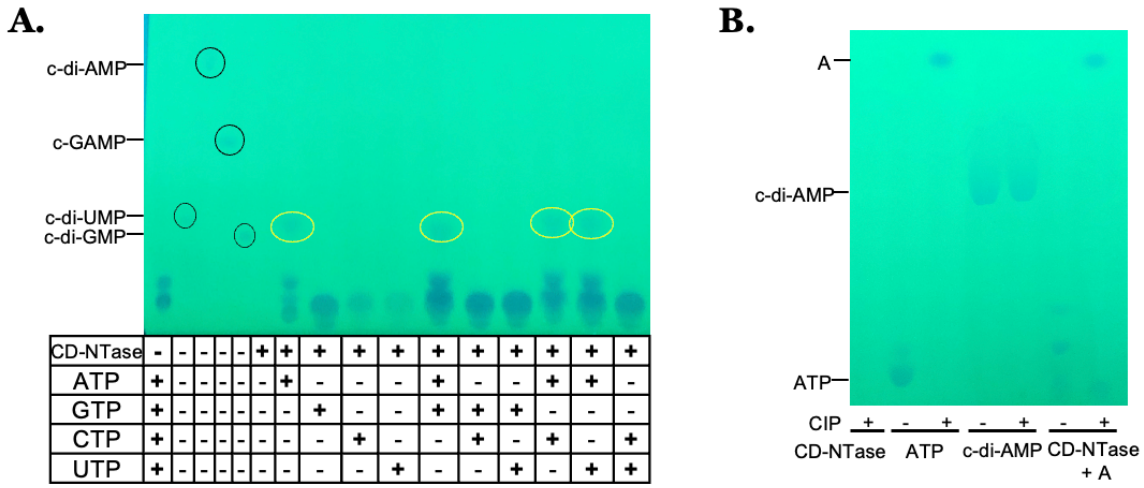

Figure 3.3. *P. fluorescens* CD-NTase utilizes ATP as substrates to synthesize products that are CIP susceptible. Silica gel thin layer chromatography (TLC), exposed under UV light (254 nm). Black circles indicate known nucleotide signaling standards. Black circles indicate known nucleotide signaling standards. **A.** *P. fluorescens* SRM1 CD-NTase utilizes ATP as substrates (yellow circles) as only ATP containing reaction had novel bands on TLC. **B.** *P. fluorescens* SRM1 CD-NTase nucleotide products were susceptible to CIP treatment. ATP was turned over into adenosine 9A) but c-di-AMP was resistant to CIP-treatment.

3.2.4 *E. coli* EDEC13E CD-NTase utilize ATP and GTP as substrates in vitro

I observed novel bands on silica gel TLC upon screening the products of EDEC CD-NTase incubated with the NTPs ATP, GTP, CTP and UTP. The *EDEC* CD-NTase showed two novel bands on TLC (**Fig. 3.4A**). The first band product was observed when GTP was added as a substrate, with ATP and GTP yielding increased band intensity. This product was resistant to CIP and P1 cleavage indicating that it might be cyclized without a 3'5' peptide bond and does not have an exposed 5' and 3' phosphate (**Fig. 3.4 & 3.5**). This band did not align with any known dinucleotide standards suggesting it might be a novel cdN. The second band product utilized ATP as the main substrate and was CIP-susceptible (**Fig. 3.4B**). This band however was later shown to be aligning with ADP, indicating the possibility of an ADP by-product being detected instead.

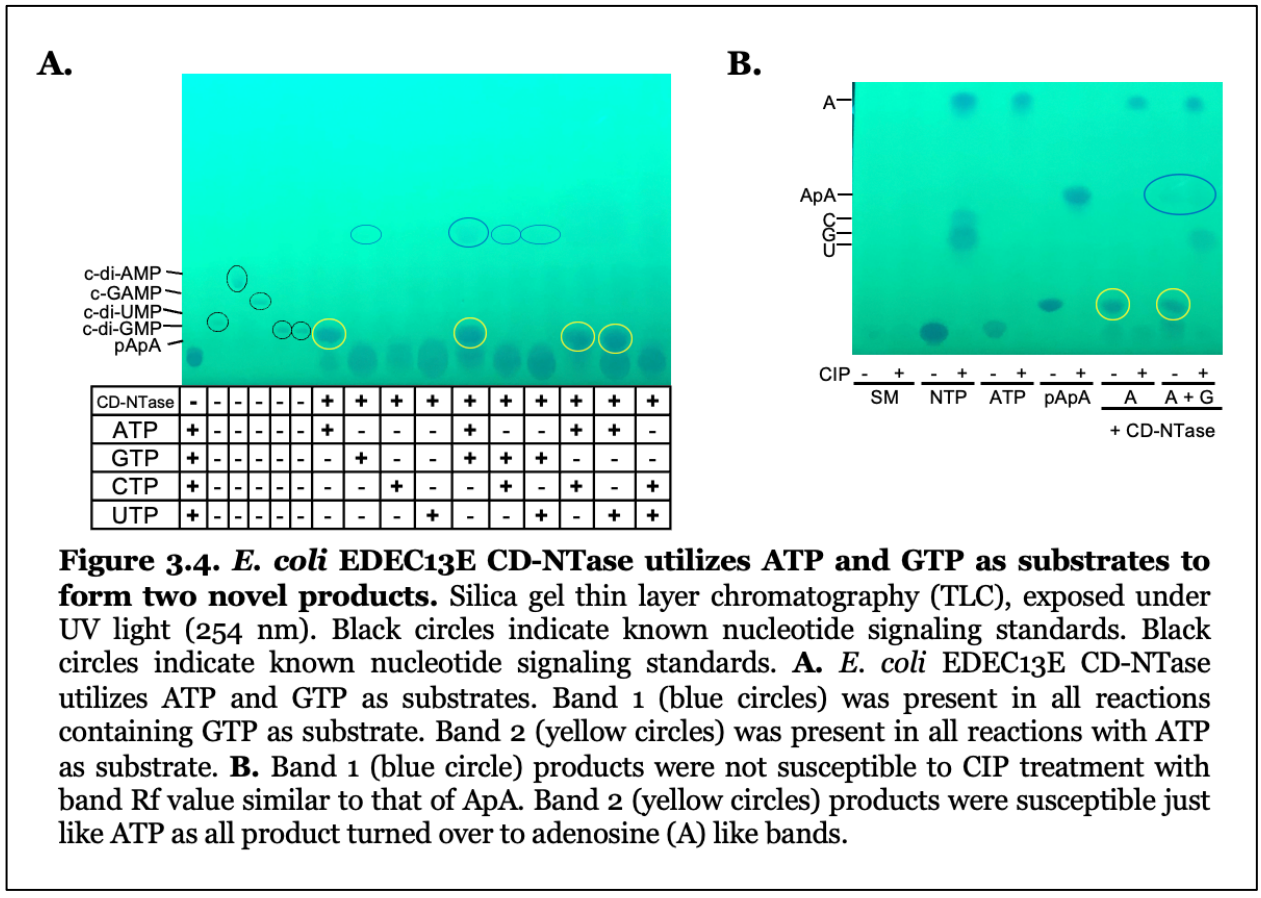

Figure 3.4. *E. coli* EDEC13E CD-NTase utilizes ATP and GTP as substrates to form two novel products. Silica gel thin layer chromatography (TLC), exposed under UV light (254 nm). Black circles indicate known nucleotide signaling standards. Black circles indicate known nucleotide signaling standards. **A.** *E. coli* EDEC13E CD-NTase utilizes ATP and GTP as substrates. Band 1 (blue circles) was present in all reactions containing GTP as substrate. Band 2 (yellow circles) was present in all reactions with ATP as substrate. **B.** Band 1 (blue circle) products were not susceptible to CIP treatment with band Rf value similar to that of ApA. Band 2 (yellow circles) products were susceptible just like ATP as all product turned over to adenosine (A) like bands.

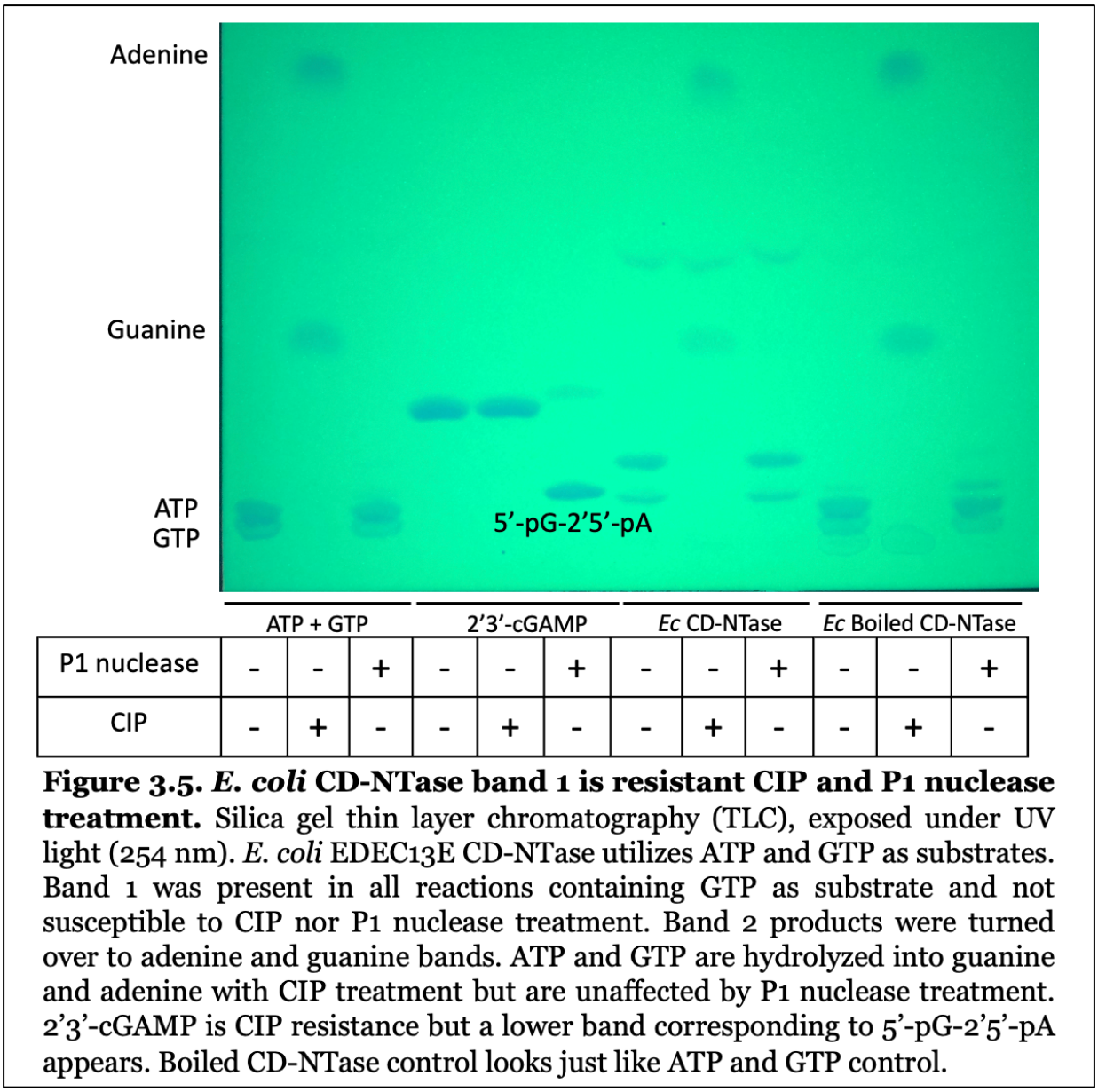

P1 nuclease	-	-	+	-	-	+	-	-	+	-	-	+
CIP	-	+	-	-	+	-	-	+	-	-	+	-

Figure 3.5. *E. coli* CD-NTase band 1 is resistant CIP and P1 nuclease treatment. Silica gel thin layer chromatography (TLC), exposed under UV light (254 nm). *E. coli* EDEC13E CD-NTase utilizes ATP and GTP as substrates. Band 1 was present in all reactions containing GTP as substrate and not susceptible to CIP nor P1 nuclease treatment. Band 2 products were turned over to adenine and guanine bands. ATP and GTP are hydrolyzed into guanine and adenine with CIP treatment but are unaffected by P1 nuclease treatment. 2'3'-cGAMP is CIP resistance but a lower band corresponding to 5'-pG-2'5'-pA appears. Boiled CD-NTase control looks just like ATP and GTP control.

Many CD-NTase enzymes function in the presence of dimetal compounds, thus EDEC activity was tested in the presence of different divalent cations. EDEC activity is dependent on MgCl2 and MnCl2 based on the nucleotide turnover analysis on TLC however, ZnSO4, NicL2 and CuCl2 also showed some levels of nucleotide turnover (**Fig. 3.6**).

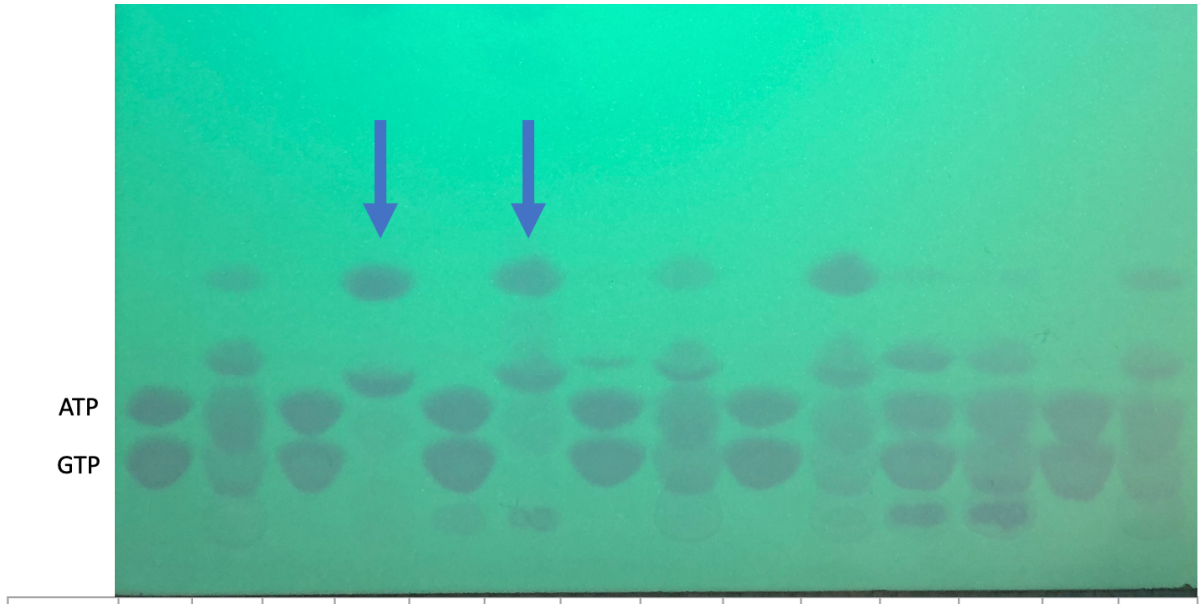

Cation	-	-	$MgCl_2$	$MgCl_2$	$MnCl_2$	$MnCl_2$	$ZnSO_4$	$ZnSO_4$	$NiCl_2$	$NiCl_2$	$CaCl_2$	$CaCl_2$	$CuCl_2$	$CuCl_2$
CD-NTase	-	+	-	+	-	+	-	+	-	+	-	+	-	+

Figure 3.6. $MgCl_2$ and $MnCl_2$ act as cofactors of *E. coli* EDEC13E CD-NTase. Silica gel thin layer chromatography (TLC), exposed under UV light (254 nm). *E. coli* EDEC13E CD-NTASE nucleotide synthesis reaction with ATP and GTP as substrates. Divalent cations were added at a final concentration of [5 mM]. CD-NTase reaction with $MgCl_2$ and $MnCl_2$ (blue arrows) added showed nearly complete depletion of ATP and GTP. Others showed control like bands.

3.2.5. Mass spec analyses show *E. coli* EDEC13E CD-NTase metabolize ATP and GTP into AMP, ADP, GMP and GDP.

To confirm our *in vitro* findings that the EDEC CD-NTase utilizes ATP and GTP to form a novel product, we analyzed the nucleotide synthesis reaction using Quadrupole Time-of-flight mass spectrometry in which all mass of compounds in a sample are identified. We prepared two controls, an enzyme control with ATP and GTP added but no enzyme and a substrate control with enzyme, but no substrates added to discern ATP, GTP and novel signals from background reaction mixture. Our reaction mixture that contained both ATP, GTP, and the purified CD-NTase showed reduction of ATP and GTP substrates with signals for AMP, ADP, GMP and GDP detected (**Fig. 3.7**). There was a greater reduction of the ATP signal compared to the GTP signal. In depth analyses for specific masses predicted for potential cyclic di nucleotides showed no signals corresponding masses of c-di-AMP, c-di-GMP, cGAMP or pApA. Moreover, no obvious signal indicating a novel compound was detected, keeping the identity of the nucleotide formed unknown. The signals at times ~1.6 and ~1.88 with mass 237.09 are HEPES molecules. We performed a similar analysis of *P. fluorescens* CD-NTase reaction which showed depletion of ATP signals and a rise in AMP signals. However, no novel signals were detected (Data not shown)

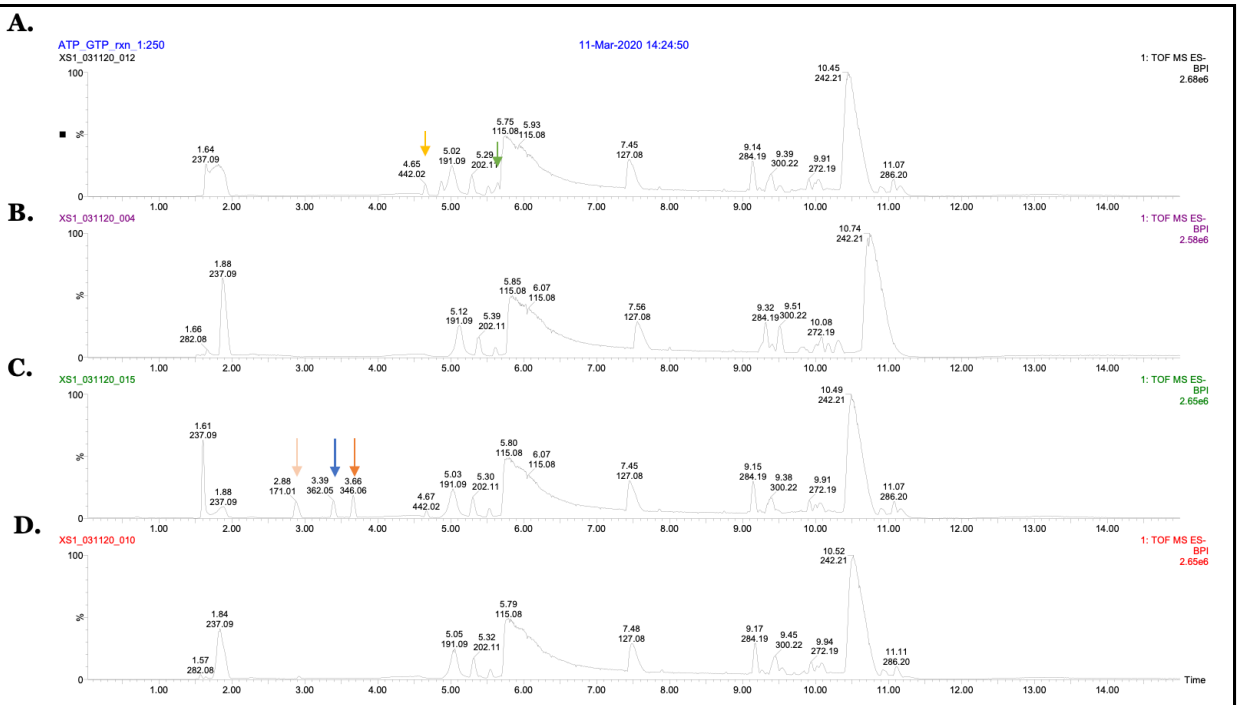

Figure 3.7. *E. coli* EDEC13E CD-NTase utilizes ATP and GTP as substrates which are CIP susceptible. Q-TOF MS analyses show *E. coli* EDEC13E CD-NTase metabolizes ATP and GTP to ADP, GDP, AMP and GMP which are CIP susceptible. **A.** Mass spectrum of ATP + GTP only reaction show ATP (yellow arrow) and GTP (green arrow) signals. **B.** *E. coli* EDEC13E CD-NTase only reaction showing background spectra. **C.** In vitro reaction of ATP + GTP + *E. coli* EDEC13E CD-NTase show decrease in ATP and GTP signals with appearance of AMP (light orange arrow), ADP (orange arrow) and GDP (blue arrow) signals. **D.** CIP treatment of the CD-NTase nucleotide synthesis reaction leads to loss of all nucleotide signals. Mass spec is representative of n=3.

3.2.6 EDEC HNH-SAVED is inhibited by addition of the CD-NTase reaction molecule

Following the unsuccessful studies to identify the nucleotide signaling molecule, we then investigated whether the HNH-SAVED domain encoded an actual endonuclease. To investigate this, we first incubated purified EDEC CD-NTase with NTPs to synthesize the cdN product. I then mixed this reaction product with purified EDEC HNH-SAVED enzyme in the presence of double stranded DNA substrates to determine whether any

degradation occurs. The resulting reaction were analyzed by gel electrophoresis to determine if there were any changes to the nucleic acid substrate (**Fig. 3.8**). The substrate only control showed three major bands indicating the presence of the pTXB1 vector in different colloidal forms (lane 1). Upon the addition of purified HNH-SAVED, this led to the appearance of multiple bands and smearing on the gel (lane 2). Unexpectedly, the incubation of the cdN products synthesized in vitro with HNH-SAVED led to the prominence of just one band with faint bands (lane 4) similar to the endonuclease absent control mixture (lane 3). This was observed a total of three times.

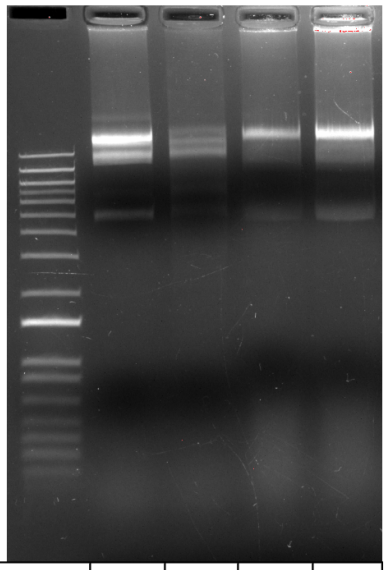

pTXB1	+	+	+	+
Ec HNH-SAVED	-	+	-	+
Ec CD-NTase rxn	-	-	+	+

Figure 3.8. *E. coli* HNH-SAVED is inactivated by the putative nucleotide signal. Gel electrophoresis of pTXB1 (Lane 1) with purified HNH-SAVED (Lane 2). The incubation of pTXB1 with nucleotide synthesis reaction (lane 3). The addition of EDEC CD-NTase nucleotide synthesis reaction to the mixture results in a single band (Lane 4) identical to controls.

3.2.7 T2 and T5 Coli Phages infect *E. coli* EDEC13E but ICP phages do not infect *V. cholerae* 2631-78.

To better study these CBASS systems in their native environment, we explored whether any of our phage libraries infect CBASS-containing hosts. EDEC13 *E. coli* cells were vulnerable to T2 and T5 phage infection suggesting this CBASS system is not sufficient to block these phages from infecting. *V. cholerae* 2631-78 CBASS showed no indication of an active system based on viability phenotype. Thus, we tested whether any of ICP phages could infect the cell. ICP 1, 2 and 3 were not able to infect *V. cholerae* 2631-78, indicating invulnerability of the cell to ICP phages. Whether or not the inability of ICP 1 to infect *V. cholerae* 2631-78 is due to the CBASS system or other factors such as receptor expression remains to be determined.

3.3 Discussion

CBASS is found in all bacterial phylogenies, including many human pathogens (89, 160). Having to adapt to various environments, they have acquired various genetic islands including various phage defense systems (23, 102). CBASS has a nucleotide synthase which produces a cyclic dinucleotide/oligonucleotide signaling molecules that binds to and activates an effector which kills off the host (86, 100). This form of abortive infection, though detrimental to the host altruistically saves the rest of the surrounding bacterial community. The CD-NTase family is a unique family of cyclic di nucleotide synthases as they produce a wide array of nucleotide molecules, from cyclic di purines or pyrimidines to tricyclic nucleotides, utilizing all four nucleotide peptides (86, 100). These CD-NTase are found associated with various effectors, the most common of which are patatin-like phospholipases in bacteria, with the original founding member of this family, CapV, being discovered in *V. cholerae* (31). CapV binds its cognate nucleotide signal and becomes activated to degrade the cellular membrane killing the host (82). However, many CD-NTases are also found associated with effectors containing a SAVED domain that is a specific nucleotide receptor (85, 88). These are fused to effector domains such as endonucleases and proteases. The majority of SAVED domains are found fused to HNH-endonuclease domains which cleave host and phage nucleic materials upon binding of a nucleotide signal to the SAVED receptor domain (88). This effector differs from the CapV mode of abortive infection but helps us better appreciate the diversity in CBASS effector response.

These systems are found in many instances with ancillary domains hypothesized to regulate or aid the CD-NTase. HORMA/TRIP13 systems attach to their cognate CD-NTase to upregulate cdN synthesis and TRIP13 removes HORMA, suppressing the

activation (107). The majority of ancillary systems discovered are E1/E2-like ubiquitin like systems which have not yet been characterized (31, 89). Prior to the publication of the mechanism of HNH-SAVED effectors, we started looking into these effector domains to determine their functions. We decided to explore this HNH-SAVED effector containing system with and without full and short length E1/E2 ancillary domains to better understand their function.

The majority of CBASS systems are predicted to be inactive in vitro (107). Thus, we started our investigation by identifying potentially active systems in vivo. Previous studies in our lab discovered that overexpression of *V. cholerae* El Tor CBASS in *E. coli* led to decreased cell viability or earlier death. Thus, we overexpressed EDEC, *V. cholerae* 2631-78 and *P. fluorescens* SRM1 CBASSs in an *E. coli* or *S. flexneri* heterologous host and found *P. fluorescens* CBASS inhibited growth in *E. coli* cells while the EDEC CBASS inhibited growth in *S. flexinerii* cells.

We then took *P. fluorescens* SRM1 and made inactivating mutations to either the CD-NTase or HNH domain to determine which component was responsible for this growth inhibition. Mutation of *P. fluorescens* SRM1 CD-NTase active sites D79A and D81A did not rescue CBASS expressing cells from growth inhibition. However, active site mutation to the HNH domain H56A H91A alone rescued the sick phenotype to that comparable to the empty vector control. As expected, a double mutant of HNH-SAVED and the CD-NTase led to a similar growth phenotype to that of HNH-SAVED single mutant and EV control. Inhibition of cdN synthesis should affect its potential effector activity, however, none was seen in the CD-NTase mutant. Thus, it would be important to verify that the mutations made for the CD-NTase did inactivate the resulting cdN synthesis activity. Another explanation is that the HNH-SAVED domain binds to multiple

signaling nucleotides. Even if it binds to similar signaling nucleotides at a lower affinity, in a highly induced state, there might be enough HNH-SAVED activated to induce abortive infection.

Since both EDEC13E and SRM1 CD-Ntases showed active phenotypes, we purified and investigated their nucleotide products in vitro. Each enzyme was incubated with various combinations of NTPs and analyzed on TLC and MS for novel products. On TLC analysis, EDEC CD-NTase exhibited two novel bands different from the NTP and boiled enzymes controls. Thus, reactions were treated with CIP phosphatase and P1 nucleases to further characterize their molecular structure. The lower band product of EDEC appeared in any ATP containing reactions. This band was susceptible to CIP treatment but not P1 nuclease treatment. This result indicated that it was a linear nucleotide with exposed phosphates with a resulting product that lined up with adenosine on TLC. The higher band however was only present in GTP containing reactions with the combination of ATP and GTP yielding much higher yields. This product was resistant to both CIP and P1 nuclease treatment, indicating that it does not have any exposed phosphate groups and that it may be a cyclic compound without 3'-5' peptide bonds. Mass spectrometric analysis confirmed both observations above with turnover of both ATP and GTP substrates with a greater utilization of GTP. This result indicates that the novel product may be a cyclic nucleotide containing both AMP and GMP with non 3'5' phosphodiester bond resistant to P1 cleavage. It does not seem to be 3'3'-cGAMP nor 2'3'-cGAMP as both are susceptible to P1 cleavage at both or one bonds, and they appear lower on TLC than our band of interest. Thus, this novel compound might be a multimer or represent a non-phosphate containing cdN. Mass spec analyses thus far have detected turnover of ATP and GTP, including phosphorylation of HEPES in the buffer solution, however, no novel signal has

been identified. This novel signal could be hidden by the presence of even greater signals in the retention time zone. Thus, we could narrow our search by changing buffer conditions to not include HEPES and analyzing the band in isolation rather than the entire reaction to determine to accentuate the signal of interest. A different approach would be to treat the reaction with a 2'5' phosphomonoesterase to determine whether there is an atypical cyclic peptide bond.

P. fluorescens SRM1 yielded products only in reactions containing ATP as substrates. Treatment of these reaction with CIP led to complete turnover to bands similar to adenosine, with no effect from P1 nuclease treatment. This result indicates that the product of *P. fluorescens* SRM1 is a linear oligonucleotide containing 5' or 3' exposed phosphates or is just a hydrolyzed ADP product of ATP. It is difficult however to discern one from the other on TLC as ADP has similar Rf values to pApA or pAp. When we subjected the reaction products to mass spectrometry analysis, we saw complete turnover of ATP and ADP, however, no novel signals were apparent. Similar to the above analyses, this novel signal could be hidden by the presence of even greater signals in the retention time zone or hard to discern due to the similarity in mass to ADP. For future mass spectrometry studies, we hope to obtain samples of pAp and cAMP and compare those standards and retention time to both ADP and pApA to better discern signals. We also hope to utilize HPLC columns before mass spec analyses to better separate molecular compounds and detect specific signals.

We were interested in studying these systems in their native environments. Thus, we tested to see whether our phage libraries for *E. coli* and *V. cholerae* could infect EDEC and *V. cholerae* 2631-78 expressing strains. EDEC was infectable with T2 and T5 phages, however, ICP phage did not form any plaques upon infection of *V. cholerae* 2631-78. This

result could be because CBASS may be active and prevent phage infection. Thus, we are planning to make a CBASS deletion strain to see if they are vulnerable to ICP phage infection. We will next determine whether T2 and T5 phage vulnerability of EDEC is mediated by EDEC CBASS by making CBASS deletion mutants and investigating whether that mutation changes its vulnerability to T2 and T5 phage infections. A broader approach would be to utilize transposon mutagenesis to identify gene disruptions that would change the plaque phenotype. We are also working on expanding our coli phage library to identify CBASS vulnerable phages. As no ICP phages infected our *V. cholerae* 2631-78 strain, we are working on acquiring other *Vibrio* phages from other laboratories and also isolating environmental *Vibrio* phages from water samples where *V. cholerae* is endemic. We currently do not have any *Pseudomonas* phages, thus are working on acquiring these phages from potential collaborators. In the meantime, we have inserted the SRM1 CBASS operon with its US and DS intergenic regions to preserve native promoter and regulatory sequences into a non-inducible plasmid and cloned these into *E. coli* host to study phage infection with coli phages. However, there has been difficulties in plaque assays as the top agar forms a hazy, uneven layer. This can be mitigated by doing liquid broth phage infection assays, in which we infect liquid cultures of bacteria and track their growth OD_{600} overtime.

Due to the higher potential of EDEC CBASS forming a cyclic nucleotide signaling molecule, we investigated whether this product is the activator of its cognate HNH-SAVED. Incubation of purified EDEC HNH-SAVED with plasmid substrates in vitro led to smearing and appearance of multiple bands on agarose gel indicating the enzyme to be active and an endonuclease. However, the disappearance of such smearing when the nucleotide synthesis reaction is added to the mixture, and the similarities of the band to

the vector only and no nuclease controls indicate the possibility that the signaling nucleotide is actually an inhibitor of HNH-SAVED. If this held true for other HNH-SAVED containing systems, this would make sense of the phenotype seen with our *P. fluorescens* SRM-1 CD-NTase mutant, which had no effect on heterologous host viability. If the inhibiting signal is no longer there, the HNH-SAVED could continue to cause death of the host under high expression. This would not explain the lower viability in the WT SRM1 CBASS expressing cells. There is the possibility that due to overexpression, there might more HNH-SAVED than can be inhibited by signaling nucleotides thus causing death of the cells. It will be important to purify *P. fluorescens* SRM1 HNH-SAVED and perform a similar assay to determine whether nuclease activity is detected without the addition of the nucleotide signaling product.

We would like to note that HNH-SAVED mechanism and regulation was investigated and published in 2019 (88). Similar to our observations, HNH-SAVED target double stranded nucleic acids. Au contraire, they saw that the signaling nucleotides produced by cognate CD-Ntases activated the HNH-SAVED, leading to disappearance of the nucleic acid on electrophoretic gel (88). They identified the nucleotide recognition sites of the SAVED domain, thus we hope to introduce SAVED mutations into EDEC HNH-SAVED and determine whether its nuclease activity is indifferent of the nucleotide signal (88). Given that EDEC CBASS contains two components compared to the four component CBASS systems of SRM1 in our study and *Enterobacter cloacae* and *Acinetobacter baumannii* used in the HNH-SAVED study, HNH-SAVED could have evolved to respond differentially to signaling nucleotides.

Our study confirms that not all CBASS systems are active at least in the conditions we tested, and investigations are limited by the availability of CBASS responsive phages.

However, we can better appreciate the evolution of CBASS in different species with some like EDEC maintaining just two core components, but *P. fluorescens* SRM1 acquiring ancillary domains. Each CD-NTase utilizes and produces signaling molecules different from each other. However, both exhibit abortive infection-like phenotypes further supporting the preservation of CBASS function across phyla but its adaptation to specific microenvironments and nucleotide availabilities. Further investigation is needed to confirm that all HNH-SAVED are activated by their cognate signaling nucleotides and further characterize their regulation in simpler two component CBASS systems.

3.4 Materials and Methods

Strains and Growth Conditions

Escherichia coli DH10b (Invitrogen) was used for cloning, protein expression, transposon library screening and phage plaque assays. *E. coli* BL21(DE3) was used for protein expression and production. EDEC13E and *V. cholerae* 2631-78 were used for phage infection assays.

All strains were grown in 2 mL of Luria-Bertani (LB) broth (0.5 % yeast extract, 1% tryptone, 1% NaCl, pH 7.5) overnight shaking at 210 rpm. EDEC13E and *V. cholerae* 2631-78 were grown at 37˚C and *P. fluorescens* SRM1 was grown at 30˚C. LB agar medium was used with 1.5% agarose. Antibiotic selections were at the following dosages: Ampicillin [100 μg/mL], Kanamycin [100 μg/mL] and Sulfamethoxazole [100 μg/mL].

Generation of site-directed mutations

For DNA base substitutions, we followed the previously established method called SPRINP as described (150). Plasmids harboring our gene(s) of interest were PCR amplified in sets of twos with each containing either a forward or reverse base substituted primer. They were then combined into a single reaction tube and incubated as described. They were then diluted with water on dialysis membranes and electrotransformed into E. coli DH10B cells as described previously. They were then recovered in 500 μL of SOC for

1 – 2 hours and spread on LB selective agar. They were incubated overnight, and positive colonies were PCR amplified and sequenced for the mutagenesis.

Viability Assay

Overnight cultures of DH10b cells harboring different CBASS operons on vectors, were back diluted to OD600 of 0.01 in 3 mL of fresh LB liquid media in large glass tubes. Cultures requiring induction were inoculated with IPTG [100 μg/mL]. Cultures were continuously grown at 37˚C shaking at 210 rpm and measured every two hours until the 8th hour. OD600 was recorded for each sample at their designated time points.

Protein purification

I purified full recombinant *E. coli* EDEC13E and *P. fluorescens* SRM1 CD-NTase via intein-tag purification (IMPACT™ Kit New England Biolabs (NEB) #E6901S). Each gene was cloned into pTXB1, a T7 polymerase promoter containing Amp^{R} vectors at NdeI and SapI restriction sites for C-terminal fusion of intein-CBD tag in *E. coli* DH10b cells.

Overnight cultures were sub-cultured 1:1000 into 1 L of LB liquid media supplemented with Amp (100 μg/mL) and grown to OD600 ~0.500 at 37˚C shaking at 210 rpm. They were then induced with IPTG (100 μg/mL) and grown further shaking at 210 rpm for 4-6 hours at 30˚C or 37˚C depending on the optimal conditions determined for each protein. EDEC and *P. fluorescens* CD-NTase were induced for 4 hrs at 30˚C and EDEC HNH-SAVED was induced for 6 hrs at 37˚C. The cultures were then collected in 300 mL centrifuge bottles and pelleted at 5000 g for 15 min at 4˚C. Cells were harvested in 100 mL of column buffer (20 mM HEPES/Tris-HCl, 500 mM NaCl pH 8.5) and homogenized using Microfluidics M-110P. They were then spun down at 25,000 g for 20

min at 4˚C and the supernatant was loaded on to a chitin column. A chitin resin (NEB™ Cat. # S6651S/L (20 mL/100 mL) column was prepared, and samples were prepared and loaded following manufacturer recommendation. Cleavage buffer consisted of 100 mM DTT in the column buffer used. Loaded columns were incubated at either 4˚C or 23˚C for 40 – 60 hours before elution. A third of the column volume was eluted using column buffer. Eluted proteins were quantified by Quick Start™ Bradford 1x Dye Reagent (BIO-RAD™ Cat. # 5000205) following manufacturer protocol using BSA standards.

Protein samples were concentrated using Amicon® Ultracentrifugal Filters following manufacturer protocol. Utilized Amicon® Ultra-4 Centrifugal Filter Units 30 kDa (Millipore™ Cat. # UFC801024) and 50 kDa (Millipore™ Cat.# UFC805024) and Amicon® Ultra-15 Centrifugal Filter Units 30 kDa (Millipore™ Cat.# UFC903008) and 50 kDa (Millipore™ Cat.# UFC905008).

SDS-PAGE

Each samples was mixed with 4X SDS-PAGE dye (200 mM Tris-HCl pH6.8, 8% SDS, 4.3 M glycerol, 6 mM bromophenol blue) with or without 400 mM DTT to 1X and boiled at 60˚C for 10 min or 95˚C for 5 min. Boiled samples were loaded onto 4–20% Mini-PROTEAN® TGX™ Precast Protein Gels, 10-well, 50 µl (BIO-RAD Cat.# 4561094) and ran for 90 min at 90 V constant or 30 min at constant 200 V. Samples were run in 1X

TG-SDS PAGE running buffer (10X buffer: 0.2501 M Tris base, 1.924 glycine, 0.03467 M SDS).

Protein Gel Coomassie Staining

Protein gels were stained using Coomassie stain (.1% Coomassie Brilliant blue, 50% MeOH, 10% glacial acetic acid (vol/vol), 40% water) overnight shaking at 100 rpm at RT. They were then decanted and de-stained using warm destaining solution (20% MeOH, 10% glacial acetic acid in water) overnight. Destaining solution was refreshed at least once when solution seemed concentrated. Images were captured using mobile device.

***In vitro* Nucleotide Synthesis Reaction**

Purified protein [5 μM] was mixed with $MgCl_2$ [2.5 mM], ATP/GTP/CTP/UTP each at [1.25 mM] in different combinations in column buffer (20 mM HEPES, 500 mM NaCl pH 8.5) in a PCR reaction tube (50 μL total). No enzyme control and no substrate controls were also prepared. They were incubated at 37˚C for 16 hrs before TLC analysis.

***In vitro* Nuclease Reaction**

Nucleotide synthesis reaction mixture was incubated with purified EDEC HNH-SAVED [5-10 μM], $MgCl_2$ [5 mM], nucleic acid substrate (1000 ng total) in 50 μL total. A no nucleotide signal control and no HNH-SAVED controls were supplemented with column buffer for a total of 50 μL. The reaction mixture was incubated at 37˚C for 1 hr then mixed with 6X EZ-Vision® Dye-as-Loading Buffer (VWR® Life Science Cat. #:

97063-166) to 1X. Each sample was run on 1% agarose gel for 45 min at 120 V and visualized using BIO-RAD ChemiDOC XRS+ Imager.

Thin Layer Chromatography

Samples were blotted (10 μL) onto silica gel thin layer chromatography glass plates (250um, THICK, 60A. FLUORES. IND.) (ANALTECH Cat. C09622) with nucleotide standards (1 μL of 10 or 100 mM). The TLC plate was incubated with running solution of n-propanol: ammonium hydroxide:water in 11:7:2 (vol:vol:vol) until the solvent front was about 1 cm from the top. The plate was then dried and visualized under UV light (254 nM). Images were captured using an iPhone 12 Pro Max and prepared using BioRender and Microsoft PowerPoint.

Mass spectrometry

Samples were analyzed using a Waters Acquity UPLC interfaced with a Waters Xevo G2-XS QTof mass spectrometer. 10 uL of sample was injected onto a Waters Acquity BEH-C18 UPLC column (2.1 x 100mm) held at 40°C. Compounds were separated using the following gradient run a 0.3 ml/min: initial conditions were 99% mobile phase A (8 mM dimethylhexylamine and 2.8 mM acetic acid in water) and 1% mobile phase B (methanol), linear ramp from 1% B at start to 40% B at 10 min, return to 1% B at 10.5 min and hold at 1% B until 15 min. Compounds were ionized by electrospray ionization operated in negative ion mode with a capillary voltage of 2.0 kV, cone voltage at 35V, source temperature of 100°C, desolvation temperature of 350°C, cone gas flow of 40 L/hr and desolvation gas flow of 600 L/hr. Data were acquired over the m/z range of 50-1500 using an MS^e method with switching of collision energy (20-80V ramp) on and off

between successive 0.2 second scans. Lockmass calibration was performed using leucine enkephalin as the lockmass compound.

Phage plaque assay

EDEC13E clones were infected with T2, T3, T4, T5, T6, T7, lambda vir, SECphi17, SECphi18 and SECphi27 coli phages. Subsequent infection studies utilized T2 and T5 phages. *V. cholerae* 2631-78 was challenged with ICP1, ICP2, and ICP3 phages.

Overnight cultures of bacteria were subcultured 1:1000 into 10-15 mL of LB and grown to OD600 of 0.02 – 0.08. Grown culture (250 μL) was then transferred into a new test tube and mixed with liquified 15 – 18 mL of MMB agar. The mixed solution was immediately poured into a large agar plate and swirled to cover the entire surface. While the plate solidified, we prepared 10-fold dilutions of each phage to be tested. After solidification of the agar, we added 5 μL of each phage dilution onto the agar surface. The plate was incubated for 18 hours and then observed for plaque formation.

CHAPTER 4:

BROADER IMPACTS AND CONCLUSIONS

Bacteria and phage continuously compete for survival in a wide variety of environments (60, 61, 68, 102). This can be seen by the rise of antimicrobial resistance in the community in response to increased antibiotic usage through communal spreading of advantageous genes (134, 161–163). It is thus crucial that we better understand some of these advantageous genetic elements to better design antimicrobial therapeutics amidst the rise of antibiotic resistance across the world. Antibiotic resistance is far outpacing the production of novel antibiotic therapeutics. Thus, taking advantage of bacterial predators such as phages to treat infections, known as phage therapy, might prove an effective method of bacterial control (164, 165). However, bacteria have several antiphage defense mechanism such as CRISPR-CAS, exonucleases, and CBASS to name a few (23, 31, 88, 89, 139, 160, 166, 167). To aid in the design of effective phage therapies, it is crucial we understand the defense mechanisms that might render them ineffective.

I sought to explore the regulation of cGAMP in the antiphage response of CBASS systems to help develop better antiphage therapeutics that bypasses these defense pathways. Specifically, I explored the role of the ancillary VC0180 and VC0181 proteins on the stability of DncV in vivo and investigated how they interact with a previously uncharacterized gene I named *bumo* in modulating DncV stability. I then broadened our horizons by investigating whether CBASS abortive functions are conserved in three other Gram-negative bacteria and exploring the function of another common effector, the HNH-SAVED nuclease, in abortive infection. I also attempted to identify the nucleotide signaling molecules synthesized by these uncharacterized CD-NTases and determine how they affect HNH-SAVED activity.

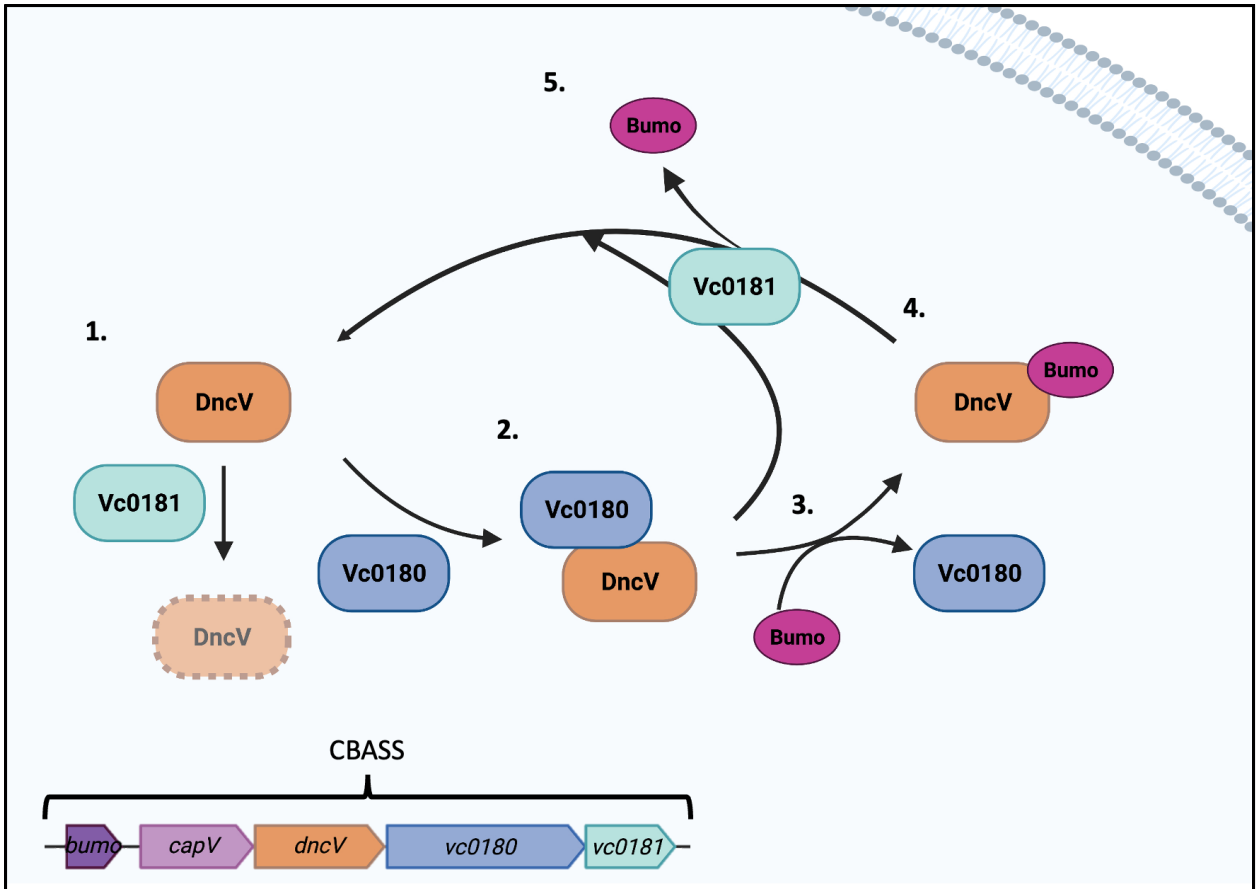

Figure 4. Model of ubiquitin-like regulation of DncV. In my theses, I show that *bumo* is part of the CBASS operon (Lower left). Even though *vc0181* is not transcribed together, it is still playing a role in regulating CBASS. **1.** Chapter 2 of my theses show evidence that DncV is degraded by VC0181 in the absence of Bumo. **2.** Moreover, there is some evidence to suggest DncV and VC0180 form a complex together. However, more work is needed to show they are forming a complex and that VC0180 is activating DncV. **3.** We think that VC0180 activates DncV to mediate the interaction of Bumo and DncV. **4.** However, more work is needed to show interaction. **5.** VC0181 could be deubiquitinating DncV or separate VC0180 from DncV to make it vulnerable to degradation.

In chapter 2 of my theses, we identified a novel component of CBASS operon, a small uncharacterized gene named Bumo for bacterial ubiquitin-like modifier, upstream of CapV. Similar proteins or genes have not been identified before in other CBASS systems. I confirmed that *bumo* is on the same transcript as *capV*, *dncV* and *vc0180* in the CBASS operon. This was further supported by 5' RACE which identified the transcriptional start

site upstream of *bumo*, midway between *vspR* and *bumo*. Contrary to our previous understanding of the CBASS operon in *Vibrio cholerae* El Tor, I discovered that *vc0181* may not be on the same transcript as the rest of the CBASS operon but still play a crucial role in modulating that response. Unlike other deubiquitinase domain encoding enzymes, my data suggest *vc0181* is a DncV-specific protease, as mutation of the active site glutamine (E39A) led to restoration of DncV in vivo. However, the protease does not seem to specifically target the N- or C-terminus of DncV, as fusions of histidine, intein nor a FLAG tag affected the decrease of DncV we observed in the presence of WT VC0181. Moreover, my data suggests that Bumo is somehow inhibiting VC0181 from degrading DncV, as the absence of Bumo leads to a disappearance of DncV. How Bumo inhibits VC0181 remains to be determined. My *in vivo* western blot analyses suggest that DncV and VC0180 form a heterodimer and higher order complexes of these dimers as evidenced by the presence of similar non-monomeric bands when detecting for either protein. However, contrary to my hypothesis that the interaction is happening at the C-terminus, the higher order structures form regardless of whether a tag is fused in the C or N terminus indicating other interactive sites might exist.

In Chapter 3, I explored the role of HNH-SAVED effector containing CBASS systems in other Gram-negative bacteria. We identified both *E. coli* EDEC13E and *P. fluorescens* SRM1 containing active CBASS systems that affected viability of heterologous hosts. However, we are still optimizing conditions to identify the exact molecules they form. EDEC CD-NTase synthesizes two products on TLC analyses, one, an ATP produced compound susceptible to phosphatase CIP and a second product produced from ATP and GTP indifferent to CIP and 3'-phosphomonoesterase, indicating a possible cyclic molecule with non 3'5'-phosphopeptide bond. *P. fluorescens* SRM1 HNH-SAVED is the

main cause of the lower cell viability in heterologous host as H56A H91A mutations restored EV-like growth, but a CD-NTase mutation had no effect. The EDEC HNH-SAVED nuclease was active in vitro in the absence of the signaling nucleotide, which instead inhibited nuclease activity as seen on agarose gel electrophoresis. My data suggests, contrary to four component CBASS systems, the simpler two component EDEC CBASS system might regulate its effector differently.

HNH-SAVED nucleases have been shown to be activated by cyclic tri-AMP in the *Enterobacter cloacae* CBASS system. Similar to our observations, HNH-SAVED targeted cleavage of double stranded nucleic acids (88). However, in our in vitro analysis of EDEC HNH-SAVED, we saw the loss of activity with the addition of nucleotide signal. They identified the nucleotide recognition sites of the SAVED domain, and thus we hope to introduce SAVED mutations that would disrupt signal binding into EDEC HNH-SAVED and determine whether it is active and unaffected by the addition of the signaling nucleotide. Given that EDEC CBASS encodes two components compared to the four component CBASS systems of SRM1 in our study and *Enterobacter cloacae* and *Acinetobacter baumannii* used in previous study, HNH-SAVED could response differentially to signaling nucleotides (87–89). Thus, we would made mutants *P. fluorescens* SRM1 HNH-SAVED and hope to determine whether its activity is affected by the addition of a nucleotide signal.

My PhD thesis thus far adds further complexity to the regulation of DncV in the CBASS response. What we once thought was only a VC0180 and VC0181 regulated system, I discovered a third component, Bumo, that inhibits VC0181 from degrading DncV. Even though *bumo*-like genes have not been identified in extensive analyses of CBASS operons across species, we are encouraged by the fact that all studies that show functional CBASS

systems included large US and DS intergenic regions of CBASS in their expression constructs, and such constructs containing the *V. cholerae* El Tor CBASS included bumo (89). However, the presence of Bumo is not enough to protect DncV from degradation from VC0181 as genetic deletion of VC0180 leads to the absence of DncV. This suggests VC0180 is important in either stabilizing DncV or mediating Bumo's inhibition of VC0181. My evidence suggests that VC0180 and VC0181 are interdependent as they are not detected *in vivo* in the absence of each other. Interestingly, although *dncV* is detectable with Δ*vc0181*, it is no longer detectable when both *vc0180 and vc0181* are deleted. Thus, the loss of DncV in the Δ*vc0180* mutant is not suppressed by the deletion of *vc0181,* suggesting they are functioning as two separate regulatory mechanisms. An important question is how does VC0181 and Bumo work in conjunction with VC0180 to stabilize and regulate DncV activity. To better decipher these regulatory networks, we would be better investigating these as two separate regulatory networks.

Even though we have evidence suggesting DncV and VC0180 form heteromers, additional studies are needed to confirm they do indeed form heterodimers and higher order complexes. This could be achieved by performing co-immunoprecipitation of either DncV or VC0180 and analyzing their bound substrates via mass spectrometry. These multimers can be separated by size and charge using HPLC then quantifying the mass of each individual signal using mass spectrometry to identify the protein substrate. To determine whether VC0180 affects DncV activity, we would quantify the synthesis of cGAMP in vivo in both WT and VC0180 KO mutants. Another approach would be to study

DncV and VC0180 in vivo in a heterologous host without CBASS. This would insulate them from the regulatory effects of Bumo and VC0181.

To better study the regulation of Bumo and VC0181, we could introduce them along with DncV into a heterologous system not containing CBASS to avoid the effects of VC0180 and repeat Western blot analyses to determine how the presence of Bumo affects DncV stability. My data suggests Bumo inhibits VC0181 via an unknown mechanism. One possibility is that Bumo binds to VC0181. However, my western blot analyses do not show evidence that Bumo binds to VC0181 directly. Their interaction might be limited due to the inclusion of c-terminal tags. This could be mitigated by utilizing the N-terminal tagged VC0181 for studies or utilizing a Bumo or VC0181 specific antibody. We did try to generate a Bumo specific antibody; however, the resulting sera bound nonspecifically with the presence of bands in both WT and Δ*bumo* strains. We sent column purified elution of VC0181 for proteomic analysis, which did not detect any Bumo. Proteomic analysis of DncV elution was inconclusive as DncV was not the major product detected, and many other products were also detected. This is not surprising because *V. cholerae* purified DncV has many bands with smears on SDS-PAGE gel further suggesting degraded DncV. We plan to confirm VC0181 specificity for DncV by incubating purified VC0181 with different protein substrates in vitro and observing degradation on SDS-PAGE gels. Another possibility is that Bumo protects DncV from VC0181 proteolysis via direct binding, as SUMO does for mammalian cGAS. This could be tested by observing whether DncV forms a heavier MW band in vivo when Bumo is present in a heterologous host lacking CBASS and VC0181. To address the possibility that VC0180 might be mediating their interaction, the interaction of DncV and Bumo will be investigated also in the presence of VC0180. Since JAMM-like deubiquitinases depend on Zn^{2+} for activity, we

are interested in determining whether this holds true by assessing VC0181 protease activity in vitro with zinc supplementation.

CBASS' function as an abortive infection system is thought to be conserved throughout all CBASS containing systems (31, 100). This has been illustrated many times for CBASS systems from *E. coli, V. cholerae, E. cloacae* and *P. aeruginosa* among many others. Moreover, the function of ancillary domain HORMA/TRIP13 is conserved between *E. coli* and *P. aeruginosa* CBASS in which HORMA activates Cdn synthesis by binding to the CD-NTase and TRIP13 dissociates the two (107). Thus, it is plausible that the function of VC0180, E1/E2-like enzyme, and VC0181, deubiquitinase-like enzyme is conserved in other systems. As mentioned previously they have not identified a small ubiquitin like modifier encoded nearby. Our transposon mutagenesis and 5'RACE led us to explore Bumo as a potential small ubiquitin-like modifier. It is important to establish whether other *bumo*-like small open reading frames (ORF) exist within intergenic regions of other four component CBASS systems with ubiquitin-like ancillary domains. Working with collaborators who are experts in bioinformatic analysis, we hope to determine whether *bumo*-like ORFs exist in other CBASS and will be crucial to establish if it is a conserved feature of four component CBASS systems with ubiquitin like ancillary domains. Preliminary analysis of *P. fluorescens* SRM1 CBASS intergenic region show multiple contenders, but none have sequence similarity to El Tor *bumo*. Moreover, similar to VC0180 and VC0181, the C-terminus of *P. fluorescens* E1/E2-like gene overlaps with the first few amino acids of the deubiquitinase-like domain encoding gene out of frame, indicating a high chance those two ancillary domains function differentially similar to that of El Tor. It would be important to verify the functions of VC0180-like and VC0181-like enzymes of *P. fluorescens* using similar experiments to that used for El Tor to

demonstrate their functions and regulation of CD-NTase is conserved across bacterial species.

Our work not only raises new questions to explore in studying CBASS, but also establishes a standard screening method for active CD-NTases using silica gel thin layer chromatography. The majority of CBASS studies utilized radiolabeled nucleotide triphosphates to determine protein activity and identify cyclic/oligonucleotide products on TLC. Though that technique remains much more sensitive than silica gel TLC, it is more time consuming and labor intensive. Silica gel TLC is comparably safer with faster results demonstrating nucleotide turnover. Thus, using purified CD-NTase we can quickly screen for NTP substrate specificity and identify potential products using standards. This technique is limited to a screening tool as some molecules such as c-di-UMP, pApA and ADP appear similarly on silica gel TLC and thus require further analysis to identify the exact molecular make-up of the compound.

We were the first to study the function of CBASS under its native host condition. Though we were not able to demonstrate CBASS responsive phage infection in *Vibrio cholerae* El Tor, we investigated the nature of DncV stability and its regulation under its native host environment. Other studies clone CBASS systems into heterologous hosts with the advantage of there being established phage libraries and isolation of these systems from other modifiers in the host. Our studies in the *V. cholerae* El Tor's natural genomic context add confidence to our findings that VC0181 is a DncV specific protease and allowed for the discovery of *bumo*, a previously uncharacterized part of CBASS. Our data

also add novel understanding that VC0181 might not be on the same operon as the rest of CBASS but still crucial in regulating the response.

Overall, my work greatly advances our understanding of DncV regulation. I have identified *bumo* as a missing piece of the ubiquitin-like CBASS system. I demonstrate that VC0181 is a DncV protease and not just an endopeptidase as its deubiquitinating domain suggests and illustrate Bumo inhibits VC0181 proteolysis of DncV via an unknown mechanism. I also demonstrate that VC0180 and VC0181 differentially regulate DncV, with VC0181 working with Bumo to regulate proteolysis of DncV and VC0180 forming multimers with DncV with yet to be defined effects, contrary to traditional ubiquitin-like systems in which E1/E2 like and DUB-like enzymes would be expected to oppose each other's functions on the same target. DncV is inhibited by folate-like molecules binding to a protein cleft on the opposite side of the active site; however, we establish DncV regulation is more complex with two more degrees of control: 1) Bumo and VC0181 control DncV levels via proteolysis, and 2) VC0180 binds to DncV to potentially affect its activity. Our findings would help better understand how to exploit these defense networks for antibacterial activity and design more effective phage-carrier genetic therapies that bypasses these defense networks to establish clinically significant effects on human

REFERENCES

1. Clemens JD, Nair GB, Ahmed T, Qadri F, Holmgren J. 2017. Cholera. Lancet 390:1539–1549.

2. Ali M, Nelson AR, Lopez AL, Sack DA. 2015. Updated global burden of cholera in endemic countries. PLoS Negl Trop Dis 9:1–13.

3. Ganesan D, Gupta S Sen, Legros D. 2020. Cholera surveillance and estimation of burden of cholera. Vaccine 38:A13–A17.

4. Pérez-Reytor D, Jaña V, Pavez L, Navarrete P, García K. 2018. Accessory toxins of vibriopathogens and their role in epithelial disruption during infection. Front Microbiol 9:1–11.

5. Herrington DA, Hall RH, Losonsky G, Mekalanos JJ, Taylor RK, Levine MM. 1988. Toxin, toxin-coregulated pili, and the toxR regulon are essential for Vibrio Cholerae pathogenesis in humans. J Exp Med 168:1487–1492.

6. Crawford JA, Krukonis ES, DiRita VJ. 2003. Membrane localization of the ToxR winged-helix domain is required for TcpP-mediated virulence gene activation in Vibrio cholerae. Mol Microbiol 47:1459–1473.

7. Miller VL, Taylor RK, Mekalanos JJ. 1987. Cholera toxin transcriptional activator ToxR is a transmembrane DNA binding protein. Cell 48:271–279.

8. Gill DM, Meren R. 1978. ADP-ribosylation of membrane proteins catalyzed by cholera toxin: basis of the activation of adenylate cyclase. Proc Natl Acad Sci U S A 75:3050–3054.

9. Mekalanos JJ, Swartz DJ, Pearson GDN, Harford N, Groyne F, De Wilde M. 1983. Cholera toxin genes: Nucleotide sequence, deletion analysis and vaccine development. Nature 306:551–557.

10. Miller VL, Mekalanos JJ. 1984. Synthesis of cholera toxin is positively regulated at the transcriptional level by toxR. Proc Natl Acad Sci U S A 81:3471–3475.

11. E. GS, N. BK, H. KB, C. BR, Jackson SM. 1994. Cystic Fibrosis Heterozygote Resistance to Cholera Toxin in the Cystic Fibrosis Mouse Model. Science (80-) 266:107–109.

12. Field M, Fromm D, al-Awqati Q, Greenough WB. 1972. Effect of cholera enterotoxin on ion transport across isolated ileal mucosa. J Clin Invest 51:796–

804.

13. Keusch GT, Jacewicz M. 1977. Pathogenesis of shigella diarrhea: VII. Evidence for a cell membrane toxin receptor involving β1 → 4-linked N-Acetyl-D-glucosamine oligomers*. J Exp Med 146:535–546.

14. Fry SK. 1992. Cholera Prevention and Control : Water Supply , Sanitation 2030:2–4.

15. Krukonis ES, DiRita VJ. 2003. From motility to virulence: Sensing and responding to environmental signals in Vibrio cholerae. Curr Opin Microbiol 6:186–190.

16. Faruque SM, Biswas K, Nashir Udden SM, Ahmad QS, Sack DA, Balakrish Nair G. 2006. Transmissibility of cholera: In vivo-formed biofilms and their relationship to infectivity and persistence in the environment. Proc Natl Acad Sci U S A 103:6350–6355.

17. Boin MA, Austin MJ, Häse CC. 2004. Chemotaxis in Vibrio cholerae. FEMS Microbiol Lett 239:1–8.

18. O'Hara BJ, Barth ZK, McKitterick AC, Seed KD. 2017. A highly specific phage defense system is a conserved feature of the Vibrio cholerae mobilome. PLoS Genet 13:1–17.

19. Meibom KL, Blokesch M, Dolganov NA, Wu CY, Schoolnik GK. 2005. Microbiology: Chitin induces natural competence in vibrio cholerae. Science (80-) 310:1824–1827.

20. Yadav M, Pal K, Sen U. 2019. Structures of c-di-GMP/cGAMP degrading phosphodiesterase VcEAL: Identification of a novel conformational switch and its implication. Biochem J 476:3333–3353.

21. Escudero JA, Mazel D. 2017. Genomic Plasticity of Vibrio cholerae. Int Microbiol 20:138–148.

22. Azman AS, Rudolph KE, Cummings DAT, Lessler J, Tor E. 2014. The incubation period of cholera: A systematic review supplement. J Infect 66:432–438.

23. Yen M, Camilli A. 2017. Mechanisms of the evolutionary arms race between Vibrio cholerae and Vibriophage clinical isolates. Int Microbiol 20:116–120.

24. Waters CM, Lu W, Rabinowitz JD, Bassler BL. 2008. Quorum sensing controls

biofilm formation in Vibrio cholerae through modulation of cyclic Di-GMP levels and repression of vpsT. J Bacteriol 190:2527–2536.

25. Alam M, Kasan NA, Sadique A, Bhuiyan NA, Ahmed KU, Nusrin S, Nair GB, Siddique AK, Sack RB, Sack DA, Huq A, Colwell RR. 2006. Seasonal cholera caused by Vibrio cholerae serogroups O1 and O139 in the coastal aquatic environment of Bangladesh. Appl Environ Microbiol 72:4096–4104.

26. Grim CJ, Choi J, Chun J, Jeon YS, Taviani E, Hasan NA, Haley B, Huq A, Colwell RR. 2010. Occurrence of the vibrio cholerae seventh pandemic VSP-I island and a new variant. Omi A J Integr Biol 14:1–7.

27. Ring J. 1804. Mr. Ring, on Diarrhœa and Cholera Morbus. Med Phys J 12:102–108.

28. Anderson WS. 1819. An Account of Cholera Morbus Epidemic in India, in 1817 and 1818. Edinburgh Med Surg J 15:354–372.

29. J S. 1856. Cholera and the Water Supply in the South Districts of London in 1854. J public Heal Sanit Rev 2:239–257.

30. Davies BW, Bogard RW, Young TS, Mekalanos JJ. 2012. Coordinated regulation of accessory genetic elements produces cyclic di-nucleotides for *V. cholerae* virulence. Cell 149:358–370.

31. Millman A, Melamed S, Amitai G, Sorek R. 2020. Diversity and classification of cyclic-oligonucleotide-based anti-phage signalling systems. Nat Microbiol 1–8.

32. Severin GB, Hsueh BY, Elg CA, Dover JA, Rhoades CR, Wessel AJ, Ridenhour BJ, Top EM, Ravi J, Parent KN, Waters CM. 2021. A Broadly Conserved Deoxycytidine Deaminase Protects Bacteria from Phage Infection. bioRxiv 2021.03.31.437871.

33. Cohn M. 1964. Non-inducible mutants of the regulator gene in the “lactose” system of Escherichia coli. J Mol Biol 8:582–592.

34. Wilson CJ, Zhan H, Swint-Kruse L, Matthews KS. 2007. The lactose repressor system: Paradigms for regulation, allosteric behavior and protein folding. Cell Mol Life Sci 64:3–16.

35. Laub MT, Goulian M. 2007. Specificity in two-component signal transduction pathways. Annu Rev Genet 41:121–145.

36. Persat A, Inclan YF, Engel JN, Stone HA, Gitai Z. 2015. Type IV pili mechanochemically regulate virulence factors in Pseudomonas aeruginosa. Proc Natl Acad Sci U S A 112:7563–7568.

37. Berg HC. 2017. The flagellar motor adapts, optimizing bacterial behavior. Protein Sci 26:1249–1251.

38. Hengge R, Gründling A, Jenal U, Ryan R, Yildiz F. 2016. Bacterial signal transduction by cyclic di-GMP and other nucleotide second messengers. J Bacteriol 198:15–26.

39. Rickenberg H V. 1974. Cyclic AMP in prokaryotes. Annu Rev Microbiol 28:353–369.

40. MAKMAN RS, SUTHERLAND EW. 1965. Adenosine 3',5'-Phosphate in Escherichia Coli. J Biol Chem 240:1309–1314.

41. Petersen S, Young GM. 2002. Essential role for cyclic AMP and its receptor protein in Yersinia enterocolitica virulence. Infect Immun 70:3665–3672.

42. Fong JCN, Yildiz FH. 2008. Interplay between cyclic AMP-cyclic AMP receptor protein and cyclic di-GMP signaling in vibrio cholerae biofilm formation. J Bacteriol 190:6646–6659.

43. D'Ari R, Jaffé A, Bouloc P, Robin A. 1988. Cyclic AMP and cell division in Escherichia coli. J Bacteriol 170:65–70.

44. Haseltine WA, Block R. 1973. Synthesis of guanosine tetra and pentaphosphate requires the presence of a codon specific, uncharged transfer ribonucleic acid in the acceptor site of ribosomes. Proc Natl Acad Sci U S A 70:1564–1568.

45. Cashel M, Gallant J. 1969. Two compounds implicated in the function of RC gene. Nature 221:838–841.

46. Römling U, Galperin MY. 2017. Discovery of the second messenger cyclic di-GMP. Methods Mol Biol 1657:1–8.

47. Ross P, Weinhouse H, Aloni Y, Michaeli D, Weinberger-Ohana P, Mayer R, Braun S, De Vroom E, Van Der Marel GA, Van Boom JH, Benziman M. 1987. Regulation of cellulose synthesis in Acetobacter xylinum by cyclic diguanylic acid. Nature 325:279–281.

48. Romling U, Galperin MY, Gomelsky M. 2013. Cyclic di-GMP: the First 25 Years of

a Universal Bacterial Second Messenger. Microbiol Mol Biol Rev 77:1–52.

49. Ryjenkov DA, Tarutina M, Moskvin O V., Gomelsky M. 2005. Cyclic diguanylate is a ubiquitous signaling molecule in bacteria: Insights into biochemistry of the GGDEF protein domain. J Bacteriol 187:1792–1798.

50. Chan C, Paul R, Samoray D, Amiot NC, Giese B, Jenal U, Schirmer T. 2004. Structural basis of activity and allosteric control of diguanylate cyclase. Proc Natl Acad Sci U S A 101:17084–17089.

51. Ausmees N, Mayer R, Weinhouse H, Volman G, Amikam D, Benziman M, Lindberg M. 2001. Genetic data indicate that proteins containing the GGDEF domain possess diguanylate cyclase activity. FEMS Microbiol Lett 204:163–167.

52. Hecht GB, Newton A. 1995. Identification of a novel response regulator required for the swarmer-to- stalked-cell transition in Caulobacter crescentus. J Bacteriol 177:6223–6229.

53. Schmidt AJ, Ryjenkov DA, Gomelsky M. 2005. The ubiquitous protein domain EAL is a cyclic diguanylate-specific phosphodiesterase: Enzymatically active and inactive EAL domains. J Bacteriol 187:4774–4781.

54. Christen M, Christen B, Folcher M, Schauerte A, Jenal U. 2005. Identification and characterization of a cyclic di-GMP-specific phosphodiesterase and its allosteric control by GTP. J Biol Chem 280:30829–30837.

55. Ryan RP, Fouhy Y, Lucey JF, Crossman LC, Spiro S, He Y-W, Zhang L-H, Heeb S, Cámara M, Williams P, Dow JM. 2006. Cell-cell signaling in Xanthomonas campestris involves an HD-GYP domain protein that functions in cyclic di-GMP turnover. Proc Natl Acad Sci U S A2006/04/12. 103:6712–6717.

56. Galperin MY. 2004. Bacterial signal transduction network in a genomic perspective. Environ Microbiol 6:552–67.

57. Simm R, Morr M, Kader A, Nimtz M, Römling U. 2004. GGDEF and EAL domains inversely regulate cyclic di-GMP levels and transition from sessibility to motility. Mol Microbiol 53:1123–1134.

58. Tischler AD, Camilli A. 2004. Cyclic diguanylate (c-di-GMP) regulates Vibrio cholerae biofilm formation. Mol Microbiol 53:857–869.

59. Tuckerman JR, Gonzalez G, Sousa EHS, Wan X, Saito JA, Alam M, Gilles-Gonzalez MA. 2009. An oxygen-sensing diguanylate cyclase and phosphodiesterase couple for c-di-GMP control. Biochemistry 48:9764–9774.

60. Sobe RC, Bond WG, Wotanis CK, Zayner JP, Burriss MA, Fernandez N, Bruger EL, Waters CM, Neufeld HS, Karatan E. 2017. Spermine inhibits Vibrio cholerae biofilm formation through the NspS–MbaA polyamine signaling system. J Biol Chem 292:17025–17036.

61. Koestler BJ, Waters CM. 2014. Bile acids and bicarbonate inversely regulate intracellular cyclic di-GMP in vibrio cholerae. Infect Immun 82:3002–3014.

62. Hufnagel DA, DePas WH, Chapmana MR. 2014. The disulfide bonding system suppresses CsgD-Independent cellulose production in Escherichia coli. J Bacteriol 196:3690–3699.

63. Hsieh M, Hinton DM, Waters CM. 2020. Cyclic di-GMP Regulation of Gene Expression 379–394.

64. Hobley L, Fung RKY, Lambert C, Harris MATS, Dabhi JM, King SS, Basford SM, Uchida K, Till R, Ahmad R, Aizawa SI, Gomelsky M, Sockett RE. 2012. Discrete cyclic di-GMP-dependent control of bacterial predation versus axenic growth in Bdellovibrio bacteriovorus. PLoS Pathog 8.

65. Tischler AD, Camilli A. 2005. Cyclic diguanylate regulates Vibrio cholerae virulence gene expression. Infect Immun 73:5873–5882.

66. Tschowri N, Schumacher MA, Schlimpert S, Chinnam NB, Findlay KC, Brennan RG, Buttner MJ. 2014. Tetrameric c-di-GMP mediates effective transcription factor dimerization to control streptomyces development. Cell 158:1136–1147.

67. Fernandez NL, Srivastava D, Ngouajio AL, Waters CM. 2018. Cyclic di-GMP Positively Regulates DNA Repair in Vibrio cholerae. J Bacteriol 200:1–13.

68. Fernandez NL, Hsueh BY, Nhu NTQ, Franklin JL, Dufour YS, Waters CM. 2020. Vibrio cholerae adapts to sessile and motile lifestyles by cyclic di-GMP regulation of cell shape. Proc Natl Acad Sci U S A 117:29046–29054.

69. Chen Z, Schaap P. 2012. Dictyostelium uses the prokaryote messenger c-di-GMP to trigger stalk cell differentiation. Nature 488:680–683.

70. Witte G, Hartung S, Büttner K, Hopfner KP. 2008. Structural Biochemistry of a Bacterial Checkpoint Protein Reveals Diadenylate Cyclase Activity Regulated by DNA Recombination Intermediates. Mol Cell 30:167–178.

71. Stülke J, Krüger L. 2020. Cyclic di-AMP Signaling in Bacteria. Annu Rev Microbiol 74:159–179.

72. He J, Yin W, Galperin MY, Chou SH. 2020. Cyclic di-AMP, a second messenger of primary importance: Tertiary structures and binding mechanisms. Nucleic Acids Res 48:2807–2829.

73. Corrigan RM, Gründling A. 2013. Cyclic di-AMP: Another second messenger enters the fray. Nat Rev Microbiol 11:513–524.

74. Woodward JJ, Iavarone AT, Portnoy DA. 2010. c-di-AMP secreted by intracellular Listeria monocytogenes activates a host type I interferon response. Science 328:1703–5.

75. Luo Y, Helmann JD. 2012. Analysis of the role of Bacillus subtilis σ(M) in β-lactam resistance reveals an essential role for c-di-AMP in peptidoglycan homeostasis. Mol Microbiol 83:623–39.

76. Gundlach J, Herzberg C, Kaever V, Gunka K, Hoffmann T, Weiß M, Gibhardt J, Thürmer A, Hertel D, Daniel R, Bremer E, Commichau FM, Stülke J. 2017. Control of potassium homeostasis is an essential function of the second messenger cyclic di-AMP in Bacillus subtilis. Sci Signal 10:1–10.

77. Pham HT, Nhiep NTH, Vu TNM, Huynh TAN, Zhu Y, Huynh ALD, Chakrabortti A, Marcellin E, Lo R, Howard CB, Bansal N, Woodward JJ, Liang ZX, Turner MS. 2018. Enhanced uptake of potassium or glycine betaine or export of cyclic-di-AMP restores osmoresistance in a high cyclic-di-AMP Lactococcus lactis mutant. PLoS Genet 14:1–23.

78. Zarrella TM, Metzger DW, Bai G. 2018. Stress suppressor screening leads to detection of regulation of cyclic di-AMP homeostasis by a Trk family effector protein in Streptococcus pneumoniae. J Bacteriol 200:1–15.

79. Schuster CF, Bellows LE, Tosi T, Campeotto I, Corrigan RM, Freemont P, Gründling A. 2016. The second messenger c-di-AMP inhibits the osmolyte uptake system OpuC in Staphylococcus aureus. Sci Signal 9:1–31.

80. Zeden MS, Schuster CF, Bowman L, Zhong Q, Williams HD, Gründling A. 2018. Cyclic di-adenosine monophosphate (c-di-AMP) is required for osmotic regulation in Staphylococcus aureus but dispensable for viability in anaerobic conditions. J Biol Chem 293:3180–3200.

81. Hu D, Liu B, Feng L, Ding P, Guo X, Wang M, Cao B, Reeves PR, Wang L. 2016. Origins of the current seventh cholera pandemic. Proc Natl Acad Sci U S A 113:E7730–E7739.

82. Severin GB, Ramliden MS, Hawver LA, Wang K, Pell ME, Kieninger AK,

Khataokar A, O'Hara BJ, Behrmann L V., Neiditch MB, Benning C, Waters CM, Ng WL. 2018. Direct activation of a phospholipase by cyclic GMP-AMP in El Tor Vibrio cholerae. Proc Natl Acad Sci U S A 115:E6048–E6055.

83. Li F, Cimdins A, Rohde M, Jänsch L, Kaever V, Nimtz M, Römling U. 2019. DncV synthesizes cyclic GMP-AMP and regulates biofilm formation and motility in Escherichia coli ECOR31. MBio 10:1–21.

84. Kranzusch PJ, Wilson SC, Lee ASY, Berger JM, Doudna JA, Vance RE. 2015. Ancient Origin of cGAS-STING Reveals Mechanism of Universal 2',3' cGAMP Signaling. Mol Cell 59:891–903.

85. Burroughs AM, Zhang D, Schäffer DE, Iyer LM, Aravind L. 2015. Comparative genomic analyses reveal a vast, novel network of nucleotide-centric systems in biological conflicts, immunity and signaling. Nucleic Acids Res 43:10633–10654.

86. Whiteley AT, Eaglesham JB, de Oliveira Mann CC, Morehouse BR, Lowey B, Nieminen EA, Danilchanka O, King DS, Lee ASY, Mekalanos JJ, Kranzusch PJ. 2019. Bacterial cGAS-like enzymes synthesize diverse nucleotide signals. Nature 567:194–199.

87. Lau R, Ye Q, Patel L, Berg K, Mathews I, Watrous J, Whiteley A, Lowey B, Mekalanos J, Kranzusch P, Jain M, Corbett K. 2019. Structure and mechanism of a cyclic trinucleotide-activated bacterial endonuclease mediating bacteriophage immunity. Mol Cell 694703.

88. Lowey B, Whiteley AT, Keszei AFA, Morehouse BR, Mathews IT, Antine SP, Cabrera VJ, Kashin D, Niemann P, Jain M, Schwede F, Mekalanos JJ, Shao S, Lee ASY, Kranzusch PJ. 2020. CBASS Immunity Uses CARF-Related Effectors to Sense 3′–5′- and 2′–5′-Linked Cyclic Oligonucleotide Signals and Protect Bacteria from Phage Infection. Cell 182:38-49.e17.

89. Cohen D, Melamed S, Millman A, Shulman G, Oppenheimer-Shaanan Y, Kacen A, Doron S, Amitai G, Sorek R. 2019. Cyclic GMP–AMP signalling protects bacteria against viral infection. Nature 574:691–695.

90. Gao J, Tao J, Liang W, Zhao M, Du X, Cui S, Duan H, Kan B, Su X, Jiang Z. 2015. Identification and characterization of phosphodiesterases that specifically degrade 3'3'-cyclic GMP-AMP. Cell Res 25:539–550.

91. Wright TA, Jiang L, Park JJ, Anderson WA, Chen G, Hallberg ZF, Nan B, Hammond MC. 2020. Second messengers and divergent HD-GYP phosphodiesterases regulate 3′,3′-cGAMP signaling. Mol Microbiol 113:222–236.

92. Hallberg ZF, Wang XC, Wright TA, Nan B, Ad O, Yeo J, Hammond MC. 2016. Hybrid promiscuous (Hypr) GGDEF enzymes produce cyclic AMP-GMP (3', 3'-cGAMP). Proc Natl Acad Sci U S A 113:1790–1795.

93. Kellenberger CA, Wilson SC, Hickey SF, Gonzalez TL, Su Y, Hallberg ZF, Brewer TF, Iavarone AT, Carlson HK, Hsieh YF, Hammond MC. 2015. GEMM-I riboswitches from Geobacter sense the bacterial second messenger cyclic AMP-GMP. Proc Natl Acad Sci U S A 112:5383–5388.

94. Hallberg ZF, Chan CH, Wright TA, Kranzusch PJ, Doxzen KW, Park JJ, Bond DR, Hammond MC. 2019. Structure and mechanism of a hypr GGDEF enzyme that activates cGAMP signaling to control extracellular metal respiration. Elife 8:1–36.

95. Zhu D, Wang L, Shang G, Liu X, Zhu J, Lu D, Wang L, Kan B, Zhang J ren, Xiang Y. 2014. Structural Biochemistry of a Vibrio cholerae Dinucleotide Cyclase Reveals Cyclase Activity Regulation by Folates. Mol Cell 55:931–937.

96. Sun L, Wu J, Du F, Chen X, Chen ZJ. 2013. Cyclic GMP-AMP synthase is a cytosolic DNA sensor that activates the type I interferon pathway. Science 339:786–91.

97. Li X, Shu C, Yi G, Chaton CT, Shelton CL, Diao J, Zuo X, Kao CC, Herr AB, Li P. 2013. Cyclic GMP-AMP Synthase Is Activated by Double-Stranded DNA-Induced Oligomerization. Immunity 39:1019–1031.

98. Liu H, Moura-Alves P, Pei G, Mollenkopf H, Hurwitz R, Wu X, Wang F, Liu S, Ma M, Fei Y, Zhu C, Koehler A, Oberbeck-Mueller D, Hahnke K, Klemm M, Guhlich-Bornhof U, Ge B, Tuukkanen A, Kolbe M, Dorhoi A, Kaufmann SH. 2019. cGAS facilitates sensing of extracellular cyclic dinucleotides to activate innate immunity . EMBO Rep 20.

99. McFarland AP, Luo S, Ahmed-Qadri F, Zuck M, Thayer EF, Goo YA, Hybiske K, Tong L, Woodward JJ. 2017. Sensing of Bacterial Cyclic Dinucleotides by the Oxidoreductase RECON Promotes NF-κB Activation and Shapes a Proinflammatory Antibacterial State. Immunity 46:433–445.

100. Kranzusch PJ. 2019. cGAS and CD-NTase enzymes: structure, mechanism, and evolution. Curr Opin Struct Biol. Elsevier Ltd.

101. Kato K, Omura H, Ishitani R, Nureki O. 2017. Cyclic GMP-AMP as an endogenous second messenger in innate immune signaling by cytosolic DNA. Annu Rev Biochem 86:541–566.

102. Faruque SM, Mekalanos JJ. 2012. Phage-bacterial interactions in the evolution of

toxigenic Vibrio cholerae. Virulence 3:556–565.

103. Wang Z, Lazinski DW, Camilli A. 2017. Immunity provided by an outer membrane vesicle cholera vaccine is due to O-antigenspecific antibodies inhibiting bacterial motility. Infect Immun 85:1–9.

104. Reyes-Robles T, Dillard RS, Cairns LS, Silva-Valenzuela CA, Housman M, Ali A, Wright ER, Camilli A. 2018. Vibrio cholerae outer membrane vesicles inhibit bacteriophage infection. J Bacteriol 200.

105. Hays SG, Seed KD. 2019. Dominant Vibrio cholerae phage exhibits lysis inhibition sensitive to disruption by a defensive phage satellite. bioRxiv 1–24.

106. Koonin E V., Makarova KS, Zhang F. 2017. Diversity, classification and evolution of CRISPR-Cas systems. Curr Opin Microbiol 37:67–78.

107. Ye Q, Lau RK, Mathews IT, Birkholz EA, Watrous JD, Azimi CS, Pogliano J, Jain M, Corbett KD. 2020. HORMA Domain Proteins and a Trip13-like ATPase Regulate Bacterial cGAS-like Enzymes to Mediate Bacteriophage Immunity. Mol Cell 77:709-722.e7.

108. Hu MM, Yang Q, Xie XQ, Liao CY, Lin H, Liu TT, Yin L, Shu HB. 2016. Sumoylation Promotes the Stability of the DNA Sensor cGAS and the Adaptor STING to Regulate the Kinetics of Response to DNA Virus. Immunity 45:555–569.

109. Vierstra RD. 2012. The expanding universe of ubiquitin and ubiquitin-like modifiers. Plant Physiol. American Society of Plant Biologists.

110. Song L, Luo ZQ. 2019. Post-translational regulation of ubiquitin signaling. J Cell Biol 218:1776–1786.

111. Lee I, Schindelin H. 2008. Structural Insights into E1-Catalyzed Ubiquitin Activation and Transfer to Conjugating Enzymes. Cell 134:268–278.

112. Noda NN, Satoo K, Fujioka Y, Kumeta H, Ogura K, Nakatogawa H, Ohsumi Y, Inagaki F. 2011. Structural basis of Atg8 activation by a homodimeric E1, Atg7. Mol Cell 44:462–475.

113. Stewart MD, Ritterhoff T, Klevit RE, Brzovic PS. 2016. E2 enzymes: More than just middle men. Cell Res 26:423–440.

114. Hennell James R, Caceres EF, Escasinas A, Alhasan H, Howard JA, Deery MJ, Ettema TJG, Robinson NP. 2017. Functional reconstruction of a eukaryotic-like

E1/E2/(RING) E3 ubiquitylation cascade from an uncultured archaeon. Nat Commun 8.

115. Mevissen TET, Komander D. 2017. Mechanisms of deubiquitinase specificity and regulation. Annu Rev Biochem 86:159–192.

116. Lake MW, Wuebbens MM, Rajagopalan K V., Schindelin H. 2001. Mechanism of ubiquitin activation revealed by the structure of a bacterial MoeB-MoaD complex. Nature 414:325–329.

117. Miranda H V., Nembhard N, Su D, Hepowit N, Krause DJ, Pritz JR, Phillips C, Söll D, Maupin-Furlow JA. 2011. E1- and ubiquitin-like proteins provide a direct link between protein conjugation and sulfur transfer in archaea. Proc Natl Acad Sci U S A 108:4417–4422.

118. Lehmann G, Udasin RG, Livneh I, Ciechanover A. 2017. Identification of UBact, a ubiquitin-like protein, along with other homologous components of a conjugation system and the proteasome in different Gram-negative bacteria. Biochem Biophys Res Commun 483:946–950.

119. Schmitz J, Wuebbens MM, Rajagopalan K V., Leimkühler S. 2007. Role of the C-terminal Gly-Gly motif of Escherichia coli MoaD, a molybdenum cofactor biosynthesis protein with a ubiquitin fold. Biochemistry 46:909–916.

120. Hershko A, Heller H, Elias S, Ciechanover A. 1983. Components of ubiquitin-protein ligase system. Resolution, affinity purification, and role in protein breakdown. J Biol Chem 258:8206–8214.

121. Burroughs AM, Jaffee M, Iyer LM, Aravind L. 2008. Anatomy of the E2 ligase fold: Implications for enzymology and evolution of ubiquitin/Ub-like protein conjugation. J Struct Biol 162:205–218.

122. Huang DT, Hunt HW, Zhuang M, Ohi MD, Holton JM, Schulman BA. 2007. Basis for a ubiquitin-like protein thioester switch toggling E1-E2 affinity. Nature 445:394–398.

123. Müller AU, Weber-Ban E. 2019. The bacterial proteasome at the core of diverse degradation pathways. Front Mol Biosci. Frontiers Media S.A.

124. Striebel F, Imkamp F, Özcelik D, Weber-Ban E. 2014. Pupylation as a signal for proteasomal degradation in bacteria. Biochim Biophys Acta - Mol Cell Res 1843:103–113.

125. Delley CL, Müller AU, Ziemski M, Weber-Ban E. 2017. Prokaryotic Ubiquitin-Like

Protein and Its Ligase/Deligase Enyzmes. J Mol Biol. Academic Press.

126. Iyer LM, Burroughs AM, Aravind L. 2008. Unraveling the biochemistry and provenance of pupylation: A prokaryotic analog of ubiquitination. Biol Direct 3:1–7.

127. Striebel F, Imkamp F, Sutter M, Steiner M, Mamedov A, Weber-Ban E. 2009. Bacterial ubiquitin-like modifier Pup is deamidated and conjugated to substrates by distinct but homologous enzymes. Nat Struct Mol Biol 16:647–651.

128. Desterro JMP, Rodriguez MS, Kemp GD, Ronald T H. 1999. Identification of the enzyme required for activation of the small ubiquitin-like protein SUMO-1. J Biol Chem 274:10618–10624.

129. Dahl JU, Urban A, Bolte A, Sriyabhaya P, Donahue JL, Nimtz M, Larson TJ, Leimkühler S. 2011. The identification of a novel protein involved in molybdenum cofactor biosynthesis in Escherichia coli. J Biol Chem 286:35801–35812.

130. Xi J, Ge Y, Kinsland C, McLafferty FW, Begley TP. 2001. Biosynthesis of the thiazole moiety of thiamin in Escherichia coli: Identification of an acyldisulfide-linked protein - Protein conjugate that is functionally analogous to the ubiquitin/E1 complex. Proc Natl Acad Sci U S A 98:8513–8518.

131. Xu X, Wang T, Niu Y, Liang K, Yang Y. 2019. The ubiquitin-like modification by ThiS and ThiF in Escherichia coli. Int J Biol Macromol 141:351–357.

132. Leimkühler S, Wuebbens MM, Rajagopalan K V. 2001. Characterization of Escherichia coli MoeB and Its Involvement in the Activation of Molybdopterin Synthase for the Biosynthesis of the Molybdenum Cofactor. J Biol Chem 276:34695–34701.

133. Lehmann C, Begley TP, Ealick SE. 2006. Structure of the Escherichia coli ThiS-ThiF complex, a key component of the sulfur transfer system in thiamin biosynthesis. Biochemistry 45:11–19.

134. Jones CJ, Utada A, Davis KR, Thongsomboon W, Zamorano Sanchez D, Banakar V, Cegelski L, Wong GCL, Yildiz FH. 2015. C-di-GMP Regulates Motile to Sessile Transition by Modulating MshA Pili Biogenesis and Near-Surface Motility Behavior in Vibrio cholerae. PLoS Pathog 11:1–27.

135. Valentini M, Filloux A. 2016. Biofilms and Cyclic di-GMP (c-di-GMP) signaling: Lessons from Pseudomonas aeruginosa and other bacteria. J Biol Chem 291:12547–12555.

136. Lau RK, Ye Q, Birkholz EA, Berg KR, Patel L, Mathews IT, Watrous JD, Ego K, Whiteley AT, Lowey B, Mekalanos JJ, Kranzusch PJ, Jain M, Pogliano J, Corbett KD. 2020. Structure and Mechanism of a Cyclic Trinucleotide-Activated Bacterial Endonuclease Mediating Bacteriophage Immunity. Mol Cell 77:723-733.e6.

137. Yoon Sh, Waters CM. 2021. The ever-expanding world of bacterial cyclic oligonucleotide second messengers. Curr Opin Microbiol 60:96–103.

138. Northrup RS, Doyle MA, Feeley JC. 1972. In vitro susceptibility of El Tor and classical Vibrio cholerae strains to trimethoprim and sulfamethoxazole. Antimicrob Agents Chemother 1:310–314.

139. Bushby SRM. 1973. Trimethoprim-sulfamethoxazole: In vitro microbiological aspects. J Infect Dis 128:S442–S462.

140. Bach MC, Finland M, Gold O, Wilcox C. 1973. Susceptibility of recently isolated pathogenic bacteria to trimethoprim and sulfamethoxazole separately and combined. J Infect Dis 128:S508–S533.

141. Chen Z, Pickart CM. 1990. A 25-kilodalton ubiquitin carrier protein (E2) catalyzes multi-ubiquitin chain synthesis via lysine 48 of ubiquitin. J Biol Chem 265:21835–21842.

142. Yang Y, He Y, Wang X, Liang Z, He G, Zhang P, Zhu H, Xu N, Liang S. 2017. Protein SUMOylation modification and its associations with disease. Open Biol. Royal Society Publishing.

143. Cuijpers SAG, Willemstein E, Vertegaal ACO. 2017. Converging Small Ubiquitin-like Modifier (SUMO) and ubiquitin signaling: Improved methodology identifies Co-Modified target proteins. Mol Cell Proteomics 16:2281–2295.

144. Cao S, Engilberge S, Girard E, Gabel F, Franzetti B, Maupin-Furlow JA. 2017. Structural Insight into Ubiquitin-Like Protein Recognition and Oligomeric States of JAMM/MPN+ Proteases. Structure 25:823-833.e6.

145. Tahmasebi S, Ghorbani M, Savage P, Gocevski G, Yang XJ. 2014. The SUMO conjugating enzyme Ubc9 is required for inducing and maintaining stem cell pluripotency. Stem Cells 32:1012–1020.

146. Cai J, Pan C, Zhao Y, Xu H, Tian B, Wang L, Hua Y. 2022. DRJAMM Is Involved in the Oxidative Resistance in Deinococcus radiodurans. Front Microbiol 12:1–10.

147. Edelheit O, Hanukoglu A, Hanukoglu I. 2009. Simple and efficient site-directed mutagenesis using two single-primer reactions in parallel to generate mutants for

protein structure-function studies. BMC Biotechnol 9:1–8.

148. Dalia AB, McDonough EK, Camilli A. 2014. Multiplex genome editing by natural transformation. Proc Natl Acad Sci U S A 111:8937–8942.

149. Dalia TN, Yoon SH, Galli E, Barre FX, Waters CM, Dalia AB. 2017. Enhancing multiplex genome editing by natural transformation (MuGENT) via inactivation of ssDNA exonucleases. Nucleic Acids Res 45:7527–7537.

150. Dalia TN, Hayes CA, Stolyar S, Marx CJ, McKinlay JB, Dalia AB. 2017. Multiplex Genome Editing by Natural Transformation (MuGENT) for Synthetic Biology in Vibrio natriegens. ACS Synth Biol 6:1650–1655.

151. Massie JP, Reynolds EL, Koestler BJ, Cong JP, Agostoni M, Waters CM. 2012. Quantification of high-specificity cyclic diguanylate signaling. Proc Natl Acad Sci U S A 109:12746–12751.

152. Lopp A, Reintamm T, Kuusksalu A, Tammiste I, Pihlak A, Kelve M. 2010. Natural occurrence of 2′,5′-linked heteronucleotides in marine sponges. Mar Drugs 8:235–254.

153. Eskildsen S, Justesen J, Schierup MH, Hartmann R. 2003. Characterization of the 2′-5′-oligoadenylate synthetase ubiquitin-like family. Nucleic Acids Res 31:3166–3173.

154. Lo R, Stanton-Cook MJ, Beatson SA, Turner MS, Bansal N. 2015. Draft Genome Sequence of Pseudomonas fluorescens SRM1, an Isolate from Spoiled Raw Milk. Genome Announc 3:10–11.

155. Hazen TH, Sahl JW, Redman JC, Morris CR, Daugherty SC, Chibucos MC, Sengamalay NA, Fraser-Liggett CM, Steinsland H, Whittam TS, Whittam B, Manning SD, Rasko DA. 2012. Draft genome sequences of the diarrheagenic Escherichia coli collection. J Bacteriol 194:3026–3027.

156. Watve SS, Chande AT, Rishishwar L, Mariño-Ramírez L, Jordan IK, Hammer BK. 2016. Whole-genome sequences of 26 Vibrio cholerae isolates. Genome Announc 4:4–6.

157. Høyland-Kroghsbo NM. 2019. Cyclic Nucleotide Signaling: A Second Messenger of Death. Cell Host Microbe 26:567–568.

158. Baker-Austin C, Oliver JD, Alam M, Ali A, Waldor MK, Qadri F, Martinez-Urtaza J. 2018. Vibrio spp. infections. Nat Rev Dis Prim 4.

159. Thorpe KE, Joski P, Johnston KJ. 2018. Antibiotic-resistant infection treatment costs have doubled since 2002, now exceeding $2 billion annually. Health Aff 37:662–669.

160. Lin J, Nishino K, Roberts MC, Tolmasky M, Aminov RI, Zhang L. 2015. Mechanisms of antibiotic resistance. Front Microbiol 6:1–24.

161. Pallasch TJ. 2003. Antibiotic resistance. Dent Clin North Am 47:623–639.

162. Torres-Barceló C. 2018. The disparate effects of bacteriophages on antibiotic-resistant bacteria. Emerg Microbes Infect 7.

163. Yen M, Cairns LS, Camilli A. 2017. A cocktail of three virulent bacteriophages prevents Vibrio cholerae infection in animal models. Nat Commun 8:1–7.

164. McDonald ND, Regmi A, Morreale DP, Borowski JD, Fidelma Boyd E. 2019. CRISPR-Cas systems are present predominantly on mobile genetic elements in Vibrio species. BMC Genomics 20:1–23.

165. Doron S, Melamed S, Ofir G, Leavitt A, Lopatina A, Keren M, Amitai G, Sorek R. 2018. Systematic discovery of antiphage defense systems in the microbial pangenome. Science (80-) 359:eaar4120.

166. Helene Thelin K, Taylor RK. 1996. Toxin-coregulated pilus, but not mannose-sensitive hemagglutinin, is required for colonization by Vibrio cholerae O1 El Tor biotype and O139 strains. Infect Immun 64:2853–2856.

167. Yildiz FH, Schoolnik GK. 1998. Role of rpoS in stress survival and virulence of Vibrio cholerae. J Bacteriol 180:773–784.

168. Shao Y, Bassler BL. 2012. Quorum-sensing non-coding small RNAs use unique pairing regions to differentially control mRNA targets. Mol Microbiol 83:599–611.

APPENDIX

Table 1. Chapter 2 Strain list

Name	Origin?	Genotype
V. cholerae El Tor C6706	*Helen et al.*(166)	WT Peru clinical strain, Strep^R
V. cholerae El Tor C6706 CR03	*Severin et al.* (82)	*ΔVSP-IΔVSP-II*
V. cholerae El Tor C6706 Δ*cbass*	SHY	*Δcbass,* Trim^R
V. cholerae El Tor C6706 Δ*dncV*	*Severin et al.* (82)	*ΔdncV*
V. cholerae El Tor C6706 *Δvc0180Δvc0181*	This study. SHY	*Δvc0180Δvc0181*, Trim^R
V. cholerae El Tor C6706 Δ*bumo*	This study. SHY	Δ*bumo*, Trim^R
V. cholerae El Tor C6706 *bumoM1**	This study. SHY	*bumoM1**, Trim^R
V. cholerae El Tor A1552	*Yildiz et al* (167)	WT Gent^R
V. cholerae El Tor A1552 pTXB1	This study. SHY	WT with pTXB1 EV, Amp^R
V. cholerae El Tor A1552 Δ*dncV* pTXB1	This study. SHY	pTXB1 Tac promoter, EV, Amp^R, Trim^R
V. cholerae El Tor A1552 pTXB1 Bumo	This study. SHY	pTXB1 Tac promoter, C-terminal InteinCBD fused Bumo, Amp^R
V. cholerae El Tor A1552 Δ*dncV* pTXB1 Bumo	This study. SHY	Δ*dncV* pTXB1 Tac promoter, C-terminal InteinCBD-Bumo, Amp^R,Trim^R
V. cholerae El Tor A1552 pET28b	This study. SHY	pET28B T7 promoter EV, Kan^R
V. cholerae El Tor A1552 Δ*bumo* pET28b	This study. SHY	pET28B T7 promoter EV, Kan^R, Trim^R
V. cholerae El Tor A1552 *bumoM1** pET28b	This study. SHY	pET28B T7 promoter EV, Kan^R, Trim^R
V. cholerae El Tor A1552 Δ*vc0181* pET28B	This study. SHY	pET28B T7 promoter EV, Kan^R, Trim^R
V. cholerae El Tor A1552 Δ*bumoΔvc0181* pET28b	This study. SHY	pET28B T7 promoter EV, Kan^R, Trim^R
V. cholerae El Tor A1552 pET28b Bumo	This study. SHY	pET28b T7 promoter C-terminal fused to Bumo-6XHIS, Kan^R
V. cholerae El Tor A1552 *bumoM1** pET28b Bumo	This study. SHY	pET28b T7 promoter C-terminal fused to Bumo-6XHIS, Kan^R, Trim^R
V. cholerae El Tor A1552 Δ*vc0181* pET28b Bumo	This study. SHY	pET28b T7 promoter C-terminal fused to Bumo-6XHIS, Kan^R, Trim^R

Table 1. (cont'd)

V. cholerae El Tor A1552 *bumoM1**Δ*vc0181* pET28b Bumo	This study. SHY	pET28b T7 promoter C-terminal fused to Bumo-6XHIS, Kan^R, $Spec^R$
V. cholerae El Tor A1552 pET28b DncV	This study. SHY	pET28B T7 promoter 6XHIS fused to C-terminal of *dncV*, Kan^R
V. cholerae El Tor A1552 Δ*bumo* pET28b DncV	This study. SHY	pET28B T7 promoter 6XHIS fused to C-terminal of *dncV*, Kan^R
V. cholerae El Tor A1552 Δ*bumo*Δ*vc0181* pET28b DncV	This study. SHY	pET28B T7 promoter 6XHIS fused to C-terminal of *dncV*, Kan^R
V. cholerae El Tor A1552 pET28b DncV	This study. SHY	pET28B T7 promoter 6XHIS fused to C-terminal of *dncV*, Kan^R
V. cholerae El Tor A1552 *bumoM1** pET28b DncV	This study. SHY	pET28B T7 promoter 6XHIS fused to C-terminal of *dncV*, Kan^R
V. cholerae El Tor A1552 Δ*vc0180* pET28b DncV	This study. SHY	pET28B T7 promoter 6XHIS fused to C-terminal of *dncV*, Kan^R, $Trim^R$
V. cholerae El Tor A1552 Δ*vc0181* pET28b DncV	This study. SHY	pET28B T7 promoter 6XHIS fused to C-terminal of *dncV*, Kan^R, $Trim^R$
V. cholerae El Tor A1552 Δ*vc0180*Δ*vc0181* pET28b DncV	This study. SHY	pET28B T7 promoter 6XHIS fused to C-terminal of *dncV*, Kan^R, $Spec^R$
V. cholerae El Tor A1552 *bumoM1**Δ*vc0181* pET28b DncV	This study. SHY	pET28B T7 promoter 6XHIS fused to C-terminal of *dncV*, Kan^R, $Spec^R$
V. cholerae El Tor A1552 pET28B VC0180-6XHIS	This study. Geoffrey Severin	pET28b T7 promoter C-terminal 6XHIS fused VC0180, Kan^R
V. cholerae El Tor A1552 Δ*bumo* pET28B VC0180-6XHIS	This study. SHY	pET28b T7 promoter C-terminal 6XHIS fused VC0180, Kan^R, $Trim^R$
V. cholerae El Tor A1552 *bumoM1** pET28B VC0180-6XHIS	This study. SHY	Nonsense mutation in first codon of *bumo* with pET28b T7 promoter C-terminal 6XHIS fused VC0180, Kan^R, $Trim^R$
V. cholerae El Tor A1552 Δ*capV* pET28B VC0180-6XHIS	This study. SHY	pET28b T7 promoter C-terminal 6XHIS fused VC0180, Kan^R, $Trim^R$
V. cholerae El Tor A1552 Δ*dncV* pET28B VC0180-6XHIS	This study. SHY	pET28b T7 promoter C-terminal 6XHIS fused VC0180, Kan^R, $Trim^R$
V. cholerae El Tor A1552 Δ*vc0180* pET28B VC0180-6XHIS	This study. SHY	pET28b T7 promoter C-terminal 6XHIS fused VC0180, Kan^R, $Trim^R$

Table 1. (cont'd)

V. cholerae El Tor A1552 *vc0180M1STOP* pET28B VC0180-6XHIS	This study. SHY	Nonsense mutation in first codon of *vc0180* with pET28b T7 promoter C-terminal 6XHIS fused VC0180, Kan^R, $Trim^R$
V. cholerae El Tor A1552 Δ*vc0181* pET28B VC0180-6XHIS	This study. SHY	pET28b T7 promoter C-terminal 6XHIS fused VC0180, Kan^R, $Trim^R$
V. cholerae El Tor A1552 *bumoM1**Δ*vc0181* pET28B VC0180-6XHIS	This study. SHY	pET28b T7 promoter C-terminal 6XHIS fused VC0180, Kan^R, $Spec^R$
V. cholerae El Tor A1552 pET28B VC0181-6XHIS	This study. SHY	pET28b T7 promoter C-terminal 6XHIS fused VC0181, Kan^R
V. cholerae El Tor A1552 *bumoM1** pET28B VC0181-6XHIS	This study. SHY	Nonsense mutation in first codon of *bumo* with pET28b T7 promoter C-terminal 6XHIS fused VC0181, Kan^R, $Trim^R$
V. cholerae El Tor A1552 Δ*capV* pET28B VC0181-6XHIS	This study. SHY	pET28b T7 promoter C-terminal 6XHIS fused VC0181, Kan^R, $Trim^R$
V. cholerae El Tor A1552 Δ*dncV* pET28B VC0181-6XHIS	This study. SHY	pET28b T7 promoter C-terminal 6XHIS fused VC0181, Kan^R, $Trim^R$
V. cholerae El Tor A1552 Δ*vc0180* pET28B VC0181-6XHIS	This study. SHY	pET28b T7 promoter C-terminal 6XHIS fused VC0181, Kan^R, $Trim^R$
V. cholerae El Tor A1552 Δ*vc0181* pET28B VC0181-6XHIS	This study. SHY	pET28b T7 promoter C-terminal 6XHIS fused VC0181, Kan^R, $Trim^R$
V. cholerae El Tor A1552 *bumoM1**Δ*vc0181* pET28B VC0181-6XHIS	This study. SHY	pET28b T7 promoter C-terminal 6XHIS fused VC0181, Kan^R, $Spec^R$
V. cholerae El Tor A1552 *dncV*-3XFLAG tag	This study. SHY	Chromosomal C-terminal fusion of 3X-FLAG tag onto *dncV*, $Spec^R$
V. cholerae El Tor A1552 *bumoM1** *dncV*-3XFLAG tag	This study. SHY	Chromosomal C-terminal fusion of 3X-FLAG tag onto *dncV*, $Spec^R$
V. cholerae El Tor A1552 Δ*vc0181 dncV*-3XFLAG tag	This study. SHY	Chromosomal C-terminal fusion of 3X-FLAG tag onto *dncV*, $Spec^R$
V. cholerae El Tor A1552 *bumoM1**Δ*vc0181 dncV*-3XFLAG tag	This study. SHY	Chromosomal C-terminal fusion of 3X-FLAG tag onto *dncV*, $Spec^R$
V. cholerae El Tor A1552 *vc0181* E39A pET28b	This study. SHY	Substitution of E39A of *vc0181* on the chromosome with pET28b EV, , $Spec^R$

Table 1. (cont'd)

V. cholerae El Tor A1552 *bumoM1* vc0181* E39A pET28b	This study. SHY	Double mutants of *bumoM1* and s*ubstitution of E39A of *vc0181* on the chromosome with pET28b T7 promoter EV, Kan^R $Spec^R$
V. cholerae El Tor A1552 *vc0181* E39A pET28b DncV	This study. SHY	Substitution of E39A of *vc0181* on the chromosome with pET28b T7 promoter 6XHIS C-terminal tagged *dncV,* Kan^R $Spec^R$
V. cholerae El Tor A1552 *bumoM1*vc0181* E39A pET28b	This study. SHY	Double mutants of *bumoM1* and s*ubstitution of E39A of *vc0181* on the chromosome with pET28b T7 promoter 6XHIS C-terminal tagged *dncV*, Kan^R $Spec^R$
V. cholerae El Tor A1552 pTYB21 DncV	This study. SHY	pTYB21 T7 promoter N-terminal Intein-CBD fused DncV, Amp^R
V. cholerae El Tor A1552 pTYB21	This study. SHY	pTYB21 T7 promoter EV, Amp^R
V. cholerae El Tor A1552 Δ*bumo* pTYB21	This study. SHY	pTYB21 T7 promoter EV, Amp^R, $Trim^R$
V. cholerae El Tor A1552 Δ*bumoΔvc0181* pTYB21	This study. SHY	pTYB21 T7 promoter EV, Amp^R
V. cholerae El Tor A1552 Δ*bumo* pTYB21 DncV	This study. SHY	pTYb21 T7 promoter N-terminal Intein-CBD fused DncV, $Trim^R$
V. cholerae El Tor A1552 Δ*bumoΔvc0181* pTYB21 DncV	This study. SHY	pTYB21 T7 promoter N-terminal Intein-CBD fused DncV Amp^R, $Spec^R$
E. coli DH10b pLAFR	*Shao et al* (168)	pLAFR, , Tet^R
E. coli DH10b pCCD7	*Severin et al* (82)	*V. cholerae* El Tor VSP-I cloned into pLAFR, Tet^R
E. coli DH10b pCCD7 cosmid library	*Severin et al* (82)	Tranposome cosmid library , Tet^R
E. coli BL21 pTXB1	This study. SHY	pTXB1 T7 promoter EV, Amp^R
E. coli BL21 pTXB1 Bumo	This study. SHY	pTXB1 T7 promoter Bumo, Amp^R
E. coli BL21 pTYB21 VC0180	This study. SHY	pTYB21 T7 promoter with N-terminal inteinCBD fused VC0180, Amp^R

Table 2. Chapter 3 Strain list

Name	Origin?	Genotype
S. flexineri pEVS141	*John Dover (Parent lab)*	pEVS143 EV, Kan^R
S. flexineri pBMW1	*John Dover (Parent lab)*	*E. coli* EDEC13E CBASS cloned into pEVS143, Kan^R
E. coli DH10b pEVS141	*Severin et al* (82)	pEVS143 EV, Kan^R
E. coli DH10b pBMW4	This study. Bella Waters.	*E. coli* EDEC13E CBASS cloned into pEVS143, Kan^R
E. coli DH10b pEVS143 *V. cholerae* 2631-78 CBASS	This study. SHY	*V. cholerae* 2631-78 CBASS cloned into pEVS143, Kan^R
E. coli DH10b pSHY34	This study. SHY	*P. fluorescens* CBASS cloned into pEVS143, Kan^R
E. coli DH10b pEVS143 *P. fluorescens CD-NTase D79A, D81A*	This study. SHY	*P. fluorescens* CBASS cloned into pEVS143 with active site mutations D79A and D81A in *CD-NTase*, Kan^R
E. coli DH10b pEVS143 *P. fluorescens hnh-saved H56A, H91A*	This study. SHY	*P. fluorescens* CBASS cloned into pEVS143 with active site mutations in HNH motif (H56A and H91A) in *hnh-saved*, Kan^R
E. coli DH10b pEVS143 *P. fluorescens CBASS* Double mutant	This study. SHY	*P. fluorescens* CBASS cloned into pEVS143 with active site mutations D79A and D81A in *CD-NTase* HNH motif (H56A and H91A) in *hnh-saved*, Kan^R
E. coli BL21 pTXB1 *Pf* CD-NTase	This study. SHY	pTXB1 with C-terminal inteinCBD fused to *CD-NTase* of *P. fluorescens* SRM1, Amp^R
E. coli BL21 pTXB1 *Ec* CD-NTase	This study. SHY	pTXB1 with C-terminal inteinCBD fused to *CD-NTase* of *E. coli* EDEC13E, Amp^R
E. coli BL21 pTXB1 *Ec hnh-saved*	This study. SHY	pTXB1 with C-terminal inteinCBD fused to *hnh-saved* of *E. coli* EDEC13E, Amp^R